# On the Control of Active End-nodes in the Smart Grid

by

Omid Ardakanian

A thesis
presented to the University of Waterloo
in fulfillment of the
thesis requirement for the degree of
Doctor of Philosophy
in
Computer Science

Waterloo, Ontario, Canada, 2015

I hereby declare that I am the sole author of this thesis. This is a true copy of the thesis, including any required final revisions, as accepted by my examiners.

I understand that my thesis may be made electronically available to the public.

**Abstract**

The electrical grid has substantially changed in recent years due to the integration of several disruptive load and generation technologies into low-voltage distribution networks, which are meant to smarten it and improve its efficiency. These technologies have subjected the grid to unprecedented amounts of variability and uncertainty that threaten its reliability and could reduce its efficiency. Even a low penetration of these disruptive technologies may cause equipment overloads, voltage deviations beyond permissible operating thresholds, and bidirectional power flows in distribution networks.

The smart grid will comprise a vast number of active end-nodes, including electric vehicle chargers, solar inverters, storage systems, and other elastic loads, that can be quickly controlled to adjust their real and reactive power contributions. Given the availability of inexpensive measurement devices and a broadband communication network that connects measurement devices to controllers, it is possible to incorporate potentially disruptive technologies into distribution networks while maintaining service reliability, using some novel control mechanisms, which are the focus of this thesis.

In this thesis, we propose a new paradigm for the control of active end-nodes at scale. This control paradigm relies on real-time measurements of the states of the distribution network and the end-nodes rather than long-term predictions. We use an optimal control framework to design mechanisms that balance a set of system-level and user-level objectives. We study control of active end-nodes in two different contexts: a radial distribution system and a grid-connected public electric vehicle charging station powered by on-site solar generation. We develop both a feedback controller and an open-loop controller, and propose centralized and distributed algorithms for solving optimal control problems. We implement and validate these control mechanisms using extensive numerical simulations and power flow analysis on a standard test system.

**Acknowledgements**

First and foremost, I thank my advisors S. Keshav and Catherine Rosenberg for their advice, guidance, and support, which have shaped my research interests and my career path. This dissertation could not have been completed without their mentorship and I have learned many invaluable lessons from them over the course of our six year relationship. I thank Keshav for teaching me how to find and formulate a research problem, and how to be more organized and efficient at work. I thank Catherine for encouraging me to understand the system and validate assumptions.

I thank Bob Singh, my supervisor at Hydro One Inc., for familiarizing me with existing planning and operation practices in the power industry. The three months that I spent there as a research intern gave me the confidence to work in this area. I am grateful to Nicole Keshav who read through this dissertation and gave me many suggestions for improving the quality of my writing.

I also thank my committee members Steven Low, Claudio Cañizares, Yuying Li, and Peter Forsyth. They helped me improve this dissertation by clarifying details and developing a deeper understanding of power systems, and distributed optimization and control.

Others have played a role in this research as well. I thank my collaborators, colleagues, and present and past members of the ISS4E research group for beneficial discussions that we have had throughout these years. In particular, I appreciate the comments that I received from Yashar Ghiassi, Rayman Preet Singh, Milad Khaki, Earl Oliver, Andy Curtis, Dariush Fooladivanda, Tommy Carpenter, Adedamola Adepetu, Elnaz Rezaei, Alimohammad Rabbani, Ankit Pat, Negar Koochakzadeh, Fiodar Kazhamiaka, and Michael Doroshenko. I have been very lucky to have great friends and know amazing people in Waterloo. I am grateful to all of them for making life more joyful and exciting for me.

I am greatly indebted to my parents for their constant encouragement and unconditional support. I would not be here without them!

Finally, I would like to thank the Natural Sciences and Engineering Research Council of Canada (NSERC) for providing funding for this research.

# Table of Contents

# List of Tables

# List of Figures

# List of Acronyms

| | |
|---|---|
| **AC** | alternating current |
| **AIMD** | additive-increase multiplicative-decrease algorithm |
| **AMI** | advanced metering infrastructure |
| **BEV** | battery electric vehicle |
| **BMS** | battery management system |
| **CSP** | charge service provider |
| **DC** | direct current |
| **DG** | distributed generation |
| **DOD** | depth of discharge |
| **DOPF** | distribution optimal power flow |
| **DR** | demand response |
| **DSO** | distribution system operator |
| **EV** | electric vehicle |
| **EVSE** | electric vehicle supply equipment |
| **GHG** | greenhouse gas |
| **HEV** | hybrid electric vehicle |

**ICE** internal combustion engine

**LP** linear programming
**LTC** transformer load tap changer

**MCC** measurement, communication, and control node
**MDP** Markov decision process
**MIP** mixed integer programming
**MPC** model predictive control

**NUM** network utility maximization

**OPF** optimal power flow

**PEV** plug-in electric vehicle (inclusive of BEV and PHEV)
**PHEV** plug-in hybrid electric vehicle
**PV** photovoltaics

**SAE** Society of Automotive Engineers
**SOC** battery state of charge

**TCL** thermostatically controlled load
**TCP** transmission control protocol
**TOU** time-of-use

**V2G** vehicle-to-grid
**VAR** volt-ampere reactive

# List of Symbols

| | |
|---|---|
| $\alpha_i^c$ | rated charge capacity of storage $i$ |
| $\alpha_i^d$ | rated discharge capacity of storage $i$ |
| $\beta_i$ | rated capacity of EV charger $i$ |
| $\delta$ | maximum one-way communication delay from an MCC node to a charger |
| $\eta_i^c$ | charge efficiency of storage $i$ |
| $\eta_i^d$ | discharge efficiency of storage $i$ |
| $\gamma_i^c$ | charge efficiency of EV battery $i$ |
| $\kappa$ | gradient step size |
| $\mathbf{A}^e$ | bus association matrix for EV chargers |
| $\mathbf{A}^g$ | bus association matrix for PV systems |
| $\mathbf{A}^l$ | bus association matrix for inelastic loads |
| $\mathbf{A}^s$ | bus association matrix for storage systems |
| $\mathbf{M}$ | distribution network topology matrix |
| $\mathcal{B}$ | set of buses |
| $\mathcal{B}_\mathcal{Z}$ | set of buses that represent balancing zones |
| $\mathcal{B}_i$ | set of buses downstream of bus $i$ |
| $\mathcal{E}$ | set of EV chargers |

| | |
|---|---|
| $\mathcal{I}$ | set of inelastic loads |
| $\mathcal{J}$ | set of PV systems |
| $\mathcal{L}$ | set of lines |
| $\mathcal{N}$ | set of lines and transformers |
| $\mathcal{N}^i$ | set of lines and transformers upstream of bus $i$ (on its unique path to the substation) |
| $\mathcal{N}_i$ | set of lines and transformers downstream of bus $i$ |
| $\mathcal{S}$ | set of battery storage systems |
| $\mathcal{T}$ | set of all time slots |
| $\mathbb{1}_{T_i}$ | indicator function defined on the set $T_i$ |
| $\mu_a$ | parameter of the Poisson distribution representing EV arrivals |
| $\mu_d$ | parameter of the Poisson distribution representing EV departures |
| $\overline{c}_i$ | maximum SOC of storage $i$ |
| $\overline{p}_i^e(t)$ | maximum acceptable charge power of EV charger $i$ in time slot $t$ |
| $\overline{p}_i^g(t)$ | available real power at PV system $i$ in time slot $t$ |
| $\overline{p}_i^s(t)$ | maximum acceptable discharge power of storage $i$ in time slot $t$ |
| $\overline{s}_i^g$ | apparent power rating of inverter $i$ |
| $\tau$ | length of a time slot |
| $\tau_c$ | length of a control interval |
| $\underline{c}_i$ | minimum SOC of storage $i$ |
| $\underline{p}_i^e(t)$ | minimum acceptable charge power of EV charger $i$ in time slot $t$ |
| $\underline{p}_i^s(t)$ | maximum acceptable charge power of storage $i$ in time slot $t$ |
| $\xi_l$ | setpoint associated with line $l$ |

| | |
|---|---|
| $\xi_0$ | setpoint associated with the substation transformer |
| $a_i$ | time slot that EV charger $i$ becomes active |
| $C(t)$ | conventional power consumed by an EV charging station in time slot $t$ |
| $C^{\max}$ | rated capacity of the line connecting an EV charging station to the grid |
| $c_i(t)$ | SOC of storage $i$ in time slot $t$ |
| $c_l$ | available capacity of line or transformer $l$ in a specific time slot |
| $d_i$ | charging deadline of EV charger $i$ |
| $e_i(t)$ | energy required to fulfill charging demand of EV $i$ in time slot $t$ |
| $f$ | cost function |
| $G^{\max}$ | installed capacity of the PV system supplying an EV charging station |
| $L^{\max}$ | rated capacity of the line connecting chargers to supply sources in a charging station |
| $p_i^e(t)$ | charge power of EV charger $i$ in time slot $t$ |
| $p_i^g(t)$ | real power contribution of solar inverter $i$ in time slot $t$ |
| $p_i^l(t)$ | real power consumption of inelastic load $i$ in time slot $t$ |
| $p_i^s(t)$ | real power contribution of storage $i$ in time slot $t$ |
| $p_i(t)$ | total real power consumed at bus $i$ in time slot $t$ |
| $P_{ij}(t)$ | real power flow from bus $i$ to downstream bus $j$ in time slot $t$ |
| $q_j^c$ | reactive power provided by capacitors at bus $j$ in a given time slot |
| $q_i^g(t)$ | reactive power contribution of solar inverter $i$ in time slot $t$ |
| $q_i^l(t)$ | reactive power consumption of inelastic load $i$ in time slot $t$ |
| $q_i(t)$ | total reactive power consumed at bus $i$ in time slot $t$ |
| $Q_{ij}(t)$ | reactive power flow from bus $i$ to downstream bus $j$ in time slot $t$ |

| | |
|---|---|
| $r_{ij}$ | resistance of line connecting bus $i$ to bus $j$ |
| $S_{ij}(t)$ | apparent power flow from bus $i$ to downstream bus $j$ in time slot $t$ |
| $T_i$ | set of time slots in which charger $i$ is active |
| $v_0$ | voltage magnitude at the substation bus |
| $v_{\text{max}}$ | upper voltage limit in the distribution network |
| $v_{\text{min}}$ | lower voltage limit in the distribution network |
| $v_i(t)$ | voltage magnitude at bus $i$ in time slot $t$ |
| $x_{ij}$ | reactance of line connecting bus $i$ to bus $j$ |
| $z_{ij}$ | impedance of line connecting bus $i$ to bus $j$ |

* Note that the upright boldface letters represent matrices and we refer to the elements of a matrix using two indices.

# Chapter 1

# Introduction

The North American power grid is the largest machine ever built. This gigantic, carbon-intensive legacy system comprises thousands of power stations producing electricity to serve demands of millions of geographically dispersed electrical loads, and has an enormous number of transmission and distribution lines and transformers connecting the power stations to distribution substations and downstream loads. Despite the scale and complexity of the power grid, its fundamental task is surprisingly simple: it delivers power to the loads while ensuring *reliability*[1] and low cost. From the early days of the grid, reliability has always been of utmost importance. This perspective has been reflected in the planning and operation of the grid. In particular, electric utilities size and operate the grid in a way that the available generation capacity almost always[2] exceeds demand peaks and the transmission and distribution capacity is almost always sufficient to deliver power to the loads. Today, North American customers take it for granted that lights turn on as they flip a switch. They do not even notice that power system operators are taking measures to constantly and precisely balance supply and demand, and to improve the service reliability on an ongoing basis.

The traditional power grid has the following characteristics:

- **Loads –** Residential and commercial loads connected to distribution feeders are mostly *inelastic*, *i.e.*, their demand cannot be controlled and shaped. Although it is difficult to accurately predict the demand of a single load at a given time, the aggregate demand of a large number of loads across the grid behaves in a relatively predictable manner. This enables the system operators to schedule their generation units in advance.

- **Customers –** In the traditional power grid, customers are information poor, control poor, yet energy rich. They do not receive real-time electricity price or other signals that indicate the state of the power system, have no means to control or schedule their loads, and are permitted to consume electricity at will as long as their demand is lower than a limit enforced by a circuit breaker.

- **Generation –** Power stations are typically centralized and dispatchable, *i.e.*, their power output can be adjusted at the request of system operators. In many countries, most power stations burn fossil fuels to produce electricity, contributing to carbon

[1] Power system reliability generally describes the continuity of electric service to customers with a voltage and a frequency within prescribed ranges.

[2] A widely accepted benchmark value for reliability in the United States is the "one-day-in-ten-years criterion", which means that the system-wide generation capacity is expected to fall short of demand once every ten years [63].

emissions. The power stations are interconnected by high voltage transmission lines forming a mesh network with many redundant pathways. Hence, there is a clear physical and structural separation between the generation resources and the loads which are connected to distribution networks.

- **Storage –** Energy storage is expensive and scarce in the traditional grid. Thus, electricity must be produced and consumed in real-time.

Remote sensing and operation has been a common practice in transmission networks. Measurement and control nodes communicate with the transmission control room using a dedicated telemetry system. However, unlike transmission networks, which are equipped with measurement devices, traditional distribution networks are not monitored in real-time for cost reasons. Hence, distribution system operators (DSOs) has no way of determining the state of the network and cannot initiate remote remedial actions. Even the location of an outage in the distribution network is often determined by customer calls, unless it affects a manned substation [63]. Given that the grid is over-provisioned by design, service reliability is not at risk, despite having poorly measured and controlled distribution circuits.

In summary, uncertainties are minimal and manageable in traditional power systems. This is because most generation units are dispatchable, the overall demand does not vary drastically over a short period of time, and the overall demand can be predicted with sufficient accuracy several hours in advance. However, the century-old grid is extremely inefficient and under-utilized; it is sized to meet the peak demand, which tends to occur only a few hours a year. This design principle is essential to preserve reliability when demand elasticity and storage capacity are very limited, but leads to a large carbon footprint. To reduce emissions and increase efficiency of the grid, various initiatives are being undertaken by governments. These initiatives have fueled the proliferation of several demand-side technologies, three of which are discussed in the next section.

## 1.1 Drivers of Change

In recent years, the traditional grid has undergone substantial changes due to the integration of several demand-side technologies into low-voltage distribution networks, aiming to improve its efficiency and reduce carbon emissions. In the following, we introduce these low-carbon technologies and briefly overview their potential impact on the grid, highlighting the growing need for control in distribution systems. A more comprehensive

impact study is presented in Chapter 2. We restrict our focus to today's most common technologies in distribution systems, namely solar photovoltaic (PV) systems, electric vehicles (EVs)[3], and battery storage systems. We also introduce measurement, communication, and control technologies that have been widely deployed in distribution systems recently.

### 1.1.1 Solar PV Systems

Solar power has reached grid parity[4] in several jurisdictions today and is expected to soon become competitive with retail electricity in many other jurisdictions, even if existing investment tax credits expire [76]. This has led to increased deployment of rooftop solar panels in residential and commercial sectors, making solar PV distributed generation one of the fastest-growing renewable generation technologies at the present time.

Unfortunately, a high concentration of inherently-variable solar generation in distribution networks is a mixed blessing. First, increased uncertainty in generation capacity both complicates generation planning [64] and increases the need for frequency regulation by fast-ramping fossil fuel power plants, which can actually *increase* overall carbon emissions[5]. Second, solar PV generation can surpass the feeder loading in some periods, resulting in *reverse power flow* and voltage rise toward the end of the feeder [48]. Reverse flows can cause protection coordination problems and the overuse of power quality and protection devices, shortening their expected life cycle. Third, curtailing inexpensive solar power, *i.e.*, accepting less solar power than what is available and displacing it by higher-priced resources, might be necessary to avoid distribution network problems in some situations [55]. However, in many jurisdictions, electric utilities need to pay for solar generation even if it is curtailed. This leads to the paradox of a large installed base of solar generation with small actual usage of solar power, yet with higher electricity bills for all.

Growing concerns over the impacts of distributed solar generation on power system planning and operation have led to the design of sophisticated inverters that are capable of on-demand curtailment of real power and reactive power adjustment in addition to their basic task of converting direct current output of PV systems to alternating current [49]. These *smart inverters* can be controlled to tackle overvoltage conditions and the problems associated with reverse flow [97, 34, 88].

[3] Our focus is on plug-in electric vehicles (PEVs), which are a subset of EVs that can be charged from the grid. But, for convenience, these two terms are often used interchangeably in this thesis.

[4] Grid parity occurs when the levelized cost of solar PV becomes less than or equal to the retail electricity price.

[5] Germany has already encountered this problem, known as the *Energiewende* paradox [29].

### 1.1.2 Electric Vehicles

The transportation sector is by far the largest consumer of petroleum, and the second largest contributor to global greenhouse gas (GHG) emissions, accounting for about 23% of the global GHG emissions in 2012 [46]. Transportation electrification could address growing concerns over climate change and petroleum scarcity. Therefore, many governments have issued mandates to incentivize the adoption of electric vehicles so as to reduce their reliance on petroleum and cut down GHG emissions. For example, the U.S. government plans to put one million EVs on the road by 2015 [98], a goal that is very unlikely to be met!

The EV market is growing fast. Global EV stock exceeded 665,000 in 2014, which is about 0.08% of the total passenger car stock at present [28], and it is anticipated that EVs will account for 64% of U.S. light-vehicle sales and will comprise 24% of the U.S. light-vehicle fleet by 2030 [17]. Several automakers, including Nissan, Chevrolet, Toyota, General Motors, Ford, Honda, Audi, BMW, BYD, and Tesla, have embraced this technological shift and have released all-electric and plug-in hybrid EV models for the mass-market.

However, widespread EV adoption poses several new challenges for electric utilities and distribution system operators. At moderate to high penetration levels, uncontrolled electric vehicle charging can increase the peak load and energy losses, congest distribution lines and transformers, and cause voltage swings and phase imbalance in the distribution system [58, 23, 80]. Unrelieved congestion can overheat transformer windings and accelerate degradation of line and transformer insulation, leading to premature equipment failure. Excessive voltage drop can cause damage to electrical appliances.

Even at low penetration levels, there are likely to be certain neighbourhoods with high penetration levels [25]. For instance, the state of California's share of total nationwide plug-in EV registrations reached 45% in 2014, accounting for 129,470 units out of 286,842 PEVs registered in the U.S. since 2010 [20]. Uncoordinated EV charging could have detrimental impacts on the distribution network in these eco-friendly and eco-trendy neighbourhoods, even if the EV penetration level is relatively low in the entire distribution network.

To accommodate the EV charging load, utilities can take either of two approaches. The first approach is to make the required investment to upgrade the distribution circuits in a piecemeal fashion. The second approach is to exploit the elasticity of the EV charging load and the broadband communication network overlaid on the distribution network

to directly control *smart* EV chargers[6] similar to the control of PV inverters. The second approach significantly reduces the required reinforcement investment to accommodate higher EV penetration levels [73]. This is studied in more detail in Chapters 4 and 5.

### 1.1.3 Battery Storage Systems

With the growing interest in battery storage systems paired with solar PV installations and the announcement of Tesla's Gigafactory, the world's largest lithium-ion battery factory, the cost per kilowatt-hour of battery storage systems is expected to fall dramatically by 2020 [65][7]. This will increase the number of battery storage systems connected to distribution feeders, as well as those integrated into the transmission network.

Battery storage systems offer several benefits to the grid. First, storage can be used to shave peaks and level loads, reducing carbon emissions, and transmission and distribution losses. Second, it helps operators better match supply with demand to maintain frequency. Indeed, the charge and discharge powers of storage systems can be adjusted even faster than the operating setpoint of fast-ramping generators that provide regulation service, making them excellent alternatives for balancing the future grid [21]. Third, storage can reduce the curtailment of solar power, which is necessary when there is a risk of over-generation or the network access link from a solar farm is overly congested and cannot transmit excess power to other locations.

Hence, the careful control of storage can reduce reverse power flow, the need for frequency regulation from the grid, wasteful and expensive solar generation curtailment, and overall carbon emissions. Whether storage systems actually offer any of these benefits depends on how they are operated in practice. For example, a control strategy that minimizes solar curtailment should not charge storage from the grid to ensure that capacity is available when the sun is shining, whereas a control strategy that provides frequency regulation services should keep storage roughly half-full at all times to support both regulation up and regulation down.

[6] Smart EV chargers choose a charging power/rate based on control signals that they receive from the grid. They are capable of charging EVs at any rate that is not greater than the maximum charge power they support.

[7] The cost per kilowatt-hour of battery packs used by market-leading EV manufacturers was approximately US$300 in 2014 [69].

### 1.1.4 Pervasive Measurement, Communication, and Control

In the past few years, millions of *smart meters* have been rolled out around the world to collect more frequent electricity consumption data from customers and, in return, receive price and other signals from the grid. The two-way communication between meters and the grid can be used to shave demand peaks and reduce the customers' electricity bill through time-of-use pricing (TOU) and demand response (DR) programs[8]. This is just an example of how customers and the electric utility can benefit from fine-grained measurements in the distribution network. But measurements will not be limited to the electricity consumption data collected by the smart meters. Inexpensive electronics for monitoring power apparatus have been developed on a large scale in recent years and it is anticipated that distribution circuits will soon be equipped with measurement, communication, and control devices [93]. This would enable the utility and customers to learn about the state of the network in near real-time and incorporate this information in their decision making.

### 1.1.5 Emerging Challenges and Opportunities

The demand-side technologies can be classified into two major types. The first type introduces uncertainties in generation and load at various time scales. These uncertainties threaten the overall reliability of the grid and mitigating them is quite costly, requiring additional operating reserves. Solar generation technologies are examples of this type. The second type provides additional control knobs to the operators, thereby increasing the flexibility of the grid and enabling it to quickly react to operating conditions. Electric vehicles and storage technologies are examples of this type. The synergy between these two types of technology could enhance system reliability if they are carefully controlled; otherwise, these technologies impose new challenges to grid operators and can impair reliability.

## 1.2 The Smart Grid Era

To address challenges posed by the integration of the three disruptive load and generation technologies discussed above, the traditional grid is morphing into an intelligent, more

[8]We note that the advanced metering infrastructure (AMI) deployed in some jurisdictions for billing purposes may not support applications that require more frequent communications between the electric utility and customers, such as demand response.

reliable and economical, and less carbon-intensive network, referred to as the "smart grid". The smart grid heavily relies on the availability of pervasive measurement, communications, and computation in distribution networks to support two-way flows of electricity and information between the grid and its customers. The possibility of receiving near real-time information enables the seamless control of *active end-nodes*, such as EV chargers, PV inverters, and storage systems, at scale to ensure reliability and efficiency. Hence, control, especially in the last mile of distribution networks, is the enabling technology for widespread adoption of these technologies.

The smart grid can be pictured as a large-scale heterogeneous system that interconnects and controls a large number of active end-nodes. To contrast it with the traditional grid, we focus on the following characteristics of the smart grid:

- **Loads –** Future loads will not be entirely inelastic. In fact, a certain population of loads will be responsive and *elastic*, where elastic loads are defined as a class of loads that can be controlled within a limited range [21]. Examples include dedicated storage, EVs, and thermostatically controlled loads (TCLs) with inherent thermal energy storage[9]. Depending on the jurisdiction, elastic loads might be controlled directly by electric utilities or the customers who own these loads. In the latter case, signals issued by the utility along with customers' input can be incorporated into the control process.

- **Customers –** Smart grid customers will be information rich, control rich, and energy frugal. They continually receive price and control signals from the grid, might install renewable generation technologies, storage, and other elastic loads within their premises, and are capable of setting and enforcing preferences and deadlines for their elastic loads. Customers seek to be 'green' and simultaneously cut their electricity bill using the control means and information that are available to them.

- **Generation –** Power generation will no longer be from a handful of very large units. Distributed generation (DG), typically from intermittent renewable energy sources such as wind and solar, will constitute a considerable share of the supply mix[10]. Small-scale renewable technologies connected to distribution feeders are mostly non-dispatchable.

[9] What differentiates EVs from other elastic loads is that they are not connected to the system at all times and they do not necessarily reconnect to the previous location. This mobility makes the EV charging load quite unpredictable.

[10] In some countries, such as Germany, the share of renewable generation has already reached a significant level.

- **Storage –** Small-scale storage in the form of EV batteries and dedicated storage systems connected to distribution feeders will become affordable and prevalent.

In effect, smart grid operators have to deal with fast-timescale dynamics that have not been present in the traditional grid. These dynamics are introduced by fluctuating supply and demand and could be observed even at low penetration of the new load and generation technologies. Thus, fast-timescale control is crucial to counteract these fluctuations, averting reliability and power quality problems.

## 1.3 Control of Active End-nodes

The smart grid will soon connect thousands of active end-nodes that, if left uncontrolled, can affect grid reliability. This poses a critical challenge to electric utilities and power system operators as existing planning and operation practices must be updated to incorporate these new technologies.

Scheduling dispatchable generation units to meet forecasted load and reserve requirements in the most cost-effective manner has been a fundamental task in traditional power system operation. This involves solving security-constrained unit commitment[11] and security-constrained economic dispatch optimization problems to perform *unit commitment* and *economic dispatch* respectively in day-ahead and real-time electricity markets [103][12]. Both problems incorporate a set of complicated constraints, including generating unit and transmission network constraints, and are cast as optimal power flow (OPF) problems [1]. However, these optimization problems traditionally do not include numerous distribution network constraints; this is because distribution networks are typically over-provisioned and unlikely to be stressed by a specific dispatch decision. Moreover, it is quite difficult to incorporate end-node objectives in the objective functions of these problems since they might be competing with OPF objectives. Thus, traditional grid operation cannot be easily extended to control solar PV inverters, EV chargers, and

[11] Unit commitment is a mixed integer programming (MIP) problem with many variables and constraints. The current leading algorithm to solve this optimization problem is NP-hard [57]. The Lagrangian relaxation of this problem can be solved more efficiently; however, the obtained solution is suboptimal because of a nonzero duality gap [57, 39].

[12] In some jurisdictions, the predicted output of large-scale renewable generators, such as wind and solar farms connected to the transmission network, is also considered in the real-time market. Short-term predictions of renewable generation are relatively accurate and, therefore, incorporating them in the real-time market could reduce the need for operating reserves.

storage systems which are connected to distribution networks [91], although this is necessary to ensure that distribution network constraints are not violated.

Using *ad hoc* controls in the distribution network can make the distribution control system unsustainable and insecure, potentially leading to chaotic situations [92]. Hence, new mechanisms are required to control the active end-nodes at scale in the distribution network. These mechanisms should be developed as extensions of the mechanisms that are already in place for balancing the grid. In the following, we specify design goals for the new control mechanisms that should be adopted by DSOs and describe a new vision of control of active end-nodes, drawing on the design of control mechanisms originally developed for the Internet.

### 1.3.1 Goals

Control mechanisms for active end-nodes are expected to satisfy the following design goals:

- **Legacy compatibility**: Given tremendous investments that have been made in the infrastructure of the grid, new control mechanisms should be compatible with existing components and operation rules of the grid.
- **Increase utilization**: To assure high reliability, the power system is traditionally designed and operated with a substantial operating margin[13]. The smart grid should maintain reliability while decreasing the operating margin, for example by shifting elastic loads to off-peak periods
- **Reduce carbon footprint**: Control mechanisms should support large-scale integration of low-carbon technologies into distribution networks with minimal curtailment, thereby minimizing the overall carbon footprint of the grid.
- **Cost efficiency**: The smart grid control architecture must be cost-effective. For example, it should improve economics of demand-side technologies, thereby increasing their adoption.
- **Fairness**: End-nodes in the smart grid may differ in their types, technologies, and service requirements. In such a heterogenous network with limited available resources,

[13]For example, the notion of n-1 reliability requires the system to reliably withstand the failure of any one of its elements.

fair power allocation is of paramount importance to avoid starvation. Control mechanisms should provide some notion of fairness to the end-nodes such as *proportional fairness* [51] which is a compromise between efficiency and fairness.

- **Scalability**: Given the number of active end-nodes that will be connected to the smart grid, the underlying control system must be scalable. This is because computing a control decision that applies to these end-nodes is a computationally intensive task.

- **Responsiveness**: To ensure reliability in the face of increased variability and uncertainty in the smart grid, control mechanisms should rapidly respond to contingencies and operator requests. Moreover, control mechanisms should not result in unnecessary invocation of existing protection mechanisms, which could cause service interruption and reduce the life cycle of protection equipment.

- **Non-disruptiveness**: Control mechanisms should have an imperceptible impact on end users' performance, *e.g.*, EV charging time and building temperature.

Additionally, an admissible control must satisfy distribution network requirements. Specifically, it should prevent line and transformer overloads, mitigate large voltage fluctuations, and avoid reverse flows towards primary distribution feeders. We note that a control mechanism should balance these *system-level* objectives with *user-level* objectives such as fairness. These two types of objectives are often competing, making the design of the smart grid control system quite challenging.

Our work is motivated by the following insight: the smart grid resembles the Internet in several ways. In both networks, control plays a critical role in satisfying certain design goals. Thus, in the following, we focus on the nature of congestion control in the Internet and the grid and discuss how feedback control strategies that run at fast timescales are employed to avoid congestion in the Internet. This gives us some clues into how similar control mechanisms might be designed to control active end-nodes in the smart grid.

### 1.3.2 Using Internet-style Control

The Internet and the power grid share some fundamental similarities [54]. In particular, they both connect geographically dispersed suppliers to geographically dispersed customers employing a two-tier network architecture. The core and access networks in the Internet, which consist of links and routers, are similar to the transmission and

distribution networks in the grid, consisting of components such as lines and transformers. These components impose certain constraints on data and electricity flow rates, and both systems embody control mechanisms to ensure that these constraints are not violated. Interestingly, both networks can be *congested* by their customers if the capacity constraint of one of their components is violated, *e.g.*, that component is loaded beyond its rated capacity.

The transmission control protocol (TCP) in the Internet employs a distributed feedback control algorithm to adjust the traffic rate of TCP endpoints in real-time so as to avoid network congestion. Specifically, using the stream of acknowledgments arriving from the receiver, the presence of congestion is inferred by endpoints from packet loss or rising delays. This allows TCP endpoints to independently adjust their traffic rate using an additive-increase, multiplicative-decrease (AIMD) method. It has been found in practice that this algorithm is stable and scales with the size of the network [85].

Reverse engineering of the TCP congestion control has revealed that this algorithm essentially determines the available resources and allocates these resources efficiently among users by implicitly maximizing a global objective function of the users' utilities that takes fairness into account [51]. The control rules that are found by solving the optimization problem in a distributed fashion [18], exploiting the hidden decomposition structure of the optimization problem (see [70] for an introduction to network utility maximization (NUM) and decomposition theory), match the control mechanisms that were earlier introduced in an ad hoc manner. Depending on the choice of the objective function, the solution to this maximization problem provides different notions of fairness, namely proportional fairness, max-min fairness, and minimum potential delay fairness. The take-away from this exercise is that it is possible to derive simple, practical, and scalable congestion control algorithms from a principled analysis of the problem.

The similarities between the Internet and the grid inspire the application of well-established resource allocation and control schemes originally developed for the Internet to control EV chargers, PV inverters, and battery storage systems in the smart grid. In particular, we believe that a distributed control mechanism that relies on real-time measurements can be used to simultaneously achieve system-level and user-level objectives. We describe our vision of active end-node control in the smart grid next.

### 1.3.3 Our Vision

The control of active end-nodes in the distribution grid based on day-ahead predictions cannot reliably and efficiently deal with the degree of uncertainty due to the stochastic

nature of loads and renewable sources, as well as EV mobility. This is because control decisions that are computed based on day-ahead forecasts are very likely to be infeasible at the time of their execution because of prediction errors, putting power system reliability at risk. Maintaining a conservative operating margin to accommodate these prediction errors results in lowering system utilization. Thus, the growing penetration of potentially disruptive load and generation technologies motivates the control of EV chargers and similarly other active end-nodes in near real-time to cope with random and large fluctuations of load and generation. Our focus in this thesis is, therefore, on control mechanisms that run on a fast timescale using real-time measurements as opposed to long-term predictions.

Active end-nodes in the distribution network can be controlled in near real-time using two different approaches. The first approach relies on real-time measurements of the distribution network state, instead of proactive power flow calculations. Given the availability of measurement nodes in the distribution network and a broadband communication network that connects them to the end-nodes, the end-nodes can learn of changes in the grid state (such as transformer and line loadings) in real-time and adjust their power consumption or production accordingly, just as the TCP endpoints in the Internet can learn of the congestion state of the network after a small delay and back off in case of congestion without having a model of the underlying network. We take this approach in Chapter 4. The second approach relies on power flow calculations (that incorporate a network model) to compute a feasible and optimal control. An optimization problem formulated for the distribution network is solved in near real-time, using measurements of elastic and inelastic loads as well as available renewable power. This requires the knowledge of real and reactive power consumptions at different buses, which can be obtained through real-time measurements of the end-nodes. We take this approach in Chapter 5.

## 1.4 Contributions

We study the control of active end-nodes in two different systems. The first one is a radial distribution system with an overlaid network of measurement, communication, and control devices. The second one is a grid-connected public charging station that uses solar power from an on-site solar generation facility as its primary supply source. We will answer the following questions in these two systems:

1. Given a distribution system with a certain penetration of smart EV chargers, how

should the utility charge EVs to satisfy a certain fairness criterion, while avoiding network overloads? Can decision making be distributed among smart EV chargers? How sensitive is the convergence speed of a distributed control algorithm to network parameters? Is convergence guaranteed in a real-world scenario where household demands and the number of connected EVs change over time?

To answer these questions, we develop a distributed feedback control mechanism for EV chargers that relies on real-time measurements of the congestion state of feeders and transformers in Chapter 4. This work has been published as [7, 8, 9].

2. Given a distribution system with a certain penetration of smart EV chargers, dedicated battery storage systems, and PV systems with smart inverters, how should the utility control these active end-nodes to simultaneously achieve multiple competing objectives without causing network overloads, overvoltage and undervoltage conditions, and reverse flows? Can this control increase the PV penetration rate reliably accommodated in the existing distribution system? Assuming that this optimal control scheme permits sharing of solar generation and stored energy within a neighborhood, what is the impact of sharing on solar curtailment compared to energy storage for different sizes and penetration levels of storage?

   To answer these questions, we develop a decentralized open-loop control mechanism for EV chargers, PV inverters, and storage systems that relies on the model of the distribution network and real-time measurements of loads and active end-nodes in Chapter 5.

3. What is the optimal energy procurement strategy for public charging stations, given minimum service requirements? How should the charge service provider (CSP) allocate the available energy fairly and efficiently among connected EVs? Given the optimal procurement and allocation strategies, what is the earliest charging deadline that permits the CSP to use the maximum amount of solar energy?

   To answer these questions, we develop an offline algorithm for EV charging that relies on daily solar radiation and EV mobility forecasts in Chapter 6. This work has been published as [10].

## 1.5 Chapter Summary

The century-old power grid has witnessed profound changes recently due to the confluence of the following factors: 1) advances in battery and renewable technologies and the

subsequent reduction in their prices, 2) strategic decisions made by governments to reduce reliance on fossil fuels in favor of renewable energy sources, and 3) the availability of inexpensive sensing, communication, and control devices, which paved the way for pervasive measurement and control in distribution networks. These changes may subject the grid to excessive amounts of variability and uncertainty that threaten its reliability and reduce its efficiency under existing grid control paradigms. This imminent threat can be addressed by harnessing the flexibility offered by the EV charging loads. In particular, fast-timescale control of smart EV chargers at scale enables operators to meet efficiency and fairness criteria, achieve objectives of the electric utility, accommodate a higher penetration of PV generation in existing distribution systems, and enhance service reliability by preventing network overloads, voltage deviations beyond operating limits, and bidirectional power flows. This is the main focus of this thesis.

# Chapter 2

# Background and Related Work

In this chapter we give a brief overview of a radial power distribution system that supplies conventional loads as well as active end-nodes, such as PV panels, EV chargers, and dedicated storage systems. We discuss terminologies related to the active end-nodes and present an infrastructure for measurement, communications, and control, enabling them to quickly react to changes in the available network capacity measured in real-time. We define an axiomatically justified fairness criterion that we use in this work.

We then give an overview of the potential impacts of the increasing penetration of active end-nodes on reliability and efficiency of the entire grid. We survey related work on direct load control to achieve user-level objectives, such as meeting the demand of elastic loads before a deadline or providing fairness, and system-level objectives, such as enhancing reliability. Balancing these two types of objectives is nontrivial, giving rise to the design of various control architectures and many plausible control schemes as discussed in this chapter.

## 2.1 Power Distribution System

The power distribution system comprises a number of step-down transformers, lines, protective switches, and power quality equipment that are essential for delivering electricity at low voltages to different types of loads in urban and rural areas [53]. We specifically focus on a radial system which has a relatively simple structure.

### 2.1.1 Structure

A radial distribution system[1] has a single source of supply, namely the distribution substation, delivering power to residential and commercial loads through feeders radiating from the substation and *laterals* (or secondary distribution lines) branching from these feeders at certain points, known as *buses*. Figure 2.1 depicts the one-line diagram[2] of a three-phase distribution network interfacing with the transmission network and power stations at the substation. The voltage is initially reduced by the substation transformer(s) and later by pad-mount and pole-top transformers, which feed a small number of customers in a neighbourhood, to the nominal supply voltage.

[1] Our work described in Chapters 4 and 5 also applies to a loop distribution system because it is operated as a radial system at any given time. However, we describe a radial system to avoid confusion when we refer to upstream and downstream nodes.

[2] A one-line diagram represents all phase conductors between two buses by a single line.

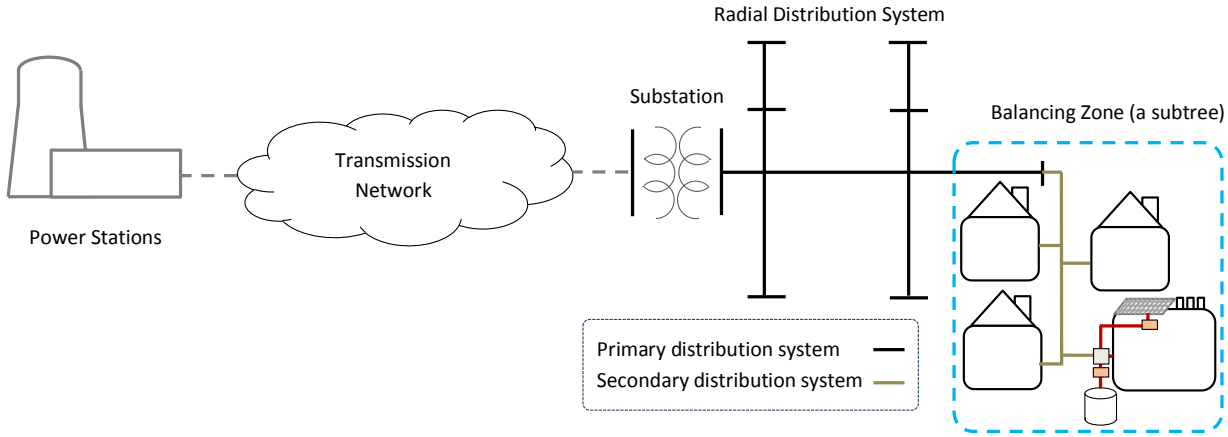


Figure 2.1: A schematic diagram of a radial distribution network that emanates from a distribution substation and consists of a number of balancing zones, one of which is illustrated here. Rooftop PV panels, storage systems, and EV chargers are connected to secondary distribution lines, similar to residential and commercial buildings.

A radial distribution system has a logical tree topology. The substation is the *root* of this tree, and electrical loads, such as homes and businesses, are its *leaves*. Radial systems have been designed with the assumption that real power flows always in the same direction, from the substation to loads. Reverse power flow can negatively affect the operation of voltage regulators and protective devices [100], and is therefore not allowed in the distribution system beyond *balancing zones*. We define a balancing zone as a subtree in which bidirectional power flow is not problematic for power quality and protection equipment. Thus, loads can be supplied by distributed generation within the same balancing zone. In today's distribution systems, a balancing zone usually starts from a distribution transformer and encompasses the low-voltage residential distribution network fed from the transformer and loads that are connected to it, as shown in Figure 2.1.

### 2.1.2 Equipment Rating and Setpoint

Resistive heating limits the capability of lines and transformers to transmit power. Hence, every line or transformer in a distribution network has a *nameplate rating* that represents

its load carrying capability without overheating[3]. Equipment loading must not exceed its nameplate rating over an extended period of time.

An electric utility can specify a *setpoint*, *i.e.*, a desired loading level, for each line or transformer in addition to its nameplate rating. The aggregate equipment loading, *i.e.*, the sum of elastic and inelastic demands supplied by this equipment, should converge to this setpoint with only a limited number of excursions above the nameplate rating. Thus, a conservative utility can ensure a very low congestion level by choosing an appropriately low setpoint. In this regard, the setpoints permit the utility to balance utilization and reliability in a distribution network.

### 2.1.3 Voltage Limits

The distribution system code requires actual service voltage to be maintained within a tolerance band, typically $\pm 5\%$ of the nominal voltage [63]. To ensure that the service voltage stays within strict bounds, electric utilities indirectly control voltage on the primary circuit, taking into account the expected voltage drop along feeders. Traditionally, voltage control in the distribution system involved the control of various devices, such as transformer load tap changers (LTCs), step voltage regulators, capacitors, and static VAR compensators.

## 2.2 An Overview of Active End-nodes

In the following, we explain technologies and terminologies related to electric vehicles, solar PV systems, and battery storage systems.

### 2.2.1 Electric Vehicles

#### Types of EVs

Electric vehicles have an on-board rechargeable battery that stores the energy required for running the vehicle. The three major types of EVs in today's mass-market are:

[3] Line ratings are usually expressed in terms of *ampacity*, whereas transformer ratings are expressed in terms of apparent power.

- *Hybrid electric vehicles (HEVs)* have an internal combustion engine (ICE) and an electric motor. The on-board battery is continually recharged with power from the internal combustion engine and regenerative braking. Unlike the other two types of EVs, HEVs do not connect to the grid to charge their batteries.

- *Plug-in hybrid electric vehicles (PHEVs)* also have an ICE and an electric motor. A PHEV battery is charged either by plugging into an electric outlet or by on-board electricity generation. Thus, a PHEV is a HEV which has a means of recharging its battery using an external source of power, *e.g.*, the grid.

- *Battery electric vehicles (BEVs)* are all-electric vehicles that have an electric motor and no ICE. These vehicles are therefore powered by a battery which is charged from the grid.

Our focus is on plug-in electric vehicles (PEVs), including PHEVs and BEVs, which connect to the grid to charge their batteries. These vehicles are examples of elastic loads.

**Battery Characteristics**

We characterize an EV battery by the following six parameters:

- *Rated capacity* is the amount of charge (in Ampere-hours) that a battery can hold.

- *Rated energy capacity* is the total amount of energy (in Watt-hours) that can be stored in the battery under the conditions predefined by the manufacturer. Hence, the rated energy capacity of a battery is equal to its rated capacity multiplied by its nominal voltage. Since most battery technologies are modular, a higher capacity battery can be made up by aggregating several battery packs.

- *Peak charge rate* is the maximum power at which the battery can be charged. For some battery technologies, this parameter depends on the state of charge (SOC) of the battery. But, we assume that a variable-rate charger can charge the battery at any rate below this maximum level.

- *Charge and discharge efficiency* is the ratio of the energy that can be restored from the battery to the energy used to charge the battery initially.

- *Maximum depth-of-discharge* is the percentage of the battery capacity that can be discharged without degrading the battery.

- *Cycle life* is the number of discharge/charge cycles the battery can handle at a specific depth-of-discharge before it fails to meet specific performance criteria.

The peak discharge rate and self-discharge are two other important battery characteristics that are not typically considered for EV batteries. It is generally assumed that the EV battery's self-discharge is negligible and the electric motor does not discharge the battery at a rate that exceeds the peak discharge rate. Moreover, we do not consider the possibility of vehicle-to-grid (V2G) in this work; thus, the peak discharge rate is not a concern.

### Supply Equipment

EV supply equipment (EVSE) has three functions according to the Society of Automotive Engineers (SAE) J1772 standard [79]. It preforms rectification, regulates voltage to a level that permits a managed charge rate, and physically couples the charger to the vehicle. The standard defines the following three allowable AC charging modes in North America:

**AC Level 1 Charging:** This method uses a standard 120V single-phase grounded outlet (ordinary household outlet). The car is plugged into the outlet using a standard J1772 connector and its on-board charger is used to charge the battery. Thus, Level 1 charging is portable and low cost, but is quite slow. It might take eight hours or more to fully charge some EV models.

**AC Level 2 Charging:** This is the primary method for private and public charging facilities [106]. Level 2 equipment has a 240V single-phase circuit and offers a wide range of charging speeds up to 80A (19.2kW). Hence, many EV models can be fully charged in less than four hours with Level 2 charging equipment.

**AC Level 3 Charging:** This method is for commercial and public fast charging, and is rarely feasible in residential areas. Level 3 charging requires an off-board charger operating with a 480V (or higher) single-phase or three-phase circuit. With this mode of charging, it is possible to fully charge an EV battery in less than an hour.

In addition to these AC charging modes, a few DC charging modes have been proposed by the SAE J1772 committee for fast recharging of EV batteries (in less than 30 minutes). This requires DC charging stations to employ special off-board chargers for high-current charging of EVs at 200–600V DC.

#### Charging Locations

Charging may take place at the following three locations:

**Home:** The primary method of charging is at home. Most people plug in their EVs on return from work and are not concerned about the charging rate as long as the battery is fully charged before starting the next trip. If the next trip occurs the following morning, drivers have ample time to charge their EVs. Thus, the battery can be charged overnight, reducing the peak demand. However, some drivers may need their EVs to make a trip late in the evening. In this case, the charging should not be delayed.

**Workplace:** EVs may be parked for almost eight hours at corporate parking lots; hence, there is plenty of time to fully charge the battery. Corporations can even take advantage of the storage capacity of the parked EVs to provide ancillary services to the grid [95], while ensuring that the batteries are fully charged by the time their employees leave. This way corporations can pay off EVSE installation costs and even profit from participating in the ancillary services market. Employees can also benefit from recharging their batteries at work (possibly at a cheaper price than the retail price of electricity).

**Public:** EV charging could be done at parking lots of supermarkets, shopping malls, airports, subway stations, libraries, and highway rest areas. Since the average parking time is relatively short in public places, deploying fast chargers at these facilities can help alleviate *range anxiety* for EV drivers.

We study residential charging in Chapter 4, workplace charging in Chapter 5, and public charging in Chapter 6.

### 2.2.2 Solar Panels and Inverters

#### Connection

Solar PV systems are broadly classified into the following two types:

**Grid-tied systems:** Grid-tied PV systems are connected to the grid using a grid intertie system, which consists of certain power electronics, including an inverter

that converts DC power into AC power. The PV system can (partly) supply a load located behind the grid intertie system and feed the excess power back to the grid when solar generation exceeds the local demand. Furthermore, solar generation can be backed up with a battery storage system. The battery charge controller can possibly be integrated into the solar inverter when the battery is connected directly to the PV system.

**Off-grid systems:** Stand-alone PV systems are designed to supply a load entirely. Hence, they are typically connected to a battery storage system, which decouples solar generation from the electricity demand.

We consider grid-tied systems in this work.

### Capacity

Grid-tied solar PV systems can be classified into the following three types based on their capacities:

**Residential:** Residential PV systems are typically installed on sloped roofs or on the rooftop of carports (parking canopies). These systems are therefore connected to secondary distribution lines and their peak capacity ranges up to 10kW. They are usually sized such that they produce approximately the amount of energy consumed by a single household over the period of a day.

**Commercial:** These systems are installed on the roof of commercial buildings and their capacity exceeds 10kW (might be on the order of a few hundred kilowatts). They connect to primary or secondary distribution lines depending on their capacity and output voltage.

**Utility-scale:** Utility-scale PV systems are ground-mount megawatt size plants that are connected either to main feeders or directly to the distribution substation via a dedicated link. These systems typically need power electronics for AC/DC conversion, an interconnection transformer, and sophisticated protection equipment.

We restrict our focus to grid-tied small-scale rooftop PV systems installed at homes and small businesses. We also study grid-connected solar parking canopies with multiple charging points.

## 2.3 Measurement, Communication and Control Infrastructure

Inexpensive electronics for monitoring and controlling power apparatus have been developed on a large scale in recent years. These power electronics can be supplemented with a transceiver, turning them into an integrated measurement, communication, and control device. We envision that future distribution networks will be equipped with *measurement, communication, and control* (MCC) nodes, which will be installed at substations, distribution transformers, and buses. The MCC nodes may cover the entire distribution network or just *hotspots*[4], where excessive overloads, voltage deviations, or reverse power flows are anticipated. We assume that the MCC nodes are interconnected by means of a reliable and broadband communication network, and that the active end-nodes are under control of the utility, so that they always react nearly immediately to signals they receive from the MCC nodes and adjust their power consumption or production according to some control rules. Thus, this measurement, communication, and control infrastructure supports the implementation of fast-timescale control mechanisms, enhancing reliability and efficiency of the network. We describe this infrastructure in more detail next.

### 2.3.1 Communication

A broadband communication network overlaid on the distribution network interconnects MCC nodes, forming a logical tree as illustrated in Figure 2.2. Specifically, every MCC node except the root MCC node installed at the distribution substation is connected to exactly one upstream MCC node and possibly several downstream MCC nodes and active end-nodes. Hence, both measurement and control signals are propagated hop-by-hop by the MCC nodes until they reach their destination. We note that the root MCC node can send signals on behalf of the (external) transmission and generation systems to force downstream loads to reduce their demand in response to generation shortfall or transmission network congestion, though this is not studied in this thesis.

[4]Partial deployment of MCC nodes at hotspots is clearly less costly. However, control mechanisms that rely on this infrastructure are incapable of tackling problems that could possibly occur in unobserved parts of the network.

### 2.3.2 Measurement

This infrastructure supports two types of measurements in a distribution network: in-network measurements performed by MCC nodes and end-node measurements performed by smart meters or other measurement devices available at the end-nodes. Control schemes may rely on either or both of these two types of measurements. We assume that both types are performed and sent periodically over the communication network to controllers at regular time slots discussed in Chapter 3; a typical time-slot duration would be 1 minute.

The MCC nodes continuously monitor the voltage level at buses, the direction of power flow in distribution feeders, and the loading of feeders and transformers. They periodically compute an average of the measured values and generate appropriate feedback, which is sent to downstream nodes using the communication network. Note that we distinguish between two possible types of feedback. The first type contains information about the *congestion state* of equipment (*e.g.*, the difference between the equipment load and its setpoint) or deviations from the nominal voltage, while the second type simply indicates the existence of congestion, overvoltage, or undervoltage.

The end-node measurement devices periodically measure real and reactive power consumptions of residential and commercial buildings as well as parameters pertaining to the active end-nodes. Specifically, they measure the available solar power, the SOC and energy demand of connected EVs, the SOC of storage systems. These measurements are sent to controllers using the communication network.

### 2.3.3 Control

The same communication network used for measurement can be used to deliver control signals to the active end-nodes. There are at least three possible approaches to the control of active end-nodes in a distribution network, as illustrated in Figure 2.3. These approaches differ in where measurement nodes are installed, what they measure, how they communicate with controllers, and how control decisions are computed based on these measurements. We discuss these approaches in the following.

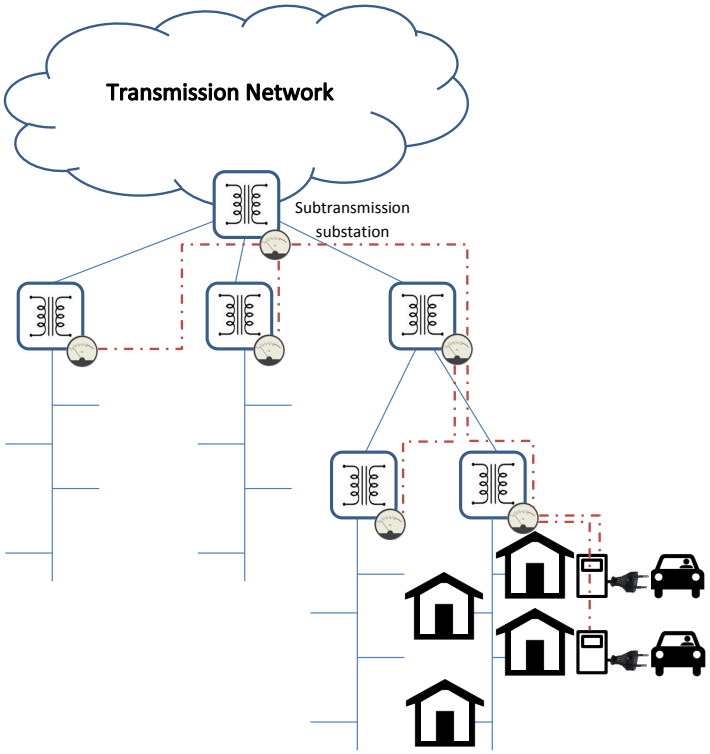


Figure 2.2: An illustration of a radial distribution system supplying inelastic loads and active end-nodes, and the overlaid communication network consisting of MCC nodes and communication links (represented by dashed lines) that connect them to each other and to downstream active end-nodes.

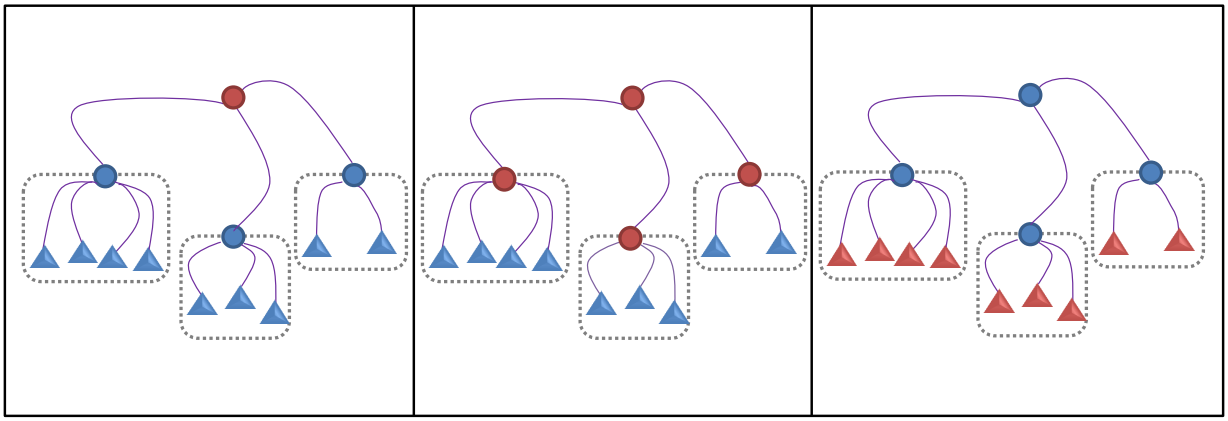

Figure 2.3: Three possible approaches to the control of active end-nodes (left: centralized; middle: hierarchical; right: distributed). Active end-nodes and MCC nodes are depicted as triangles and circles, respectively, measurement nodes are blue and controllers are red. Dotted boxes represent balancing zones.

### Centralized Control

In a centralized approach, the root MCC node installed at the substation computes the optimal control in every time slot based on measurements received from all MCC nodes. We assume that MCC nodes installed at the edge of the balancing zones collect measurements from downstream active end-nodes and send them to the root MCC node right away. Control signals generated by the root MCC node are then forwarded on through the network until they reach the active end-nodes.

### Distributed Control

In a distributed approach, active end-nodes independently adjust their power consumption or production rate based on control signals that they periodically receive from MCC nodes located on their path to the substation. Hence, every MCC node should send feedback (in the form of congestion prices defined in Chapter 4) to all active end-nodes located in its subtree. Every round of feedback is initialized by the root MCC node by flooding a request packet in the network.

#### Hierarchical Control

In a hierarchical approach, the root MCC node and MCC nodes installed at the edge of balancing zones do not perform measurements; they instead collaborate in solving the optimal control problem using only end-node measurements. Specifically, the root MCC node receives measurements from all end-nodes via the MCC nodes installed at the edge of balancing zones (defined in Section 2.1.1), while each of these MCC nodes receives measurements from active end-nodes in its subtree. The root MCC node subsequently computes certain values required for decoupling the optimal control problem at the level of balancing zones. These values are sent to the MCC nodes installed at the edge of balancing zones, enabling these nodes to independently compute the optimal control for active end-nodes in their subtree. Hence, each active end-node receives control signals from the MCC node that controls the corresponding balancing zone. This scheme is used in Chapter 5.

## 2.4 Fairness and Resource Allocation

It is crucial for scheduling policies to ensure that users are treated *fairly* and no user is starved of service in a system with constrained resources that are shared by many users. Fairness can be defined in different ways depending on the context and application. This has motivated the development of an optimization framework to unify various fairness criteria for computer systems with single or multiple types of resources.

We attribute a *utility*, *i.e.*, a measure of satisfaction, to every user. We assume that users are greedy and their utility increases with the amount of resources allocated to them in an interval that spans over one or several time slots. A fair allocation is a feasible allocation that optimizes an objective function defined in terms of the utility of all users. The choice of the objective function therefore determines the fairness criterion. In this work, we adopt a fairness criterion called *proportional fairness*. A proportionally fair allocation is a scale invariant Pareto-optimal solution, which is consistent with axioms of fairness in game theory [105]. It is shown in [50] that proportional fairness is achieved if we maximize a global objective function defined as the sum of the logarithm of the utility function of all users.

In the following chapters, we extend the notion of fair scheduling to power distribution systems with a certain population of controlled loads, such as EV chargers. Our goal is to allocate the available real power to EV chargers in a fair and efficient manner. We

attribute a utility to each EV owner. This utility is defined in different ways in different chapters. In particular, the EV owner utility is defined as the instantaneous charge power of the charger in Chapters 4 and 5, whereas it is defined as the total energy charged into the battery by the charger over the charging interval in Chapter 6.

## 2.5 Distribution System Impacts of EVs and PV Systems

Solar PV distributed generation and different types of elastic loads, such as EVs and TCLs, are becoming ubiquitous in the distribution system [30, 28]. In view of this, many studies have explored the potential impacts of large-scale integration of these technologies on the electrical grid through the intensive use of steady-state and dynamic simulations [5, 48]. Performing these impact studies for a given power system is indeed quite complex owing to uncertainties about the point of connection and the size of these technologies, and also the degree of correlation that might exist between loads and local renewable generation[5].

We remark that elastic loads, except for EVs, have been connected in large numbers to distribution feeders for a long time and operators never considered them a threat to power system reliability. With the availability of low cost communications in recent years, elastic loads, such as air conditioners, and space and water heaters, have been even utilized in some jurisdictions to shave the peak demand and to provide regulation service to the grid (see for example the *peaksaver* program in Ontario [45]). But unlike these loads, demands of EV chargers are significant, relatively unpredictable, and highly correlated. For example, EVs can be charged at up to 80A at 240V with AC Level 2 charging [79], an instantaneous demand of 19.2kW, which is equivalent to the average demand of about ten average homes in North America. This section discusses the potential impacts of EV and PV adoption on the distribution system.

### 2.5.1 EV Adoption

Studies on the impact of EV charging on distribution, transmission, and generation systems go back to the 1980s. An early paper by Heydt in 1983 [42] anticipates that the load increase due to the future penetration of EVs falls within generation planning limits; however, distribution circuits may be inadequate to accommodate the charging of EVs;

[5] For example, the workplace EV charging load is strongly correlated with solar generation, while the home-level EV charging load is usually correlated with wind generation.

therefore, transformer overloading and voltage deviations are anticipated. In this regard, load management strategies are necessary to alleviate peak loading stresses. A similar observation is made by Rahman, *et al.* [75]. The authors anticipate that with future penetration of EVs, certain distribution branches may be subject to significant overloads, even if the entire system has sufficient capacity. This is attributed to the nonuniform growth of the EV charging load in a distribution network.

The potential impacts of EV integration into the distribution network, including increased energy losses, transformer and branch congestion, voltage deviations that affect power quality, and phase imbalance, have been explored extensively in the literature [38, 44, 73, 74, 58, 23]. In recent work, Fernández, *et al.* [73] assess the impact of uncontrolled EV charging on large-scale distribution system planning in two real distribution networks. They show that the minimum reinforcement investment required to accommodate 62% EV penetration can increase the total actual network costs in a situation without EVs up to 19%. Furthermore, energy losses increase up to 20% and 40% of actual values in off-peak hours for 35% and 62% EV penetration respectively. The incremental investment can be reduced by 60-70% if a smart charging strategy is adopted.

In an effort to underscore the need for coordinated charging, Qian, *et al.* [74] analyze the impact of four different EV charging strategies on a typical UK distribution system. In the case of uncontrolled domestic charging, where EVs start charging nearly simultaneously, the daily peak load increases by 17.9%, 35.8% for 10%, and 20% EV market penetration levels respectively. This drastic increase in the peak load overloads several branches and transformers, emphasizing the need for control.

In a similar line of work, Lopes, *et al.* [58] evaluate the impact of EV integration into a typical medium voltage distribution network in terms of branch congestion levels and voltage profiles for different charging strategies. The authors show that the voltage lower limit is almost reached at several distant buses in the scenario with 10% EV penetration and uncoordinated charging. However, the lower voltage limit is reached only when EV penetration reaches 52% if a smart charging strategy is adopted. The branch congestion level is only slightly higher for the case of 52% EV penetration and smart charging than the case of 10% EV penetration and uncoordinated charging, indicating the effectiveness of a smart charging strategy in relieving congestion.

Clement Nyns, *et al.* [23] also study the impact of low to moderate EV penetration on distribution system losses and voltage deviations. Their results imply that with 30% EV penetration, uncoordinated charging leads to more than 10% voltage deviations, whereas coordinated charging keeps voltage deviations below 10% at all times. Moreover, for all charging periods and seasons, power losses noticeably decrease with coordinated

charging.

The impact of EV adoption on aging of distribution transformers is explored by Gong, *et al.* [38] and Hilshey, *et al.* [44]. In [38], a transformer thermal model is used to study the impact of Level 2 EV charging on aging of the distribution transformers installed at residential neighbourhoods. Monte Carlo simulation results show that with poor coordination of charging times, the transformer insulation life is greatly affected at relatively high EV penetration rates. Simulation results presented in [44] indicate that coordinated charging of EVs can reduce the annual transformer aging rate by more than 12.8% and 48.9% compared to uncoordinated charging when EV chargers are Level 1 and Level 2 respectively.

The above studies show that uncoordinated charging of a large population of EVs could have detrimental impacts on the existing distribution networks. Upgrading distribution circuits alone, would be quite costly for DSOs as discussed in [73]. Therefore, DSOs must incorporate a control strategy to reduce the required distribution reinforcement investment.

### 2.5.2 PV Adoption

The exponential growth of global PV cumulative installed capacity [30] has given impetus to the study of solar integration into power distribution networks and of the resultant architectural, technical, and operational problems, such as adverse impacts on power quality, protection coordination, voltage profiles, and feeder and transformer loading [100, 48]. The potential steady-state and transient impacts of PV systems on volt/var control, power quality, and power system operation depend on the penetration level and interconnection of PV units, their interactions with loads and distribution equipment, and control system behavior, making it extremely complex to understand their potential impact.

Several attempts have been made to quantify the extent of local and system-wide problems associated with PV integration. In [94], it has been shown using simulations of a test network with rooftop PV systems connected to secondary distribution lines that a 30% penetration of PV systems can be accommodated without any change to voltage control systems. Should the PV penetration increase to 50%, overvoltage is observed in simulations; this suggests that the voltage control systems must be adjusted or re-engineered at this penetration. Another study examines the impacts of high penetration of residential PVs on protection and voltage control schemes of the distribution system [13]. The conclusion is that high penetration of PVs complicates the coordination of protection equipment and creates unacceptable voltage swings (beyond pre-defined limits) on

feeders. In [43], a control methodology is described for grid-scale battery storage systems to address the negative impacts of PV integration; this methodology enables storage systems to provide voltage stability and frequency regulation, and improves the economics of distributed solar generation.

## 2.6 Taxonomy of Related Work on Control of EV Chargers

The control of smart EV chargers is essential to address the potential distribution network problems discussed in Section 2.5, while satisfying user-level objectives. Additionally, EV chargers and other elastic loads can be controlled to support higher penetrations of distributed renewable generation, and provide system services such as frequency regulation [3]. This section only surveys control mechanisms that aim to mitigate the negative impacts of EVs on the distribution network and to optimize certain user-level objectives[6]. We defer the discussion on the control of elastic loads to safely accommodate a higher penetration of distributed solar generation and to enhance the overall reliability and cost-effectiveness of the power system to Section 2.7.

We focus on control schemes that do not put customers in the control loop, meaning that the customers may specify deadlines and preferences but cannot impede or delay the execution of control decisions that are computed by the utility based on their input. We refer to these schemes as *direct control* schemes. Unlike direct load control schemes, price-based schemes assume some specific response from the customers to changes in the electricity price. This fundamental assumption does not necessarily hold in practice and the demand response is neither predictable nor immediate, rendering these schemes of limited practical value [21]. For this reason, these control schemes are not discussed in this section.

We categorize existing work into two categories based on the objectives they seek to achieve. The first category encompasses approaches that take the perspective of the electric utility and satisfy a system-level objective, whereas the second category encompasses approaches that take the perspective of users and satisfy a user-level objective, noting that users are either EV owners or CSPs. Furthermore, there are several possible approaches to control EV chargers. In particular, EV chargers have been controlled using a schedule computed the prior day (known as *pre-dispatch scheduling*) or in near real-time, and control decisions are made independently by EV chargers (a fully distributed

[6] We exclude EV control mechanisms for delivering electricity to the grid (*i.e.*, V2G applications).

| | Objective | Pre-dispatch | Real-time | |
|---|---|---|---|---|
| | | | Centralized | Decentralized |
| Utility | Avoid network congestion | [83] | [81, 82] | [102, 44, 41] |
| | Improve voltage profiles | [23, 99] | [26, 12] | |
| | Minimize losses | [23, 84, 83] | [26] | |
| | Flatten the load | [84, 36] | | [56, 36] |
| | Shave the peak load | [90, 62] | [96] | [32] |
| | Minimize the cost of generation | | [26] | |
| Users | Minimize charging cost | [90, 78, 60, 83] | [104] | [47] |
| | Minimize charging time | | [108] | [86] |
| | Maximize EV owners' convenience | | [102] | [102] |
| | Maximize CSP's revenue | | [22] | |
| | Fair power allocation to EVs | | [87] | [32] |

Table 2.1: Taxonomy of related work

approach), jointly by EV chargers and intermediate control nodes installed at transformers (a decentralized approach), or entirely by a computer cluster at the utility control center (a centralized approach). Table 2.1 shows a taxonomy of existing work on coordinated charging according to their objectives and control approaches.

### 2.6.1 Pre-Dispatch Scheduling

Pre-dispatch scheduling approaches compute charging schedules for EVs by solving an optimization problem in advance of power delivery. In some cases, this optimization problem falls within the general class of optimal power flow problems [99, 23, 83, 62]. Solving the OPF problem requires a precise model of the distribution network and inelastic loads, as well as the knowledge of the point of connection of EV chargers and arrival and departure patterns of EVs. These parameters are difficult to determine or estimate in practice. Hence, pre-dispatch scheduling approaches either maintain a conservative operating margin to accommodate estimation uncertainties or perform power flow calculations for numerous instantiations of random variables (*e.g.*, EV arrival and departure times, their initial SOC, and their point of connection). The former typically results in system under-utilization and the latter significantly increases the computation time.

For example, Mehboob, *et al.* [62] solve a distribution optimal power flow (DOPF)

problem to determine the hourly EV charging schedule and hourly tap and capacitor settings that minimize the system peak. This optimization problem incorporates voltage and feeder capacity constraints as well as EV charging constraints. They employ a genetic algorithm based approach to solve this DOPF problem. This approach generates many feasible EV load samples and performs power flow calculations for each set of samples to find the day-ahead optimal solution.

A DOPF problem is also formulated in [83] to control EV charging loads, taps, and capacitor switching decisions for the next day in an unbalanced three-phase distribution system. The authors consider various objectives and the distribution substation capacity constraint in the nonlinear programming problem. Specifically, they minimize the total energy drawn by the local distribution company and its cost, the total feeder losses, and the total cost of EV charging over the period of a day. The proposed day-ahead hourly scheduling approach is evaluated on the IEEE 13-node test feeder and a real distribution feeder. Compared to the uncontrolled charging case, their approach prevents undervoltage conditions and reduces the peak demand and losses.

Several other pre-dispatch scheduling approaches simply use the optimal control framework without relying on power flow calculations. In these cases, control might be computed more efficiently; however, it does not necessarily respect distribution network constraints such as voltage limits. Following is an overview of the most relevant work in this area.

In recent work, Gan, *et al.* [36] and Ma, *et al.* [60] use distributed control to obtain a day-ahead charging schedule for EVs. In [36], the EV charging control problem is formulated as a discrete optimization problem with the objective of flattening the aggregate demand served by a transformer. A stochastic decentralized control algorithm is proposed to find an approximate solution to this optimization problem. It is shown that this algorithm almost surely converges to one of the equilibrium charging profiles. To facilitate real-time implementation of this controlled charging scheme, the authors also propose an online version of their decentralized control algorithm in which EVs participate in negotiation on their charging profiles as they plug in for charging, over time. In [60], a decentralized algorithm is proposed to find the EV charging strategy that minimizes individual charging costs. It is shown that the optimal strategy obtained using this algorithm converges to the unique Nash equilibrium strategy when there is an infinite population of EVs. In the case of homogeneous EV populations, this Nash equilibrium strategy coincides with the valley-filling maximizing strategy, *i.e.*, the globally optimal strategy.

In [90], a deterministic optimization problem is formulated to find a fleet charging

schedule which minimizes the overall charging cost, subject to the available power, the battery capacity, and the charging power constraints. The optimization problem is deterministic because it is assumed that the connection and disconnection times of EVs, their energy demands, the price of electricity, and the total wind generation are known *a priori*. The authors also compare linear and quadratic approximations of the EV battery model in terms of violations of the battery boundaries (minimum and maximum charge levels) for the obtained charging schedule.

A similar line of work by Rotering, *et al.* [78] explores the possibility of using plug-in hybrid EVs for regulation and ancillary services while charging their batteries with minimum cost. Specifically, dynamic programming is employed to find a charging schedule that minimizes the EV charging cost based on forecasts of the electricity price, EV driving patterns, and energy demands in three different scenarios. If the control is incapable of supplying the energy demand, it is assumed that the lack of charge is fulfilled by the internal combustion engine consuming gas, which is presumably more expensive than electricity.

The relationship between the load factor, the load variance, and losses is investigated in [84]. The authors formulate three optimization problems to minimize the load variance, to maximize the load factor, and finally to minimize losses. These optimization problems are solved by a centralized approach using day-ahead load predictions, noting that the first two problems are convex and can be solved more efficiently compared to the third one. It is shown through simulations that if the distribution system is radial with all loads connected at the end, solutions to these three problems are identical, motivating the use of load factor or load variance as the objective function rather than losses. In any case, for practical systems the performance of the algorithm that minimizes the load variance is quite similar to the one that minimizes losses.

### 2.6.2 Near Real-time Control

The near real-time computation of charging schedules improves utilization and reliability of the power system compared to the pre-dispatch computation of the schedules by continuously adapting the charging rate of EV chargers to the available capacity of the network. Hence, smart EV chargers use higher rates when the distribution network has sufficient capacity, reducing these rates once the network becomes congested. The real-time charging schedule could be computed using either a centralized or a decentralized/distributed approach. In the following, we survey related work in each category.

### Centralized Approaches

Coordinated charging of EVs at parking facilities with a certain total available amount of power is the focus of [87, 22, 104, 108]. In [108], the problem of charging scheduling in a charging station with stochastic EV arrivals, variable electricity prices, and intermittent renewable generation is modelled as a constrained stochastic optimization problem which can be studied using the Markov decision process (MDP) framework. The objective is to minimize the mean waiting time of EVs. In [104], the scheduling problem of EV charging with stochastic arrivals and renewable generation is formulated as an infinite-horizon MDP. The objective is to maximize a social welfare function that takes into account total customer utility, the electricity cost associated with the charging schedule, and the penalty for failing to meet the deadlines. In [22], it is assumed that the CSP uses collocated renewable sources and supplements the renewable with the energy purchased from the grid. The authors formulate an online scheduling problem with the objective of maximizing the operating profit of the CSP while meeting the charging deadlines. This optimization problem is of the mixed integer type. Admission decisions are made based on EV arrivals, output of renewable sources, and the electricity price. The scheduler can further optimize on the time and quantity of the energy purchased from the grid. In an effort to provide a notion of fairness, an optimization problem is formulated in [87] that maximizes a weighted average of the state of charge of parked EVs in the next time step, subject to the amount of energy available from the utility, the maximum energy that can be absorbed by EVs, and the ramp rate of EV batteries. Each weight term incorporated in the objective function is a function of the energy price, and the remaining charging time and the present SOC of the corresponding EV. The authors use four computational intelligence-based algorithms, namely the estimation of distribution algorithm, the particle swarm algorithm, the genetic algorithm, and the interior point method, to solve this optimization problem and compare their performance.

A DR strategy is proposed in [81, 82] to avoid transformer and feeder congestion by controlling non-critical and controllable loads, including EVs. This strategy determines household demand limits using a simple algorithm which protects the distribution network from congestion, and issues the obtained limits to in-home controllers. Subsequently, every in-home controller determines which appliances should be on based on the priorities and preferences set by users in advance. The effect of the proposed DR on consumers comfort is quantified using comfort indices introduced in [82]. Nevertheless, the proposed DR strategy does not guarantee congestion prevention because appliances might be turned on to satisfy users' preferences even when the transformer is congested.

Deilami, *et al.* [26] propose a real-time smart load management algorithm to coordi-

nate EV chargers; this algorithm minimizes the total cost of generation and anticipated losses, while respecting user preferences. To solve this problem, their approach is to use the maximum sensitivities selection method, which selects EVs for charging from a queue sorted based on the sensitivity of the loss function to EV charging loads. A load flow analysis is performed in each time step to evaluate the objective function and ensure that system constraints, including voltage limits and the available generation capacity, are not violated. Nevertheless, this approach does not deal with line and transformer congestion.

A two-stage controller based on a model predictive control (MPC) formulation is designed in [12] to regulate charging of a time-varying number of EVs and control a fixed number of distributed generation inverters under the assumption that the load is periodic with period length of 24 hours. Using approximate power flow equations for radial distribution networks, the proposed controller charges EV batteries to a desired SOC while tracking an optimal reachable reference voltage at every bus. The proposed scheme handles plug-and-play charging requests (as EVs join or leave the system) by updating reference voltages to ensure stability and reliability under the new dynamics. This plug-and-play operation comes at the price of delaying charging of EVs that have arrived recently until bus voltages converge to the updated reference values. Note that this control scheme does not address branch and transformer congestion problems in the distribution network.

Turitsyn, *et al.* [96] aim at maximizing the utilization of the excess distribution circuit capacity while keeping the probability of a circuit overload negligible by controlling EV chargers. Using one-way broadcast communication, the authors regulate EV charging start times by computing a single EV connection rate and sending to chargers periodically. This rate determines, on average, how many EV chargers can start charging per unit time.

In summary, most existing work on real-time centralized control of EV chargers suffers from the scalability problem. Moreover, the central controller is a single point of failure in the distribution network. These issues can be addressed by distributing control among the EV chargers and possibly other control nodes as suggested in [91]. We review real-time decentralized control schemes next.

### Decentralized Approaches

We now turn our attention to decentralized and fully distributed control schemes that run in near real-time. These schemes are the closest to what we propose in Chapter 4. Specifically, they are scalable, robust, and use real-time information instead of predictions. However, unlike our scheme, they suffers from three major shortcomings. First, they do

not use a realistic model of the distribution network, which includes all branches and transformers and their operational constraints. Second, they do not evaluate the proposed solution using power flow analysis when it is not originally found using power flow calculations. Instead, many of them focus on flattening the demand of the entire distribution network, ignoring bus voltages and loading of distribution lines and transformers. Third, they do not balance efficiency and fairness of the control algorithm. In fact, fairness is not a design goal of most of these approaches. In the following, we discuss these schemes.

Wen, *et al.* [102] propose a novel approach to the EV charging control problem, where a subset of EVs are selected for charging in every time slot such that user convenience is maximized and branch flow constraints are met. This selection problem is posed as a combinatorial optimization problem, whose convex relaxation can be solved in a control center using linear programming. An efficient decentralized algorithm is then proposed based on the alternating direction method of multipliers to determine the set of EVs that must be charged in a given time slot. Using numerical simulations for different EV penetration levels, the proposed centralized and decentralized approaches are compared in terms of performance, computational complexity, and communication overhead. Moreover, the authors study effects of the control timescale, and the rounding method, which maps continuous selection variables into 0 and 1, on the performance of the decentralized algorithm. We note that this paper only addresses branch congestion and ignores other operational constraints of the distribution network, does not use power flow analysis to validate that computed charging schedules are feasible, and finally does not attempt to provide fairness to connected EVs.

Fan [32] borrows the notion of congestion pricing from the Internet to reduce the peak load while providing weighted proportional fairness to end users. Exploiting two-way communications between the utility and users, congestion prices are sent to users, enabling them to adapt their demands to the capacity of the market in a fully distributed fashion. The user preference is modelled as a willingness-to-pay parameter, *i.e.*, the weight factor in the utility function of users. The proposed algorithm is then applied to EV charging to obtain a charging rate allocation. Interestingly, the total EV charging load varies with the range from which the weight factors can be chosen. Thus, the utility has to limit this range to ensure that the total load is not greater than the market capacity. Convergence behavior of the algorithm is studied using both an analytical approach and a simulation-based approach. We note that this work does not model the distribution network and does not incorporate the capacity constraints of distribution lines and transformers and the charge rate constraints of EV chargers.

In [86], AIMD-based control schemes are used for distributed control of a set of EV chargers that share only a single constrained resource. The EV chargers independently

increase their demands by an additive factor until the shared resource becomes congested; following this event, they reduce their demands by a multiplicative factor to relieve congestion. Unlike our work, the authors study the problem from the user perspective rather than the utility perspective; they consider various scenarios and user-level objectives, and propose an AIMD-like congestion control algorithm for each scenario. Moreover, this work is not based on the theory of network utility maximization and uses an arbitrary choice of AIMD.

In [41] a control mechanism is designed to deal with the transformer overloading by modelling the transformer thermal limit as a constraint. Specifically, the authors formulate the EV charging problem as an open-loop centralized control problem with the objective of minimizing the SOC deviations from 1 and also minimizing the control effort subject to the capacity constraint of batteries and EV chargers, temperature constraint of the substation transformer, and the target SOC specified by EV owners. Using the dual decomposition method, an iterative price-coordinated implementation of this control mechanism is proposed which allows EV owners to compute their charging rate locally. A receding-horizon feedback mechanism is employed to account for unexpected disturbances, including fluctuations in inelastic demands, changes in the number of connected EVs, changes in the ambient temperature, and modelling errors. Note that this work deals with the substation transformer overloading problem and cannot prevent distribution line overloads. Furthermore, it does not use power flow analysis to validate the operation of the proposed algorithm in a test distribution network.

Li, *et al.* [56] aim at flattening the load at the distribution network level by extending the "max-weight algorithm" to the EV charging control problem. Control rules solve an optimization problem that minimizes the L2 norm of the aggregate load. It is shown that in the long term the solution to this optimization problem can be made arbitrarily close to the solution of the optimization problem that minimizes the variance of the aggregate load. The former problem can be solved in real-time. Using numerical simulations of the IEEE 37-bus and 123-bus test feeders, the performance of the algorithm is compared with static charging algorithms that use perfect knowledge and imperfect forecast of the base load for different penetration levels. Note that the authors do not attempt to address distribution network problems due to the simultaneous charging of EVs and their objective is merely to flatten the load.

Jin, *et al.* [47] propose an EV charging scheduling algorithm to minimize the energy bill of users, and, at the same time, flatten the aggregated load imposed on the power grid. Their approach is comprised of a grouping algorithm and a sliding window iterative scheduling algorithm. The grouping algorithm reduces the computation and communication overhead of the scheduling algorithm. It runs at a centralized coordinator, which is

called the information center, and classifies the EV population into several groups based on a similarity metric defined in terms of the start and end charging times, the energy requirement of an EV, and the maximum charge rate of its charger. Once EV groups are formed, the information center computes and broadcasts the charging characteristic of every group. The charging schedule is then computed using a sliding window iterative scheduling algorithm. Specifically, EVs belonging to each group solve an optimization problem to minimize the group bill and compute their charging schedule locally in a specific slot of every cycle, while charging schedules of other groups remain unchanged. When the charging rates of EVs within a group are determined, they send their updated charging profiles to the information center. The information center broadcasts real-time price/load information at the beginning of each slot of each cycle to coordinate EV chargers. When the algorithm converges, the obtained charging schedule also optimizes the total generation cost. We note that this work does not take fairness into account and does not address distribution network problems due to the simultaneous charging of EVs.

Hilshey, *et al.* [44] propose two automaton-based strategies for coordinating EV charging to limit the power supplied by transformers and decelerate their aging. Their approach is to compare the transformer aging status against four thresholds to determine whether the number of EVs being charged should be increased, decreased, or held constant in the next time period. Once the number of active chargers is determined, one of the proposed decentralized automaton-based strategies is used for admission control. The first strategy is a first-come first-served strategy in which every EV sends a charge request to the transformer. If the request is denied due to congestion, it is queued and processed again in the next time slot. The second strategy is probabilistic; it allows chargers to specify urgency by agreeing to pay a higher rate. If charging is not urgent and the request is denied, the charge request is sent to the transformer in the next time slot with a probability $p$. If charging is urgent and the request is denied, a request is sent to the transformer in every future time slot until it is admitted. Note that both control strategies do not provide fairness, and are only applicable to a single transformer supplying fixed-rate EV chargers. Moreover, the aging thresholds are chosen in an ad hoc manner.

## 2.7 Joint Control of EVs and PV Systems

Assuming the availability of an infrastructure for pervasive measurement, communications, and control, a number of studies explore the possibility of using different types of elastic loads (such as EVs) to smooth out fluctuations of renewable generation and track the difference between demand and supply in real-time [21, 89, 37, 40]. These studies employ

a direct load control mechanism to achieve a desired response to power system dynamics from a large population of elastic loads. Hence, the focus of these studies is on providing power system control services as opposed to achieving the objectives of the electric utility and enhancing the end-use performance, the direction pursued in this thesis. In fact, we are not aware of any related work that has exploited the flexibility of elastic loads to stabilize voltage, relieve congestion, prevent bidirectional flows, and minimize curtailment in a distribution system with a high concentration of solar PV generation.

Furthermore, control will not be limited to elastic loads in the smart grid. Smart inverters can also be controlled by the utility to address growing concerns over widespread adoption of PV systems and simultaneously enhance the EV charging service. Since elastic loads and PV systems have opposite impacts on distribution circuits, it is reasonable to extend the optimal control framework to jointly control elastic loads and PV inverters. This integrated control system enables the grid to safely accommodate higher penetrations of distributed solar generation and electric vehicles, while enhancing the overall reliability and cost-effectiveness of the power system. We study this problem in Chapter 5. To the best of our knowledge, no related work exploits the synergy between solar PV generation and EV charging loads in the distribution network to simultaneously achieve the above-mentioned objectives.

## 2.8 Chapter Summary

Large-scale integration of elastic loads and solar PV systems can negatively impact reliable and economical generation, transmission, and distribution of power if these end-nodes are not controlled properly. This has given impetus to the design of mechanisms to control these active end-nodes. The extensive body of literature that has been developed around the control of elastic loads can be divided into several categories based on the following criteria:

- **Time of control:** The control algorithm can run in near real-time or several hours in advance of power delivery.
- **Information needs:** The control algorithm may require the precise model of the distribution network along with load and generation forecasts, or rely on recent measurements of certain network parameters only.
- **Control scheme:** Control decisions can be computed in a centralized or decentralized manner.

- **Optimization time horizon:** Control objectives can be myopic or defined over a time horizon.

We believe that a control scheme that fully meets the design goals specified in Chapter 1 must be decentralized and based on real-time measurements. The infrastructure presented in this chapter supports the implementation of this control scheme. This scheme should enhance reliability and cost-effectiveness of the power system, satisfy user-level and device-level objectives, and mitigate adverse impacts of large-scale adoption of solar PV systems and EVs, including large voltage fluctuations, network congestion, reverse flow, and violation of voltage limits. None of the control schemes surveyed in this chapter can meet our design goals and satisfy these objectives simultaneously. This calls for the design of scalable control schemes, similar to the TCP congestion control scheme originally developed for the Internet, to balance system-level and user-level objectives.

# Chapter 3

# System Model

Several studies suggest that disruptive load and generation technologies will primarily affect distribution networks [82, 100], which are not typically monitored in real-time for cost reasons. Exploiting the availability of pervasive measurement, broadband communication, and decentralized decision making in the smart grid, different control mechanisms can be designed to effectively mitigate the adverse impacts of these technologies on distribution systems.

In this chapter we describe a simplified model of a radial distribution system and time-slotted models for loads, PV systems, EV chargers, and dedicated storage systems that will be used throughout this work, and present the set of assumptions that are common to the next three chapters.

## 3.1 Distribution System Model

### 3.1.1 Network Model

Consider a tree graph $\mathcal{G} = \{\mathcal{B}, \mathcal{L}\}$ that represents the topology of a radial system (as seen in Figure 3.1), comprising a set $\mathcal{B}$ of buses and a set $\mathcal{L}$ of lines that connect these buses just as edges of a graph connect its vertices. We denote the set of buses that each represents the root of a balancing zone by $\mathcal{B}_{\mathcal{Z}} \subset \mathcal{B}$, the set of buses located downstream of bus $i$ by $\mathcal{B}_i$, the set of all network elements (lines and transformers) by $\mathcal{N}$, the set of elements on the unique path from the substation to bus $i$ by $\mathcal{N}^i$, and the set of elements that belong to the subtree rooted at bus $i$ by $\mathcal{N}_i$.

To simplify the analysis, we study the radial system on a per-phase basis, ignoring the dependency between phases. We model homes, businesses, and other end-nodes connected to laterals as single-phase constant complex power loads, *i.e.*, their power consumption is voltage-independent. We encode the topology of the network into a matrix $\mathbf{M}$, where $\mathbf{M}_{ij}$ is 1 if bus $i$ is supplied by line or transformer $j$, and is 0 otherwise. Hence, for every bus $i$, $\mathbf{M}_{ij}$ is 1 when $j \in \mathcal{N}^i$.

We denote the setpoint associated with a line $l$ by $\xi_l$ and the setpoint associated with the substation transformer by $\xi_0$[1]. We assume that setpoints are expressed in Watts for distribution lines and transformers, remarking that the electric utility can easily translate line and transformer ratings which are expressed in Amperes and Volt-amperes,

[1]The equipment setpoint is its ideal operating point below its nameplate rating, defined in Section 2.1.2.

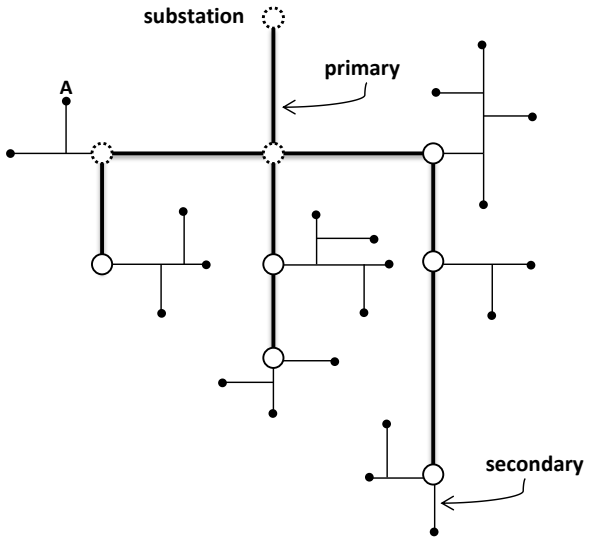


Figure 3.1: A schematic diagram of a radial distribution system representing primary and secondary lines, buses, and loads. Dotted circles represent buses that supply a load connected at point A. We refer to them as upstream buses when we talk about that load.

respectively, into setpoints using conservative estimates of the power factor and the operating voltage at corresponding nodes to err on the side of caution.

To study the dynamics of the system, we use a time-slotted model with time slots of equal length $\tau$ (typically of the order of seconds). We assume that during a single time slot, the network configuration, the demand of inelastic loads, the solar power generated by each panel, the output of each storage system, and the number of plugged-in EVs and corresponding charge powers do not change. This assumption permits us to study a dynamical system as a sequence of time slots. To simplify the conversion between energy and power units, we use *Watt-*$\tau$ as the unit of energy transmitted, produced, or consumed. For instance, if an EV is charged at the constant rate of 1 Watt in a 1 minute time slot, it consumes 1 Watt-minute of energy.

### 3.1.2 Simplified DistFlow Model

Power flow in a radial distribution system can be approximated with single-phase recursive branch flow equations, known as *DistFlow* equations [14, 15, 16]. This specific formulation leads to efficient solution methods for computing bus voltages and branch flows, given real

and reactive powers drawn from or injected to every load bus. We present the DistFlow model and a linearized model based on an approximation that ignores power losses.

Consider the distribution system in a time slot $t$. For each bus $i \in \mathcal{B}$, we denote the voltage magnitude at this bus measured on a per unit basis by $v_i(t)$ and real and reactive powers drawn from this bus by $p_i(t)$ and $q_i(t)$, respectively. Let bus 0 be the substation bus and $v_0$ be its voltage magnitude, which is assumed to be known. We use the substation bus voltage as the base value for voltage in a per-unit system; hence, $v_0$ is equal to 1p.u. in this work. We denote the impedance of a line connecting bus $i$ to bus $j$ by $z_{ij}= r_{ij} + \mathbf{j}x_{ij}$, where $\mathbf{j}$ is the imaginary unit, and $r_{ij}$ and $x_{ij}$ are the line resistance and reactance, respectively. We also denote the sending-end apparent power flow from bus $i$ to bus $j$ by $S_{ij}(t)= P_{ij}(t) + \mathbf{j}Q_{ij}(t)$, where $P_{ij}(t)$ and $Q_{ij}(t)$ are real and reactive power flows at the sending-end. The DistFlow model can be described with the following equations:

$$P_{ij}(t) = p_j(t) + \sum_{k \neq i:(j,k)\in\mathcal{L}} P_{jk}(t) + r_{ij}\frac{P_{ij}(t)^2 + Q_{ij}(t)^2}{v_i(t)^2} \tag{3.1}$$

$$Q_{ij}(t) = q_j(t) + \sum_{k \neq i:(j,k)\in\mathcal{L}} Q_{jk}(t) + x_{ij}\frac{P_{ij}(t)^2 + Q_{ij}(t)^2}{v_i(t)^2} \tag{3.2}$$

$$v_j^2(t) = v_i^2(t) - 2(r_{ij}(t)P_{ij}(t) + x_{ij}(t)Q_{ij}(t)) + (r_{ij}^2 + x_{ij}^2)\frac{P_{ij}(t)^2 + Q_{ij}(t)^2}{v_i(t)^2} \tag{3.3}$$

where $\frac{P_{ij}(t)^2+Q_{ij}(t)^2}{v_i(t)^2}$ is the square of the current magnitude that is being carried by the line connecting bus $i$ to bus $j$, meaning that the quadratic terms in the above equations represent line losses. We note that an OPF problem that incorporates the DistFlow model is not convex and, therefore, finding its solution(s) will be of exponential complexity in the number of nodes.

Since losses are typically quite smaller than real and reactive power flow components, an approximation that ignores the higher order loss terms introduces only a small error on the order of 1%. We refer to this approximate power flow model as *simplified DistFlow*. This model was originally proposed in [16] and has been used several times to formulate convex optimal control problems for distribution networks, see for example [97, 33]. The

simplified DistFlow equations can be written as follows after unfolding recursions:

$$P_{ij}(t) = \sum_{k \in \mathcal{B}_i} p_k(t) \tag{3.4}$$

$$Q_{ij}(t) = \sum_{k \in \mathcal{B}_i} q_k(t) \tag{3.5}$$

$$\begin{aligned} v_j^2(t) &= v_i^2(t) - 2(r_{ij} P_{ij}(t) + x_{ij} Q_{ij}(t)) \\ &= v_0^2 - 2\left( \sum_{k \in \mathcal{B}} p_k(t) \sum_{(m,n) \in \mathcal{L}^j \bigcap \mathcal{L}^k} r_{mn} + \sum_{k \in \mathcal{B}} q_k(t) \sum_{(m,n) \in \mathcal{L}^j \bigcap \mathcal{L}^k} x_{mn} \right) \end{aligned} \tag{3.6}$$

where $\mathcal{B}_i$ is the set of buses downstream of bus $i$ and $\mathcal{L}^j \bigcap \mathcal{L}^k$ is the set of lines that supply both bus $j$ and bus $k$. Observe that these equations are linear in the squared voltage magnitudes, and real and reactive power flows.

We remark that these linearized branch flow equations (3.4-3.6) allow us to enforce capacity and voltage limits in optimal control problems without losing computational tractability. We expand on this in Chapter 5.

Note that we use an even more simplified power flow model in Chapter 4 for the purpose of controlling EV chargers on a fast timescale. This approximate model relies on the assumption that the power factor is close to unity in the distribution system and losses are negligible. Thus, it completely ignores the reactive power flow and line losses, and describes only the real power flow as in Equation (3.4).

## 3.2 Component Models

This section presents time-slotted models that pertain to inelastic loads, solar inverters, battery storage systems, and EVs. These models describe the operation and dynamics of these components.

### 3.2.1 Residential and Commercial Loads

Residential and commercial loads are typically supplied by lateral feeders, branching from load buses. To simplify the presentation, we assume that these laterals are single-phase. We denote the set of inelastic loads connected to the distribution network by $\mathcal{I}$, and the

real and reactive power consumptions of an inelastic load $i$ in a given time slot $t$ by $p_i^l(t)$ and $q_i^l(t)$, respectively. These values are assumed to be fixed during a time slot and can be predicted quite accurately in the beginning of a time slot using measured values of previous time slots.

### 3.2.2 Solar Photovoltaic Systems

Consider a rooftop PV system that is connected via a smart inverter to the electrical service panel of a residential or a commercial building, supplied by a lateral. This small-scale PV system is single phase and does not need an interconnection transformer. The smart inverter converts the DC output of the system to AC at nominal supply voltage and frequency and provides a wide range of capabilities at the request of operators. These capabilities include injecting or absorbing reactive power and on-demand curtailment of real power[2] [49].

We use the inverter model of [97, 34]. We ignore losses associated with inverters and simultaneously control real and reactive power outputs of inverters in every time slot. We denote the set of PV systems in the distribution network by $\mathcal{J}$, and the available solar power, the inverter's rated apparent power capacity, the real power output, and the reactive power output of the PV system $i$ in a given time slot $t$ by $\overline{p}_i^g(t)$, $\overline{s}_i^g$, $p_i^g(t)$, and $q_i^g(t)$, respectively. Given that the rated apparent power capacity of the inverter is known and the available solar power is measured in this time slot, we have the following inequalities for real and reactive power contributions for this PV system:

$$p_i^g(t) \geq 0 \tag{3.7}$$

$$p_i^g(t) \leq \overline{p}_i^g(t) \tag{3.8}$$

$$p_i^g(t)^2 + q_i^g(t)^2 \leq \overline{s}_i^{g2} \tag{3.9}$$

Note that a negative value of $q_i^g(t)$ means that the inverter is consuming reactive power, while a positive value means that it is injecting reactive power in that time slot.

[2] Modern inverters can synthesize reactive power just as they produce real power. Despite the fact that the current IEEE 1547 standard for integration of distributed energy resources requires inverters to operate at unity power factor, the use of inverters to assist with voltage regulation is currently an active area of research as they can be controlled on a faster timescale compared to load tap changers and switched capacitors. This possibility is indicated in the proposed IEEE 1547.8 standard.

### 3.2.3 Battery Storage Systems

Battery storage systems are connected via an interface for AC/DC conversion and a battery management system (BMS) to the electrical service panel of residential and commercial buildings and distribution feeders. The BMS monitors the battery SOC, communicates with external devices, and ensures that charge and discharge operations are within limits of its safe operating area. The BMS enables the battery storage system to store the solar power generated by the local PV system or neighbouring systems, to serve the local demand, and to supply neighbouring loads, if permitted. This system can also immediately adopt any *feasible* charge or discharge power desired by a remote controller.

Our battery model assumes that the battery is only capable of absorbing or injecting real power. We denote the set of battery storage systems in the distribution network by $\mathcal{S}$ and the real power injection of the battery storage system $i$ in a given time slot $t$ by $p_i^s(t)$, where a negative value of $p_i^s(t)$ indicates that the battery is charging in this time slot (acting as a load) and a positive value indicates that it is discharging (acting as a generator). A feasible $p_i^s(t)$ is required to be between the effective maximum charge and discharge powers, denoted $\underline{p}_i^s(t)$ and $\overline{p}_i^s(t)$:

$$-\underline{p}_i^s(t) \leq p_i^s(t) \leq \overline{p}_i^s(t) \tag{3.10}$$

In this model, the effective maximum charge and discharge powers of the battery depend on its SOC (a number in $[0\ 1]$ interval), and the maximum charge and discharge powers supported by the BMS, denoted $\alpha_i^c$ and $\alpha_i^d$. Specifically, we have:

$$\underline{p}_i^s(t) = \min\{\alpha_i^c, (\overline{c}_i - c_i(t)) \times \frac{b_i}{\eta_i^c}\} \tag{3.11}$$

$$\overline{p}_i^s(t) = \min\{\alpha_i^d, (c_i(t) - \underline{c}_i) \times b_i \times \eta_i^d\} \tag{3.12}$$

where $b_i$ is the energy capacity of the battery, $\eta_i^c$ and $\eta_i^d$ are its charge and discharge efficiencies, and $c_i(t)$, $\underline{c}_i$, and $\overline{c}_i$ are its current, minimum, and maximum states of charge respectively. These two constraints prevent storage from overflowing or underflowing.

We can now write the state of charge evolution of the battery:

$$c_r(t+1) = \begin{cases} c_i(t) - \eta_i^c \times \frac{p_i^s(t)}{b_i} \times \tau & \text{if } -\underline{p}_i^s(t) \leq p_i^s(t) \leq 0 \\ c_i(t) - \frac{p_i^s(t)}{\eta_i^d \times b_i} \times \tau & \text{if } \quad 0 < p_i^s(t) \leq \overline{p}_i^s(t) \end{cases} \tag{3.13}$$

where $\tau$ is the length of each time slot.

### 3.2.4 Electric Vehicle Chargers

Similar to other appliances, smart EV chargers connect to the electric circuit of a residential or commercial building. They can be supplied either by local solar and storage systems or by the lateral. We assume that EV batteries cannot be discharged to offer system services as in the vehicle-to-grid case. This is a key difference between EVs and storage systems in our model. We also assume that EV chargers only consume real power.

A smart charger is called *active* when an EV is plugged in and ready for charge. An active smart charger can provide any feasible charge power desired by operators. We denote the set of EV chargers connected to the distribution network by $\mathcal{E}$ and characterize the charging load of an EV $i$ by its maximum and minimum demands in a given time slot $t$, which are denoted by $\overline{p}_i^e(t)$ and $\underline{p}_i^e(t)$ and defined:

$$\overline{p}_i^e(t) = \min\{\beta_i, e_i(t)\} \tag{3.14}$$

$$\underline{p}_i^e(t) = \min\{\overline{p}_i^e(t), \frac{e_i(t)}{d_i}\} \tag{3.15}$$

where $e_i(t)$ is the amount of energy required to fill the battery[3], $\beta_i$ is the maximum charge power supported by the charger, and $d_i$ is the charging *deadline* of the EV expressed in number of time slots. Hence, a feasible charging rate for this time slot, denoted $p_i^e(t)$, must be between the maximum and minimum demands:

$$\underline{p}_i^e(t) \leq p_i^e(t) \leq \overline{p}_i^e(t) \tag{3.16}$$

and the amount of energy required to fill the battery evolves according to the following equation:

$$e_i(t+1) = e_i(t) - \gamma_i^c \times p_i^e(t) \times \tau \tag{3.17}$$

where $\gamma_i^c$ is the charge efficiency of the battery and $\tau$ is the length of each time slot.

We note that the minimum demand of chargers would be zero if fulfilling charging demands by deadlines is not guaranteed by the charging scheme.

### 3.2.5 Bus Injection

Given the load models, we can obtain total real and reactive powers that are drawn from the distribution network at every bus. To this end, we use the binary matrices $\mathbf{A}^l$, $\mathbf{A}^e$, $\mathbf{A}^g$,

[3] A charger $i$ sets $e_i(t)$ to zero if it is inactive at the beginning of time slot $t$. Hence, $\underline{p}_i^e(t) = \overline{p}_i^e(t) = 0$ in that time slot.

and $\mathbf{A}^s$ to encode the point of connection of inelastic loads, EV chargers, PV systems, and battery storage systems, noting that elements of these matrix are referred to using two indices. For example, $\mathbf{A}^l_{ij}$ is 1, if an inelastic load indexed by $i$ is connected under a load bus $j$, and is 0 otherwise. The other matrices are defined in a similar way. Thus, real and reactive powers drawn from bus $j$ in time slot $t$ are obtained as follows:

$$p_j(t) = \sum_{i:\mathbf{A}^l_{ij}=1} p^l_i(t) + \sum_{i:\mathbf{A}^e_{ij}=1} p^e_i(t) - \sum_{i:\mathbf{A}^g_{ij}=1} p^g_i(t) - \sum_{i:\mathbf{A}^s_{ij}=1} p^s_i(t) \tag{3.18}$$

$$q_j(t) = \sum_{i:\mathbf{A}^l_{ij}=1} q^l_i(t) - \sum_{i:\mathbf{A}^g_{ij}=1} q^g_i(t) - q^c_j \tag{3.19}$$

where $q^c_j$ represents the total reactive power provided by shunt capacitors connected to bus $j$. We assume that $q^c_j$ is fixed, and set it to zero when no shunt capacitor is connected to a bus.

## 3.3 Assumptions

We now state the assumptions that are made in this chapter and also in Chapter 2.

A1 Distribution system losses are assumed to be negligible.

A2 The communication network is ubiquitous, broadband, reliable, and has a low latency. The end-to-end communication delay is on the order of a few milliseconds.

A3 MCC nodes can detect overloads, reverse flows, and over-voltage and under-voltage incidents sufficiently quickly so that any transient problem is within system tolerances and the protection system will not be invoked.

A4 Line and transformer overloads cannot be inferred from local measurements performed at end-nodes. Therefore, congestion must be explicitly signalled to the end-nodes.

A5 Active end-nodes are tamper-resistant and under control of the electric utility. Thus, any control signal sent to them is assured of a cooperative response.

A6 Active end-nodes can instantly adjust their power production or consumption to the level desired by operators. This impacts the loading of lines and transformers that supply these end-nodes almost immediately as power flows in the grid at the speed of light.

A7 EV batteries can be charged at any rate that does not exceed the maximum charge power supported by their charger, independent of their SOC. This variable rate charging has negligible impact on the lifetime of batteries.

A8 EVs are not capable of delivering power back to the grid as is the case in V2G.

A9 Battery storage systems and smart EV chargers do not consume reactive power and operate at unity power factor.

A10 Smart inverters can synthesize reactive power. We assume that their real and reactive power outputs can be jointly controlled on a fast timescale.

## 3.4 Chapter Summary

Real-time control can reliably and economically address congestion, voltage, and reverse flow problems that might occur due to the integration of residential PV systems, storage technologies, EV chargers, and other elastic loads. We presented an approximate linear branch flow model for radial distribution systems that neglects losses. Branch flow equations given by this model can be incorporated in the formulation of convex optimal control problems. We developed a time-slotted model for active end-nodes that are common in today's distribution networks. We concluded this chapter by summarizing the assumptions that we have made in modelling loads and active end-nodes.

# Chapter 4

# Congestion Management in Distribution Networks

In this chapter, we consider a radial distribution system that supplies homes and EV chargers. We explore the real-time power allocation to smart EV chargers to satisfy efficiency and fairness criteria and avoid congestion in the distribution network. Inspired by Internet congestion control mechanisms, we design a distributed feedback control mechanism for smart chargers using measurements of the congestion state of feeders and transformers. Our approach deals with line and transformer overloads but does not address voltage problems, since the underlying model ignores reactive power flows and resistive losses. We tackle these problems in Chapter 5.

## 4.1 Introduction

Uncontrolled charging of EVs can congest lines and transformers and cause voltage swings in the distribution system at moderate to high penetration levels [58, 80]. Even at low penetration levels, uncontrolled charging may lead to congestion in certain neighbourhoods, due to a non-homogeneous distribution of EVs in the distribution network [25]. Unrelieved congestion can overheat transformer windings and accelerate degradation of line and transformer insulation, leading to premature equipment failure. Although distribution system congestion can be relieved by upgrading system components piecemeal, this approach is both expensive and time-consuming. A more promising alternative is for the utility company to directly control smart EV chargers so that system components are rarely overloaded. This is the motivation for our work in this chapter.

The real-time computation of the charging rate for smart chargers achieves higher utilization than prediction-based scheduling approaches by continuously adapting the charge power of smart EV chargers to the *measured* available capacity of the network. In this approach, enabled by the widespread adoption of measurement and communication technologies in future distribution systems, information about the congestion state of lines and transformers is sent from measurement nodes to smart chargers in the form of feedback. This allows the chargers to independently adjust their charge power, using a higher rate when there is available capacity and reducing it when the distribution network becomes congested. Note that during demand peaks, the available capacity of the network may not allow chargers to charge connected EVs at their maximum rate[1]. Therefore, it is desirable to continuously allocate the available capacity in a fair manner among EV chargers. Computing the charge power for EV chargers, given the available network

[1] In fact, this is a best-effort service. Hence, in the rare event that the grid is overly congested some EVs might not be fully charged by their deadlines.

capacity, can be viewed as an optimization problem whose solution is an allocation that simultaneously satisfies efficiency and fairness criteria.

Drawing on the design of congestion control protocols in packet-switched networks [85], we formulate a nonlinear convex optimization problem for a snapshot of the system to obtain an allocation of charge powers which is both proportionally fair [50], and scale-invariant Pareto optimal [105]. We propose a TCP-inspired iterative distributed algorithm for solving the optimization problem and for computing the optimal control using dual decomposition [70] and the projected subgradient method [18]. More specifically, we decompose the dual optimization problem into several subproblems, each solved independently by a charger to adjust its charge power. These subproblems are coordinated by a master problem through *congestion prices* [50], which are computed based on the congestion state of distribution lines and transformers and communicated to EV chargers periodically. Hence, unlike TCP endpoints that infer congestion, the degree of congestion is explicitly signalled to the chargers.

We first consider a *quasi-static* setting, where household demands and the number of active chargers are fixed during a time slot, and then extend our study to a *dynamic* setting, where household demands and the number of active chargers change over time. We validate, using power flow analysis on a standard test distribution system, that our control algorithm does not violate operational limits of the distribution network and rapidly converges from large disturbances to a stable operating point in both static and dynamic settings. We investigate the sensitivity of our control algorithm to EV arrivals and departures, EV penetration levels, the rated capacity of EV chargers, and the choice of control parameters and setpoints.

This work draws on the seminal work of Low and Lapsley on flow control [59]. The authors proved and evaluated, using extensive simulations, that a distributed price-based iterative algorithm that takes a control action in every iteration converges as long as changes are sufficiently small in every iteration. Hence, our proposed control is also stable under some conditions. We analyze the convergence speed of the control algorithm in the worst case, provide engineering insights into the dynamic operation of the real-time distributed control algorithm, and discuss different design choices for control parameters to meet utility performance requirements.

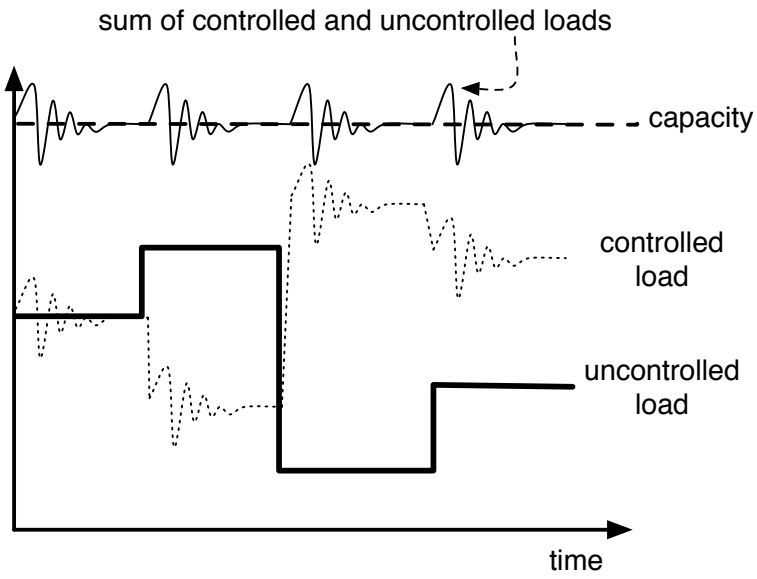


Figure 4.1: Available network capacity changes on a slower timescale than the timescale of control for active end-nodes.

## 4.2 System Model

We study a radial distribution system that supplies residential customers connected to secondary distribution lines. This radial system is equipped with MCC nodes described in Section 2.3, supporting low-latency communication and fast timescale control of the state of the power system. We assume that some customers have smart chargers at home, enabling them to recharge their EV battery when they arrive home, but no customer owns rooftop PV or dedicated storage systems. Hence, distribution lines and transformers must serve the total demand of homes and EV chargers.

It is also assumed that the aggregate home load imposed on a distribution line or transformer varies on a slower timescale than the timescale on which EV chargers can be controlled. This assumption allows us to study the control problem for a sequence of time slots of length, $\tau$, each representing a snapshot of the system in which the aggregate household demand, the available network capacity, and the number of active chargers are fixed (see Figure 4.1). The length of each time slot is chosen to be sufficiently small (on the order of several seconds) so that the aggregate household demand does not change much in each time slot in a real-world scenario.

In this chapter, we focus on a single time slot that represents a snapshot of the system and design a stable controller for this time slot. Hence, we drop the time index of all variables that are constant in this time slot. We divide each time slot into intervals of equal length $\tau_c$; hence, we have $\frac{\tau}{\tau_c}$ control intervals in every time slot. We assume that the charge power of a smart charger is fixed during one interval, but can change from one interval to another. This permits smart chargers to set their rates at certain times within a time slot. We use a time index for the charge rates of every charger when we discuss the iterative algorithm that adjusts these rates in every interval of the same time slot. The time index denotes the control interval in this case.

We formulate our control problem based on a simple DC power flow model assuming that EV chargers are single-phase constant power loads. This model neglects the dependency between phases, the reactive power flow, and line losses completely, and only describes the flow of real power in each phase of our radial system using Equation (3.4). Thus, the real power carried by the line that connects bus $n$ to downstream bus $m$ is:

$$\begin{aligned} P_{nm} &= \sum_{j \in \mathcal{B}_n} p_j \\ &= \sum_{j \in \mathcal{B}_n} \left( \sum_{i:\mathbf{A}^l_{ij}=1} p^l_i + \sum_{i:\mathbf{A}^e_{ij}=1} p^e_i \right) \end{aligned} \tag{4.1}$$

where $\mathcal{B}_n$ is the set of buses downstream of bus $n$, including bus $m$.

We use power flow analysis in Section 4.8 to check numerically if EV charging controls computed based on this model are feasible for the system under consideration, thereby validating our approach in this specific case.

## 4.3 Problem Formulation

We cast the EV charging control problem in each time slot as a centralized optimization problem. Our goal is to allocate power fairly and efficiently among active EV chargers without causing network congestion, *i.e.*, persistent overloads.

### 4.3.1 Objective Function

We assert that EV owners prefer to finish charging their EVs as soon as possible. This is due to the stochastic nature of EV departures from home and the likelihood of short trips

in the evening. Thus, it is reasonable to assume that the EV owner utility just depends on the current charge power adopted by its charger, regardless of the future charging schedule. We therefore define the utility of the EV owner $i$ as $p_i^e$.

Our optimization problem is to maximize the sum of the logarithm of the utility function for EV owners. This choice of the objective function guarantees that the optimal control is proportionally fair to EV owners, as discussed in Section 2.4. For notational simplicity, we denote $\log(p_i^e)$ by $U_i$ and remark that $U_i$ is infinitely differentiable, increasing, and strictly concave on its domain.

### 4.3.2 Constraints

We incorporate the capacity constraint of distribution lines and transformers, and the peak charging capacity of EVSE, in our optimization problem. We cannot control voltage within limits at distribution buses because reactive power flows are ignored in our model.

#### Equipment Capacity Constraint

Distribution lines and transformers should not be loaded above their setpoint for an extended period of time to avoid overheating and reduce the risk of equipment failure. Hence, for every line or transformer, control must limit the total demand of downstream homes and EV chargers to the equipment setpoint. We obtain the following capacity constraint for a line or transformer $l$ installed between bus $n$ and bus $m$:

$$\sum_{j \in \mathcal{B}_n} \sum_{i:\mathbf{A}_{ij}^e=1} p_i^e \leq c_l \qquad \forall\, l : (n,m) \in \mathcal{L},\ t \in \mathcal{T} \tag{4.2}$$

where $c_l = \xi_l - \sum_{j \in \mathcal{B}_n} \sum_{i:\mathbf{A}_{ij}^l=1} p_i^l$ is called the *available capacity* of this equipment and is fixed in each time slot.

#### EV Charger Constraint

An active smart charger can charge the connected EV at any rate that satisfies this constraint:

$$0 \leq p_i^e \leq \overline{p}_i^e \qquad \forall\, i \in \mathcal{E}, t \in \mathcal{T} \tag{4.3}$$

We remark that $\overline{p}_i^e = 0$ if charger $i$ in inactive.

### 4.3.3 Centralized Optimization Problem

We formulate the following optimization problem for a time slot to distribute the available real power among active EV chargers in a proportionally fair manner, ensuring that lines and transformers are not overloaded:

$$\max_{\mathbf{p}^e} \sum_{i \in \mathcal{E}} U_i \tag{4.4}$$

$$\begin{aligned} \text{subject to} \quad & 0 \leq p_i^e \leq \overline{p}_i^e && \forall\, i \in \mathcal{E} \\ & \sum_{j \in \mathcal{B}_n} \sum_{i : \mathbf{A}_{ij}^e = 1} p_i^e \leq c_l && \forall\, l : (n, m) \in \mathcal{L}, \end{aligned}$$

The above problem is a convex optimization problem because it maximizes an objective function that is the sum of concave functions (and is therefore concave) and the constraints form a convex set. We refer to the second constraint of this optimization problem as the *coupling constraint*; it couples EV chargers connected to different buses of the distribution network since they share at least one line or transformer on their unique path to the substation. The solution to this optimization problem is a proportionally fair power allocation to active EV chargers that satisfies equipment capacity and charger constraints. We refer to this solution as optimal control.

In the next section, we write the dual problem and apply the dual decomposition method to obtain a set of decoupled subproblems and a master problem that coordinates them. We then design an iterative distributed algorithm to solve these subproblems independently at charging points.

## 4.4 Controller Design

The centralized optimization problem presented in the previous section is a standard network utility maximization problem which can be solved in a distributed fashion [70]. The distributed approach is more scalable and robust compared to a centralized approach as it reduces the computation overhead and distributes decision making.

Our plan is, therefore, to design a distributed algorithm that solves the Lagrangian dual of the centralized optimization problem. We apply the dual decomposition method to obtain a set of decoupled subproblems that are controlled at the higher level by a master problem through congestion prices. The proposed algorithm requires solving the master

problem and these subproblems in an iterative fashion until convergence to primal and dual solutions. From a control theory standpoint, solutions to these problems constitute our control and congestion prices are feedback.

### 4.4.1 Dual Problem

Consider the Lagrangian relaxation of the optimization problem (4.4):

$$g(\lambda) = \max_{0 \preceq \mathbf{p}^e \preceq \overline{\mathbf{p}}^e} \left\{ \sum_{i \in \mathcal{E}} \log(p_i^e) + \sum_{l:(n,m) \in \mathcal{L}} \lambda_l (c_l - \sum_{j \in \mathcal{B}_n} \sum_{i:\mathbf{A}_{ij}^e = 1} p_i^e) \right\}, \tag{4.5}$$

where $\mathbf{p}^e = (p_1^e, \ldots, p_{|\mathcal{E}|}^e)$ and $\overline{\mathbf{p}}^e = (\overline{p}_1^e, \ldots, \overline{p}_{|\mathcal{E}|}^e)$ are vectors of charge powers and maximum charge powers of EV chargers, respectively, and $\lambda = (\lambda_1, \ldots, \lambda_{|\mathcal{L}|})$ is a vector of Lagrangian multipliers associated with the coupling constraints. The dual problem is

$$\begin{aligned} &\min_{\lambda} g(\lambda) \\ &\text{subject to} \qquad \lambda \succeq 0, \end{aligned} \tag{4.6}$$

which can be written in this form by taking out the term that depends on Lagrangian multipliers from the maximization:

$$\begin{aligned} &\min_{\lambda} \left\{ \sum_{l \in \mathcal{L}} \lambda_l c_l + \max_{0 \preceq \mathbf{p}^e \preceq \overline{\mathbf{p}}^e} \left\{ \sum_{i \in \mathcal{E}} f_i(p_i^e; \lambda) \right\} \right\} \\ &\text{subject to} \qquad \lambda_l \geq 0 \qquad \forall l \in \mathcal{L}, \end{aligned} \tag{4.7}$$

where

$$f_i(p_i^e; \lambda) = \log(p_i^e) - p_i^e \left( \sum_{j:[\mathbf{A}^e \times \mathbf{M}]_{ij} = 1} \lambda_j \right), \tag{4.8}$$

and $[\mathbf{A}^e \times \mathbf{M}]_{il}$ is equal to 1 if charger $i$ is downstream of (and therefore supplied by) line or transformer $j$. Hence, $\sum_{j:[\mathbf{A}^e \times \mathbf{M}]_{ij}=1} \lambda_j$ is the sum of Lagrangian multipliers associated with capacity constraints of lines and transformers that supply charger $i$. In fact, these lines and transformers are located on the unique path from charger $i$ to the substation.

Since dual variables are not introduced for EV charger constraints, we restrict the maximization over $\mathbf{p}^e$ to $[\mathbf{0}\ \overline{\mathbf{p}}^e]$ (see Section 3.4.2 in [18]). We note that $f(\mathbf{p}^e; \lambda)$ represents

$f$ as a function of $\mathbf{p}^e$ parameterized by $\lambda$, and $f_i(p_i^e;\lambda)$ is concave and has a unique maximum as it is the sum of two concave functions of $p_i^e$.

Importantly, strong duality holds in this case because all inequality constraints are affine. We can write the following KKT optimality conditions for the original optimization problem:

$$\left[\frac{1}{\sum_{j:[\mathbf{A}^e\times\mathbf{M}]_{ij}=1}\hat{\lambda}_j}\right]_0^{\overline{p}_i^e} = \hat{p}_i^e \qquad \forall i \in \mathcal{E} \tag{4.9}$$

$$\hat{\lambda}_l\Big(\sum_{j\in\mathcal{B}_n}\sum_{i:\mathbf{A}_{ij}^e=1}\hat{p}_i^e - c_l\Big) = 0 \qquad \forall\, l:(n,m)\in\mathcal{L} \tag{4.10}$$

$$\sum_{j\in\mathcal{B}_n}\sum_{i:\mathbf{A}_{ij}^e=1}\hat{p}_i^e \le c_l \qquad \forall\, l:(n,m)\in\mathcal{L} \tag{4.11}$$

$$0 \le \hat{p}_i^e \le \overline{p}_i^e \qquad \forall i \in \mathcal{E} \tag{4.12}$$

$$0 \le \hat{\lambda}_l \qquad \forall l \in \mathcal{L} \tag{4.13}$$

where $\hat{\mathbf{p}}^e$ and $\hat{\lambda}$ are the primal and dual solutions and $[c]_a^b = \min\{\max\{c,a\},b\}$. The first condition, which is the stationarity condition, states that the gradient of Lagrangian vanishes at the optimal point, and the second condition, which is the complementary slackness condition, implies that either the optimal Lagrangian multiplier is zero or the corresponding line or transformer is *fully utilized*, *i.e.*, the line or transformer load has reached its setpoint.

### 4.4.2 Dual Decomposition

Writing the Lagrangian dual problem in the form of (4.7) reveals its hidden decomposition structure. Specifically, each EV charger can locally solve a subproblem given by

$$\max_{0\le p_i^e\le\overline{p}_i^e} f_i(p_i^e;\lambda) \tag{4.14}$$

provided that it knows the sum of the Lagrangian multipliers corresponding to the lines and transformers on its unique path to the substation. It turns out that Lagrangian multipliers play the role of congestion prices (or shadow prices [51]).

These subproblems are controlled by a master problem by means of congestion prices. The master problem is responsible for updating the congestion prices. It can be written in

the following form

$$\min_{\lambda \succeq 0} \left\{ \sum_{l \in \mathcal{L}} \lambda_l c_l + \sum_{i \in \mathcal{E}} f_i^*(p_i^e; \lambda) \right\}. \tag{4.15}$$

where $f_i^*(p_i^e; \lambda)$ is the optimal value of (4.14) for a given vector of Lagrangian multipliers. We remark that the objective function of the master problem is linear in $\lambda$ and its derivative with respect to a Lagrangian multiplier, $\lambda_l$, is

$$\frac{\partial g}{\partial \lambda_l}(\lambda) = c_l - \sum_{j \in \mathcal{B}_n} \sum_{i: \mathbf{A}_{ij}^e = 1} p_i^e \tag{4.16}$$

### 4.4.3 Control Rules

Our approach is to solve the dual optimization problem using an iterative distributed algorithm that runs every $\tau_c$. Each iteration of this algorithm corresponds to a control interval and is comprised of two separate phases. In the first phase, the congestion price of every line or transformer is updated by the corresponding MCC node. Specifically, the MCC node updates its congestion price by solving the master problem using the gradient projection method. Then, in the second phase, the new charge power of every EV is computed by its smart charger. Specifically, the smart charger solves the subproblem given the most recent prices that are received.

We now derive control rules for updating congestion prices and adjusting charging rates by solving the master problem and the subproblems, respectively. These control rules constitute the distributed algorithm outlined in Section 4.5. In Section 4.6, we specify sufficient conditions for convergence of this algorithm to primal and dual solutions.

We use $p_i^e(t)$ and $\lambda_l(t)$ to denote the charge power of EV charger $i$ and the congestion price computed for $l$ in the control interval $t$ of the time slot that we consider, respectively.

#### Control Rule for Updating the Congestion Price

Since the dual function is differentiable, we can adopt the gradient method with a projection onto the positive orthant to solve the master problem (4.15). The following rule updates the congestion price for line or transformer $l$ that connects bus $n$ to downstream bus $m$ in the opposite direction of the gradient of the dual function, using its value in the

control interval $t$.

$$\lambda_l(t+1) = \max\{\lambda_l(t) - \kappa(c_l - \sum_{j\in\mathcal{B}_n}\sum_{i:\mathbf{A}^e_{ij}=1} p^e_i(t)), 0\} \tag{4.17}$$

Here, the gradient step size, denoted $\kappa$, is a sufficiently small positive constant that balances control responsiveness and stability.

Note that $c_l - \sum_{j\in\mathcal{B}_n}\sum_{i:\mathbf{A}^e_{ij}=1} p^e_i(t)$ is indeed the congestion state of $l$, *i.e.*, the difference between the equipment loading and its setpoint. The congestion state is *measured* by the corresponding MCC node in every control interval. This greatly enhances the implementation of this control rule because MCC nodes can update their congestion price based on measurements, without requiring smart chargers and home smart meters to report their demands in every iteration.

#### Control Rule for Adjusting the Charging Rate

Let us denote the latest congestion price vector received by a smart charger by $\lambda(\bar{t})$, where $\bar{t} \geq t - \frac{\delta}{\tau_c}$ as congestion prices must be received by smart chargers after $\delta$ milliseconds, which is an upper bound on the one-way latency from an MCC node to its downstream EV chargers.

The subproblem (4.14) can be easily solved by finding the stationary point of $f_i(p^e_i(t); \lambda(\bar{t}))$.

$$f_i'(p^e_i(t); \lambda(\bar{t})) = \frac{1}{p^e_i(t)} - \sum_{j:[\mathbf{A}^e\times\mathbf{M}]_{ij}=1} \lambda_j(\bar{t}) \overset{\text{set to}}{=} 0 \rightarrow$$

$$p^e_i(t) = \min\left\{\frac{1}{\sum_{j:[\mathbf{A}^e\times\mathbf{M}]_{ij}=1}\lambda_j(\bar{t})}, \overline{p}^e_i\right\} \tag{4.18}$$

We call $\sum_{j:[\mathbf{A}^e\times\mathbf{M}]_{ij}=1}\lambda_j(\bar{t})$ the *path price* of EV charger $i$.

## 4.5 Distributed Control Algorithm

We now describe two algorithms that run at MCC nodes and EV chargers in every control interval and implement the control rules of Section 4.4.3.

Algorithm 1 implements the control rule (4.17) for updating the congestion price at an MCC node based on the measured equipment load. Specifically, every $\tau_c$ milliseconds the root MCC node initiates the price update phase by computing and sending its congestion price to MCC nodes that are directly connected to it. Upon receiving the congestion price(s), an intermediate MCC node computes and sends its own congestion price along with the received price(s) to the next level. The price update phase ends once congestion prices are received by smart chargers.

**Algorithm 1:** Congestion price update at MCC node $l$ with setpoint $\xi_l$

**input**: $\xi_l$, $\kappa(>0)$

**while** *true* **do**

  Measure load

  congestion state $\leftarrow \xi_l -$ load

  price $\leftarrow \max\{\text{price} - \kappa \times \text{congestion state}, 0\}$

  Send price along with all received prices to child nodes

  Wait until the next **message from parent** or the next **clock tick** (if root)

**end**

Algorithm 2 describes how a smart charger computes its charge power, in accordance with the control rule (4.18). The charge power is computed only after receiving congestion prices from MCC nodes located on its unique path to the substation and computing the path price. Once the charge power is computed, the charger starts charging at this rate. Remark that the charge power of a charger does not change drastically in one control interval because $\kappa$ limits the extent of the change in the congestion price of MCC nodes and hence the charge power.

## 4.6 Convergence Analysis

This section investigates the impact of control parameters (the gradient step size and the control timescale) on stability and convergence speed of the algorithm. We first study the conditions under which the proposed distributed control algorithm converges to the solution of the centralized optimization problem (4.4) in a static setting, *i.e.*, no EVs arrive or depart and the change in the magnitude of uncontrollable loads is negligible. We then study the worst-case rate of convergence.

**Algorithm 2:** Rate adjustment at EV charger $i$

**input**: $\overline{p}_i^e$, new congestion prices

**while** *true* **do**

  $\lambda \leftarrow$ new congestion prices

  path price $\leftarrow \sum_{l \in \text{upstream nodes}} \lambda_l$

  rate $\leftarrow \min\{\frac{1}{\text{path price}}, \overline{p}_i^e\}$

  Start charging the battery at rate

  Wait until the next **message from parent**

**end**

### 4.6.1 Proof of Stability

Given that strong duality holds, the primal optimum is equal to the dual optimum. Therefore, in the static setting, we only need to show that the distributed control algorithm converges to the solution of (4.6). We then verify convergence in a dynamic setting both by studying the worst-case change in home loads, and through extensive numerical simulations.

Let $\overline{L}$ be the length of the longest path from the substation to a charger; $\overline{E}$ be the maximum number of active EV chargers sharing a line or a transformer[2]; $\overline{p}_{\text{max}} := \max_{i \in \mathcal{E}} \overline{p}_i^e$ be the maximum charge power supported by EV chargers; and $\delta$ be the maximum communication delay between the root MCC node and a charger.

**Theorem 1** *Starting from any initial vector of feasible charge powers* $0 \preceq \mathbf{p}^e \preceq \overline{\mathbf{p}}^e$ *and congestion prices* $\lambda \succeq 0$*, the distributed control algorithm converges to the primal-dual optimal values if the following conditions hold:*

*(1)* $\tau_c \geq \delta$

*(2)* $0 < \kappa < \kappa^* = \frac{2}{\overline{p}_{max}^2 \overline{L}\overline{E}}$

*Proof*: The first condition guarantees that the control action at each MCC node, which leads to a price update, is taken only after all chargers have reacted to the previous control action. In this case, the continuous time system reduces to the discrete-time system studied in [59] and our theorem reduces to Theorem 1 proved in that work. The second condition maps directly to the necessary condition for Theorem 1 in [59]. □

[2] Assuming that the substation transformer is equipped with an MCC node, $\overline{E}$ would be the total number of EV chargers in the distribution network.

### 4.6.2 Convergence Speed in the Worst Case

We now prove that the control algorithm exhibits monotone convergence even in the worst case and use this to compute an upper bound on the convergence time.

The control algorithm converges most slowly when there is the greatest need for a decrease in EV charging demand, together with the least possible decrease in the charging rate in each iteration. Note that each iteration of the control algorithm reduces the EV load by a multiplicative factor, which corresponds to the sum of the non-negative congestion prices sent by upstream MCC nodes. Thus, the worst case is when home demands are initially zero and every EV charger is charging at its maximum rate $\overline{p}_i^e$. Subsequently, a *single* line or transformer becomes overloaded due to an increase in the aggregate home demand to its peak[3]. We assume that prior to the change in the aggregate home demand, control has stabilized, with the gradient step size equal to $\kappa^*$. To simplify the presentation, we also assume that EV chargers are identical; thus, $\overline{p}_i^e = \overline{p}$ for all $i$.

We first prove that system convergence after the described change in the aggregate home demand is monotone.

#### Monotonic Convergence

Suppose that the change in the aggregate home demand happens in the beginning of a time slot, denoted $t_0$. Given that the system has been under-utilized before $t_0$, all congestion prices are zero at time $t_0$. We denote the line or transformer that becomes overloaded due to this change by $l$, and the aggregate charging demand that it supplies at time $t$ by $y_l(t)$. Hence, $y_l(t_0^+) > c_l$ as its loading exceeds its setpoint after $t_0$. We now prove that $y_l$ converges *monotonically* to $c_l$.

[3] If multiple lines and transformers become congested at the same time, EV charge powers reduce at a faster rate since they depend on the sum of congestion prices. Thus, it would not be the worst case.

The total EV charging load supplied by $l$ is

$$\begin{aligned} y_l(t) &= \sum_{j\in\mathcal{B}_n}\sum_{i:\mathbf{A}^e_{ij}=1} p^e_i(t) = \sum_{j\in\mathcal{B}_n}\sum_{i:\mathbf{A}^e_{ij}=1} \min\{\frac{1}{\sum_{k:[\mathbf{A}^e\times\mathbf{M}]_{ik}=1}\lambda_k(t)}, \overline{p}\} \\ &= \sum_{j\in\mathcal{B}_n}\sum_{i:\mathbf{A}^e_{ij}=1} \min\{\frac{1}{\lambda_l(t)}, \overline{p}\} \\ &= \sum_{j\in\mathcal{B}_n}\sum_{i:\mathbf{A}^e_{ij}=1} \frac{1}{\lambda_l(t)} \qquad\qquad \text{if } \lambda_l(t) > \frac{1}{\overline{p}} \\ &= \frac{|E(l)|}{\lambda_l(t)} \end{aligned} \tag{4.19}$$

where $|E(l)|$ is the number of EV chargers downstream of $l$. Note that the second line of (4.19) is derived from the first line since $l$ is the only congested line or transformer, and therefore the congestion price of other lines and transformers is zero.

We remark that $y_l$ remains constant for a few iterations after $t_0$ until $\lambda_l$ exceeds the threshold $\frac{1}{\overline{p}}$, starting from zero. Let $t_s$ be the beginning of the first control interval in which the condition $\lambda_l(t) > \frac{1}{\overline{p}}$ holds, then $y_l$ starts decreasing when EV chargers receive the updated price of $l$. The following equation can be derived from (4.19) for $t \geq t_s$:

$$\begin{aligned} y_l(t) - y_l(t+1) &= |E(l)|(\frac{1}{\lambda_l(t)} - \frac{1}{\lambda_l(t+1)}) \\ &= |E(l)|\frac{\lambda_l(t+1) - \lambda_l(t)}{\lambda_l(t)\lambda_l(t+1)} = |E(l)|\frac{\kappa(y_l(t) - c_l)}{\lambda_l(t)\lambda_l(t+1)} \end{aligned} \tag{4.20}$$

The following theorem states that monotonic convergence of our control is guaranteed in the worst case.

**Theorem 2** *If, in a distribution network, the length of the longest path from the substation to an EV charger is at least 2, for all $t > t_0$, $y_l(t) \geq c_l$ if $y_l(t_0) \geq c_l$.*

*Proof.* We prove this theorem by contradiction. Suppose for some $\tilde{t} \geq t_s$ we have $y_l(\tilde{t}) \geq c_l$, and $y_l(\tilde{t}+1) < c_l$, or equivalently $y_l(\tilde{t}) - y_l(\tilde{t}+1) > y_l(\tilde{t}) - c_l$. From (4.20) we have:

$$|E(l)|\frac{\kappa(y_l(\tilde{t}) - c_l)}{\lambda_l(\tilde{t})(\lambda_l(\tilde{t}) + \kappa(y_l(\tilde{t}) - c_l))} > y_l(\tilde{t}) - c_l$$

The following inequality is obtained by canceling out the $y_l(\tilde{t}) - c_l$ term from both sides of the above inequality

$$\frac{|E(l)|}{\lambda_l(\tilde{t})} - \frac{\lambda_l(\tilde{t})}{\kappa} > y_l(\tilde{t}) - c_l$$

But $\frac{|E(l)|}{\lambda_l(\tilde{t})} - \frac{\lambda_l(\tilde{t})}{\kappa} \leq 0$ since

$$\begin{aligned} |E(l)|\kappa &= |E(l)|\frac{2}{\overline{p}^2\overline{LE}} \\ &\leq \frac{2}{\overline{p}^2\overline{L}} \\ &\leq \frac{1}{\overline{p}^2} \qquad \text{since } \overline{L} \geq 2 \\ &\leq \lambda_l(\tilde{t})^2 \end{aligned}$$

Thus $y_l(\tilde{t}) - c_l < \frac{|E(l)|}{\lambda_l(\tilde{t})} - \frac{\lambda_l(\tilde{t})}{\kappa} \leq 0$. This contradicts our assumption that $y_l(\tilde{t}) - c_l \geq 0$. Therefore, we conclude that $\tilde{t}$ does not exist, and $y_l$ does not go below $c_l$. □

**An Upper Bound**

The monotonic convergence of the control algorithm enables us to compute an upper bound on the time that it takes until the algorithm converges to the region specified by $\pm\rho$ around the setpoint.

Let $\Delta$ be the overload of $l$ at $t_0$; hence, $y_l(t_0) - c_l = \Delta$. We first compute an upper bound on the time between $t_0$ and $t_s$, denoted $\delta_s$, during which $y_l$ does not change:

$$\begin{aligned} \delta_s &\leq \lceil \frac{\frac{1}{\overline{p}} - 0}{\kappa(y_l(t) - c_l)} \rceil \times \tau_c \\ &= \lceil \frac{1}{\overline{p}\kappa\Delta} \rceil \times \tau_c \end{aligned} \tag{4.21}$$

Let $t_{\text{conv}}$ be the beginning of the first control interval in which the loading of $l$ goes below the level $c_l + \rho$, and $\delta_{\text{conv}}$ be an upper bound on the time between $t_s$ and $t_{\text{conv}}$. We compute $\delta_{\text{conv}}$ now. Since $y_l(t) - c_l \geq \rho$ for $t < t_{\text{conv}}$, we can write $\lambda_l(t) = \frac{|E(l)|}{y_l(t)} < \frac{|E(l)|}{c_l + \rho}$ for $t_s \leq t < t_{\text{conv}}$. From (4.20) we obtain:

$$y_l(t) - y_l(t+1) > \kappa\rho\frac{(c_l + \rho)^2}{|E(l)|} \tag{4.22}$$

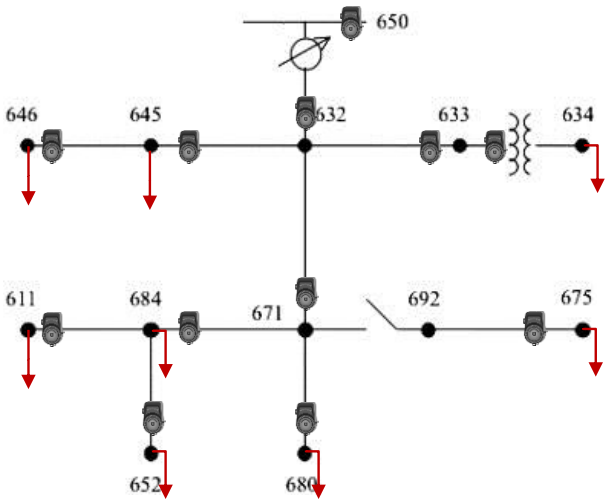


Figure 4.2: A one-line diagram of our test distribution network. An MCC node is depicted as a meter in this figure.

for $t_s \leq t < t_{\text{conv}}$.

To compute $\delta_{\text{conv}}$ we approximate the decaying decrease rate of the line or transformer loading (after $t_s$) with a constant value equal to $\kappa\rho\frac{(c_l+\rho)^2}{|E(l)|}$:

$$\begin{aligned}\delta_{\text{conv}} &= \left(\lceil |E(l)| \frac{y_l(t_0) - (c_l+\rho)}{\kappa\rho(c_l+\rho)^2} \rceil + 1\right) \times \tau_c \\ &= \left(\lceil \frac{(\Delta-\rho)|E(l)|}{\kappa\rho(c_l+\rho)^2} \rceil + 1\right) \times \tau_c \end{aligned} \tag{4.23}$$

Thus, $\delta_{\text{conv}} + \delta_s$ is an upper bound on the convergence time in the worst case.

## 4.7 Test Distribution System

We evaluate our control algorithm by means of power flow analysis using the Open Distribution System Simulator (OpenDSS) [31] on the IEEE 13-bus test feeder [52], a 4.16kV three-phase radial distribution system (Figure 4.2). For the purpose of our simulations, we modify this test system by changing loads. In this section, we discuss the

details of the modified distribution system, as well as our approach to model home and EV loads.

This distribution network is supplied by a three-phase 5MVA transformer that steps down the transmission line voltage from 115kV to 4.16kV. For simplicity, we treat buses as load aggregation points with directly connected home loads and EV chargers and do not model the transformers and feeders radiating from them, although that analysis would be a straightforward extension to what we describe below. Using the parameters provided in [52], we set the nameplate rating of every feeder to its ampacity at $50^{\circ}C$. The nameplate rating of the substation transformer and the in-line transformer are also set to 5MVA and 500kVA, respectively. We assume that all loads, including homes and EV chargers, are single-phase and are connected between a phase and neutral of load buses 634, 645, 646, 675, 680, 684, 652, 611. We further assume that EV chargers are identical, either Level 1 (a maximum load of 1.8kW) or Level 2 (a maximum load of 7.2kW), consume real power only, and that the reactive power consumption of every home is 30% of its real power consumption, a conservative assumption.

### 4.7.1 MCC Nodes

An MCC node measures the real power carried by phase conductors at each bus (Figure 4.2). Similarly, the substation transformer load is measured by an MCC node installed at the substation bus and the loading of the in-line transformer, connected between buses 633 and 634, is also measured by an MCC node installed at bus 634. All MCC nodes are interconnected using a communication network which forms a logical tree overlaid on the radial distribution system. Thus, for example, the MCC node installed at phase B of bus 632 is the parent of MCC nodes installed at phase B of buses 633, 645, and 671, and the MCC node installed at the substation is the parent of MCC nodes installed at phases A, B, and C of bus 632.

### 4.7.2 Power Flow

To run a power flow study, we specify the real and reactive power injected at every load bus. The OpenDSS simulator performs power flow calculations for every iteration of the algorithm, controls regulator taps automatically, and returns the complex power that flows in different branches and the voltage magnitude at different buses. Assuming that real power flows measured by MCC nodes match the actual real power flows calculated by OpenDSS, we use the actual values in our control algorithm to update congestion

| | Bus | 680 | 634 | 675 | 645 | 646 | 684 | 652 | 611 |
|---|---|---|---|---|---|---|---|---|---|
| | Phase | abc | abc | abc | bc | bc | ac | a | c |
| Static | Aggregated home load (kW) | 600 | 100 | 400 | 100 | 300 | 100 | 200 | 200 |
| | Number of chargers | 80 | 40 | 40 | 40 | 40 | 40 | 40 | 40 |
| Dynamic | Number of homes | 450 | 50 | 300 | 50 | 200 | 50 | 150 | 150 |
| | Percentage of chargers | 10% | 5% | 5% | 5% | 5% | 5% | 5% | 5% |

Table 4.1: Simulation scenarios for dynamic and static settings.

prices. We then compute the charge power of EV chargers using the new prices sent by upstream MCC nodes, and update the real power consumed at every bus accordingly. We also update the aggregate home load at every bus using the synthetic load model described in Section 4.7.3. This allows us to run a power flow study for the next time slot.

### 4.7.3 Home Load Model

We assume that our test distribution system supplies 3300 households and a finite population of EV chargers that are connected to selected load buses, as explained in Table 4.1. Note that numbers provided in this table are for each phase of a load bus.

To evaluate our control algorithm using power flow and to study its fast (sub-second) timescale dynamics, we need fine-grained measurements (100-millisecond timescale) of household loads, which we lack[4]. Therefore, we generate synthetic load traces using the Markov models developed in [6] to represent the real power consumption of homes during on-peak, mid-peak, and off-peak periods. These models are derived from fine-grained measurements of real power consumed in 20 homes over four months. To compute the aggregate home load consumed at each bus, we add individual household demands that we synthesized, ignoring losses. Our simulations span over three days in winter and the aggregate household demand in this period is illustrated in Figure 4.6. The peak of the aggregate home load is 4.44MW; hence, the distribution system is never congested over these three days in the absence of EV charging demands.

[4]We note that a real world implementation of the proposed algorithm only requires measurements of the branch power flow and transformer loading at the MCC nodes and does not rely on smart meter data or other measurements at the home level. This is explained in Section 4.4.3.

### 4.7.4 EV Model

We assume that each household owns at most one EV and EV owners have installed a dedicated smart charger at home. We assume that the capacity of EV batteries is 24kWh (the battery capacity of a Nissan Leaf EV [66]). In our simulations, EVs disconnect from their charger every day after 6am following a Poisson distribution with parameter $\mu_d$, and return to the system and connect to their charger after 4pm on the same day, following a Poisson distribution with parameter $\mu_a$, with a fully discharged battery. Thus, the number of active chargers changes over time. Since the EV population is finite, a higher value of $\mu_a$ (or $\mu_d$) creates a larger burst of arrivals around 4pm (or departures around 6am).

## 4.8 Performance Evaluation

We use power flow analysis in this section to study:

- the effect of uncontrolled EV charging on the test distribution system (Section 4.8.1),
- the convergence speed of the distributed algorithm to specified setpoints (Section 4.8.2),
- the operation of our control algorithm in a dynamic setting (Section 4.8.3),
- the efficiency and utilization of the controlled system, compared to the uncontrolled case and the theoretical maximum (Section 4.8.4), and
- the operation of the congestion control algorithm with a realistic number of MCC nodes (Section 4.8.5).

We define the *efficiency* as the average energy stored in an EV battery in a day and measure the *congestion* of a line or a transformer by the amount of energy it supplied above its nameplate rating; we refer to this as the *overload* below.

### 4.8.1 The Need for Control

Figure 4.3 shows the effect of uncontrolled EV charging on the distribution network using Level 2 chargers operating at the maximum rate when active. We find that a population

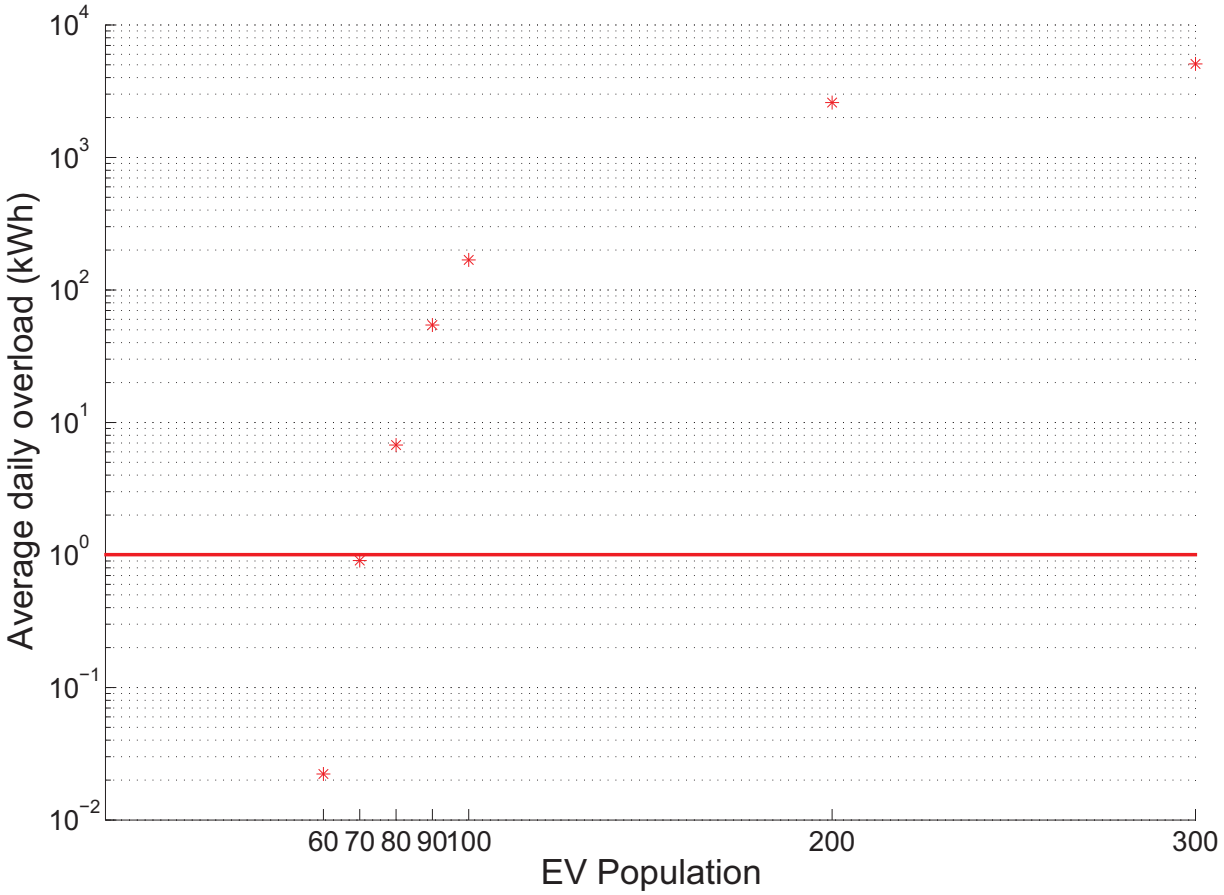


Figure 4.3: Average daily overload versus EV population in an uncontrolled scenario with AC Level 2 chargers. Note that the Y-axis is logarithmic scale.

of only 90 EVs in a neighbourhood comprised of 3300 homes leads to a non-negligible overload of 54kWh/day. To avoid congestion without controlled charging, either the EV penetration level must be kept low or distribution circuits must be reinforced. For example, if the utility requires an overload of less than 1kWh/day, depicted by a horizontal line in Figure 4.3, without controlled charging, the EV population must be kept below 70, which is equivalent to 2.1% EV penetration. Even when overall EV penetration is low, this may not be true for certain neighbourhoods and uncontrolled charging will be problematic in these cases.

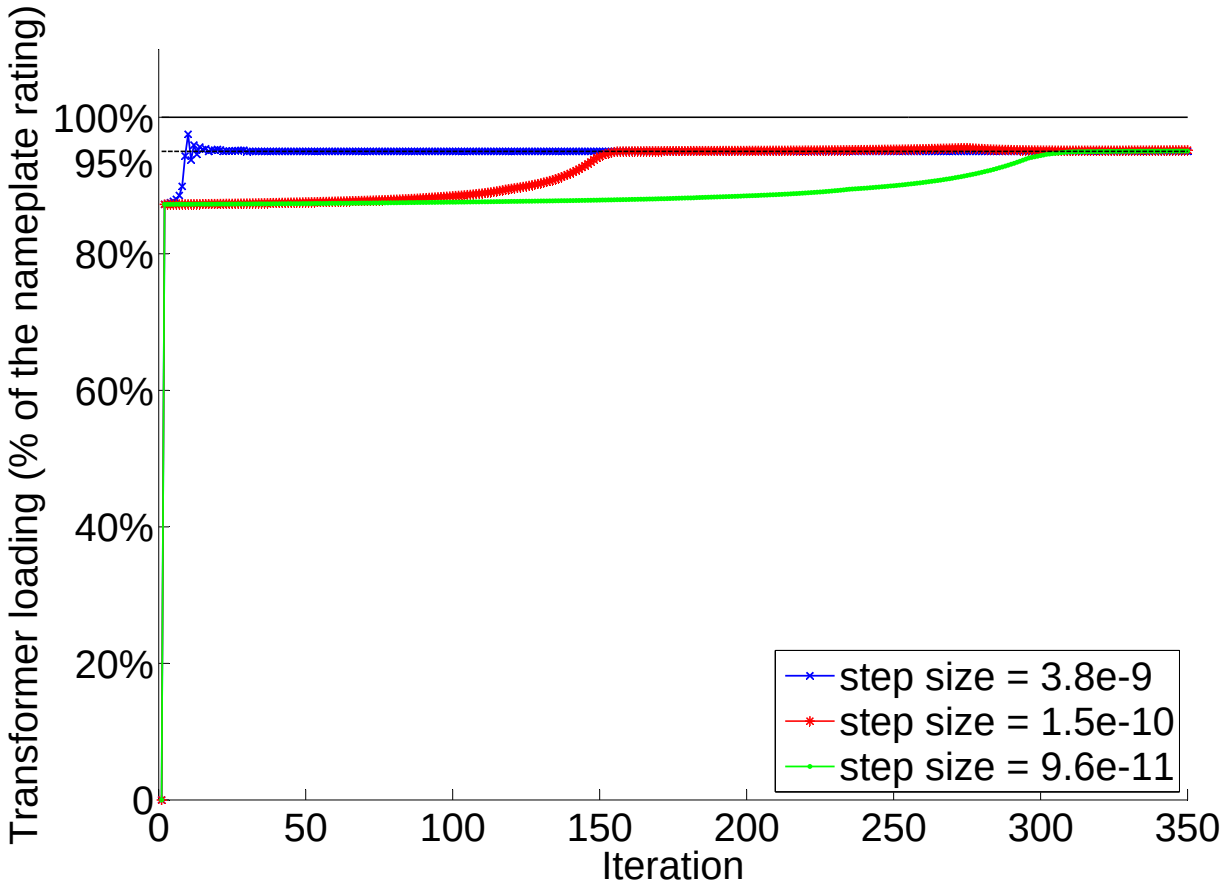


Figure 4.4: Choice of the step size, $\kappa$, determines how the substation transformer load changes over time. In this case, the transformer setpoint is 95% of its nameplate rating.

### 4.8.2 Rate of Convergence

We now study the number of iterations that it takes to achieve convergence for different values of $\kappa$, assuming that the setpoint of each line or transformer is set to 95% of its nameplate rating, that EV chargers are Level 1, and that home loads are fixed. Table 4.1 summarizes our simulation scenario in this static setting.

In this scenario, the maximum charging rate is 1800W, so the maximum step size for which the convergence of the algorithm is guaranteed is $\kappa^* = \frac{2}{1800^2 \times 800 \times 5} = 1.54 \times 10^{-10}$ (from Theorem 1). As we increase the value of $\kappa$, the control system transitions from an

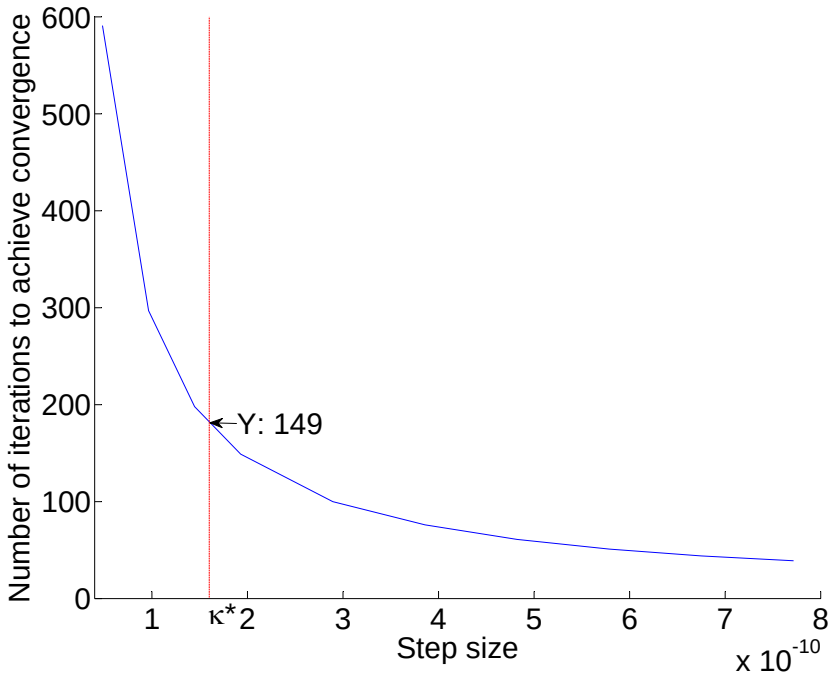


Figure 4.5: Number of iterations to achieve convergence.

over-damped system to an under-damped system, and eventually to an unstable system for $\kappa > 3.8 \times 10^{-9}$, which is larger than $\kappa^*$. Figure 4.4 shows how the loading of the substation transformer varies over different iterations for three different values of $\kappa$ that are smaller than, equal to, and larger than $\kappa^*$.

The value of $\kappa$ also controls the number of iterations it takes to achieve convergence, that is, when the loading of a line or transformer is within $\pm 1\%$ of its setpoint. Figure 4.5 shows that the number of iterations required for convergence deceases exponentially as we increase the value of $\kappa$. When the step size is equal to $\kappa^*$, it takes 149 iterations to achieve convergence (about 15 seconds if $\tau_c = 0.1$s). Note that in most cases the algorithm converges to $\pm 5\%$ of the setpoint after only 20-40 iterations. Also note that choosing time-varying step sizes may speed up convergence of the algorithm. However, finding the step size that will produce the biggest change in the dual objective value requires nonlocal information, and is therefore difficult to implement in practice for large networks.

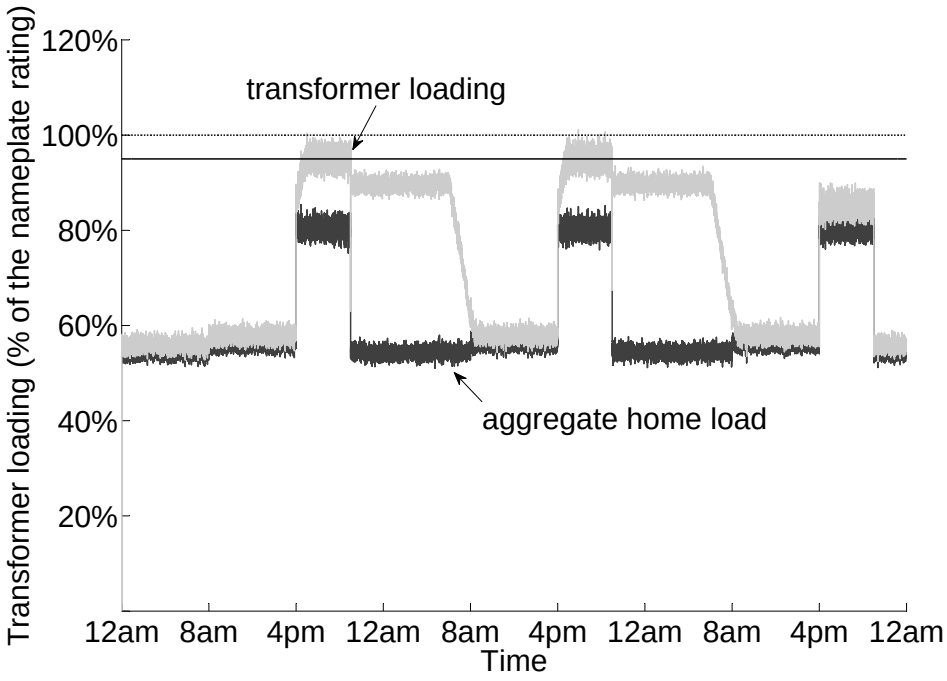


Figure 4.6: Substation transformer loading (the light grey curve) and the aggregate household demand (the dark grey curve) in a dynamic setting where 900 Level 1 smart EV chargers are controlled using the proposed distributed algorithm. The setpoint of the substation transformer is 4.75MVA (the solid line), the control timescale is set to 1 second, and the step size is set to $\kappa^*$.

### 4.8.3 Performance Evaluation in a Dynamic Setting

We now investigate the scenario in which household demands and the number of active EV chargers vary over time. We refer to this as the dynamic setting in Table 4.1. In our simulations, we fix the value of the step size to be $\kappa^*$, and study six different values for the setpoint of the substation transformer, which are 4.75MVA, 4.8MVA, 4.85MVA, 4.9MVA, 4.95MVA, and 5MVA. We consider two different values of $\tau_c$, 1s and 0.5s, and two modes of EV charging, AC Level 1 (1.8kW maximum) and AC Level 2 (7.2kW maximum) [79]. We repeat each simulation 10 times, using 10 different arrival and departure patterns generated by setting $\mu_d = \mu_a = 0.1$ per second. Thus, on average, one EV connects and disconnects every 10 seconds after 4pm and 6am, respectively. These arrival and departure patterns are intentionally chosen to stress test the system.

Figure 4.6 shows a single simulation trace of the overall system load over time when

the transformer setpoint is 4.75MVA, the control timescale is 1 second, and the EV population is 900. The home loads have evening peaks, with loads at night and at mid-day being roughly equal. Note that even when EVs are not charging, the transformer load is slightly higher than the aggregate home load, due to line losses. We note that the transformer load is computed by means of power flow analysis.

When EV chargers are active, the overall load is close to the setpoint, with rare excursions above the nameplate rating. Each such excursion contributes to the *overload*. Clearly, the lower the setpoint, the lower this overload. To illustrate this, Figure 4.7 shows the average daily overload versus the transformer setpoint when the EV population is 500. It can be seen that the overload is generally smaller when the setpoint is lower, but increases as we use slower control timescales for a fixed setpoint value. It also increases significantly with the charging level, and grows exponentially with the setpoint if we fix the control timescale and the charging level.

Table 4.2 shows the minimum and maximum voltage levels recorded in our power flow simulations for the dynamic setting using our proposed control algorithm when the transformer setpoint is 4.9MVA, the control timescale is 1 second, the EV population is 500, and all chargers are either Level 1 or Level 2. It can be seen that the voltage magnitude at every bus stays within $\pm 5\%$ of the nominal distribution voltage at all times. This implies that fast timescale control of smart chargers does not create a major voltage problem in our test distribution network, given its voltage regulation capability. Moreover, the gradual change in the charge power of EV chargers, as discussed in Section 4.5, does not cause severe voltage fluctuations, making flicker a non issue.

### 4.8.4 Efficiency

We now study the efficiency of our control scheme. Consider the situation in which all EVs arrive at 4pm and stay in the system until 6am the next day. We numerically compute an upper bound on the number of EVs that can be fully charged in this time interval by simply dividing the integral of the difference between the nameplate rating and the aggregate home load (after incorporating losses) over this interval by the battery capacity (*i.e.*, 24kWh). We find that a maximum of 900 EVs can be fully charged between 4pm and 6am the next day, under these ideal conditions. With our control algorithm, using Level 2 charging, if we set the setpoint of the substation transformer to 4.8MVA to obtain a very small overload (approximately 1kWh/day), up to around 700 EVs can be fully

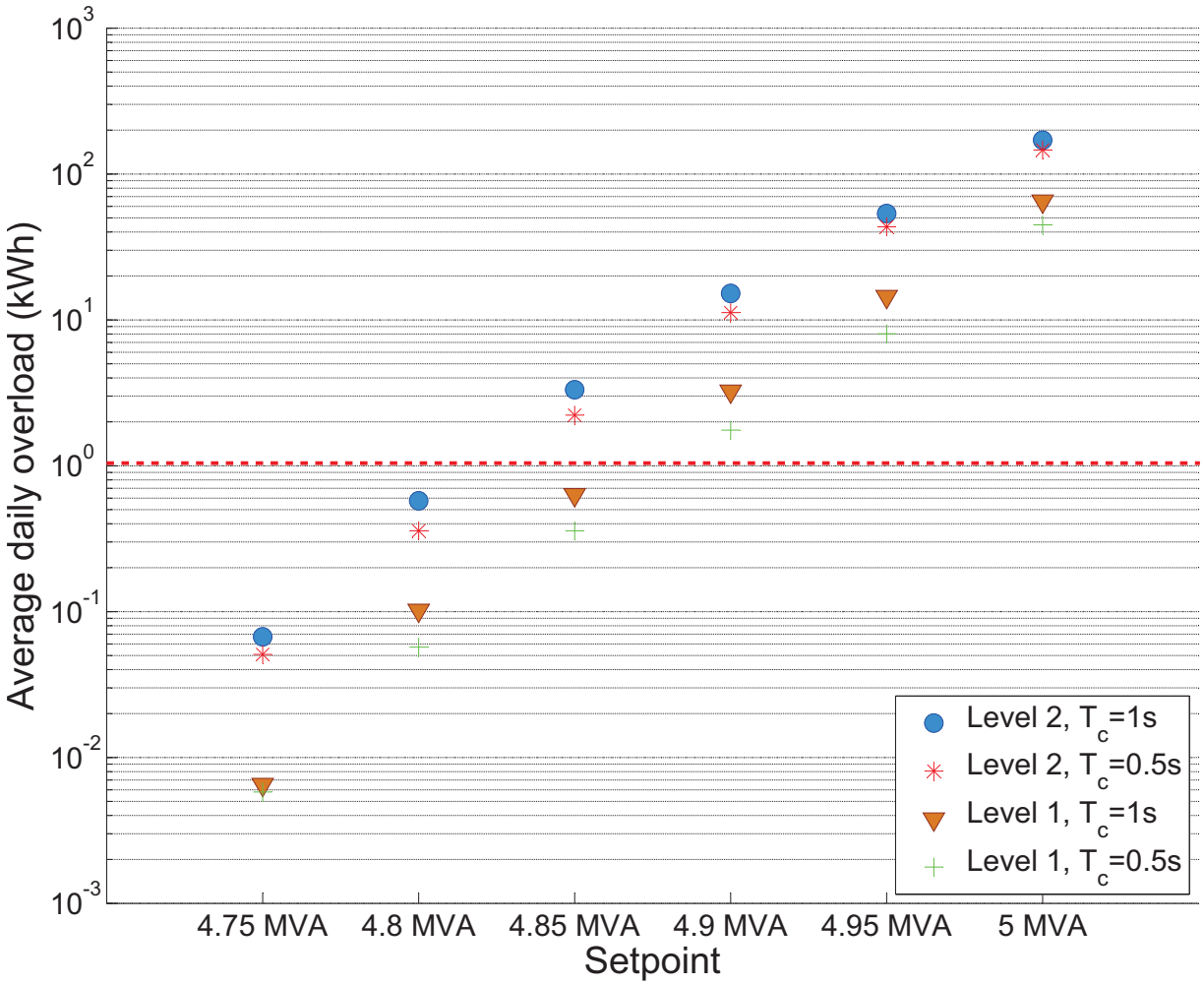


Figure 4.7: Average daily overload versus the substation transformer setpoint when the EV population is 500. Note that the Y-axis is logarithmic scale.

| | L1 Chargers | | L2 Chargers | |
|---|---|---|---|---|
| | min | max | min | max |
| SUB | 1.000 | 1.000 | 1.000 | 1.000 |
| 632a | 1.008 | 1.031 | 0.999 | 1.027 |
| 632b | 1.007 | 1.029 | 1.007 | 1.038 |
| 632c | 1.006 | 1.029 | 1.007 | 1.036 |
| 671a | 0.994 | 1.026 | 0.966 | 1.018 |
| 671b | 1.008 | 1.038 | 1.001 | 1.044 |
| 671c | 0.977 | 1.027 | 0.968 | 1.028 |
| 680a | 0.991 | 1.024 | 0.956 | 1.012 |
| 680b | 1.006 | 1.036 | 0.995 | 1.042 |
| 680c | 0.974 | 1.026 | 0.957 | 1.025 |
| 633a | 1.008 | 1.030 | 0.999 | 1.026 |
| 633b | 1.005 | 1.028 | 1.006 | 1.036 |
| 633c | 1.004 | 1.028 | 1.005 | 1.035 |
| 634a | 1.001 | 1.024 | 0.993 | 1.019 |
| 634b | 0.995 | 1.021 | 0.997 | 1.028 |
| 634c | 0.993 | 1.025 | 0.994 | 1.031 |
| 692a | 0.994 | 1.026 | 0.966 | 1.018 |
| 692b | 1.008 | 1.038 | 1.001 | 1.044 |
| 692c | 0.977 | 1.027 | 0.968 | 1.028 |
| 675a | 0.990 | 1.025 | 0.963 | 1.016 |
| 675b | 1.005 | 1.036 | 0.998 | 1.042 |
| 675c | 0.974 | 1.027 | 0.965 | 1.028 |
| 645b | 0.989 | 1.017 | 0.995 | 1.024 |
| 645c | 0.998 | 1.026 | 1.005 | 1.039 |
| 646b | 0.981 | 1.014 | 0.987 | 1.018 |
| 646c | 0.995 | 1.025 | 1.005 | 1.041 |
| 684a | 0.990 | 1.024 | 0.963 | 1.015 |
| 684c | 0.972 | 1.026 | 0.963 | 1.027 |
| 652a | 0.980 | 1.019 | 0.954 | 1.009 |
| 611c | 0.969 | 1.026 | 0.960 | 1.026 |

Table 4.2: Voltage magnitudes (p.u.) per phase and node in a dynamic setting where 500 smart EV chargers are controlled using the proposed distributed algorithm.

charged, which compares well with the maximum of 900 EVs, especially when recalling that without control we cannot charge more than 70 EVs to obtain the same level of overload.

### 4.8.5 Impact of Partial Deployment of MCC Nodes

The test distribution system described in Section 4.7 is a small network thoroughly monitored by the MCC nodes installed at the substation, distribution transformers, and buses. However, a real distribution network could have hundreds of line segments and monitoring the power flow in every part of the network requires widespread deployment of MCC nodes, which is quite costly and impractical at the present time. This motivates us to study the operation of the congestion control mechanism with a realistic number of MCC nodes.

We argue that MCC nodes should be installed wherever congestion is likely to happen because congestion can only be detected locally. In reality, congestion is not likely to happen in all parts of a distribution network and the network has a certain number of *hotspots*. We call a hotspot a line or a transformer that i) is susceptible to overload, *i.e.*, the margin between its loading and its nameplate rating is small or ii) is anticipated to supply a large number of EVs. We expect the number of hotspots to be relatively small (especially at low EV penetration rates) and that the utility would know or could predict their locations. Hence, it is reasonable to install MCC nodes at these locations.

Consider the following three cases where MCC nodes are installed 1) only at hotspots, 2) at hotspots and buses on the path from the substation to the hotspots, and 3) everywhere as illustrated in Figure 4.2. We create a hotspot in our test distribution system by making a slight change to the dynamic scenario presented in Table 4.1 and compare these three cases based on the amount of overload. Specifically, we increase the number of homes supplied by phase B of bus 646 to 300, and reduce the number of homes supplied by each phase of bus 680 to 150. This creates a single hotspot, *i.e.*, phase B of the line segment between buses 645 and 632 becomes congested when all EV chargers are Level 1 and 500 EVs are uniformly distributed in the network. We choose the setpoint of all lines and transformers to be 98% of their nameplate rating. Results of power flow simulations show that the last two cases are similar in terms of the average daily overload ($\sim$20.35kWh), while the first case leads to a slightly higher daily overload of 20.46kWh. This indicates that the benefit from installing MCC nodes at non-hotspot locations is insignificant and our scheme does not necessitate a pervasive MCC deployment.

## 4.9 Engineering Insights

This section provides guidelines for choosing the control parameters and setpoints based on the results of our simulations, assuming that the utility limits the amount of risk that it is willing to take. For simplicity, we confine our study to the substation transformer which is the potential bottleneck in this network, although our study applies to arbitrary distribution systems with more than one transformer. Thus, we have just one setpoint to select.

### 4.9.1 Choosing Control Knobs

Recall that the gradient step size, $\kappa$, should be set to $\kappa^*$ to improve control responsiveness and to ensure stability simultaneously.

Choosing $\tau_c$ is a more complex problem. Faster control timescales reduce the overload but increase the communication overhead at the same time. If communication is not a bottleneck, then $\tau_c$ should be set as small as possible. Of course, this is lower bounded by the communication delay, as stated by Theorem 1.

Communication overhead can be reduced by using multicast to send packets from an MCC node to its children. With multicasting we can implement the control algorithm by sending at most $\mathcal{O} = |\mathcal{E}| + |\mathcal{N}| - 1$ packets in every control interval, where $|\mathcal{E}|$ is the number of EV chargers and $|\mathcal{N}|$ is the number of MCC nodes. Hence, $\mathcal{O}$, $2 \times \mathcal{O}$, and $10 \times \mathcal{O}$ packets must be transmitted per second when the control timescale is 1 second, 0.5 second, and 0.1 second, respectively. Thus the control timescale can be chosen properly given the communication medium and protocol.

### 4.9.2 Choosing Setpoints

Recall that equipment overloading increases the risk of failure and outages. The choice of line and transformer setpoints depends on the amount of risk the utility is willing to take. Specifically, the utility chooses the equipment setpoint for a given EV population and a charging level such that the overload does not exceed an acceptable level.

For example, in the above scenario (where we have only one setpoint to select) the transformer setpoint could be as high as 4.85MVA to obtain an overload of 1kWh/day (depicted by a dashed line in Figure 4.7), when the EV population is 500 and all EV chargers are Level 1.

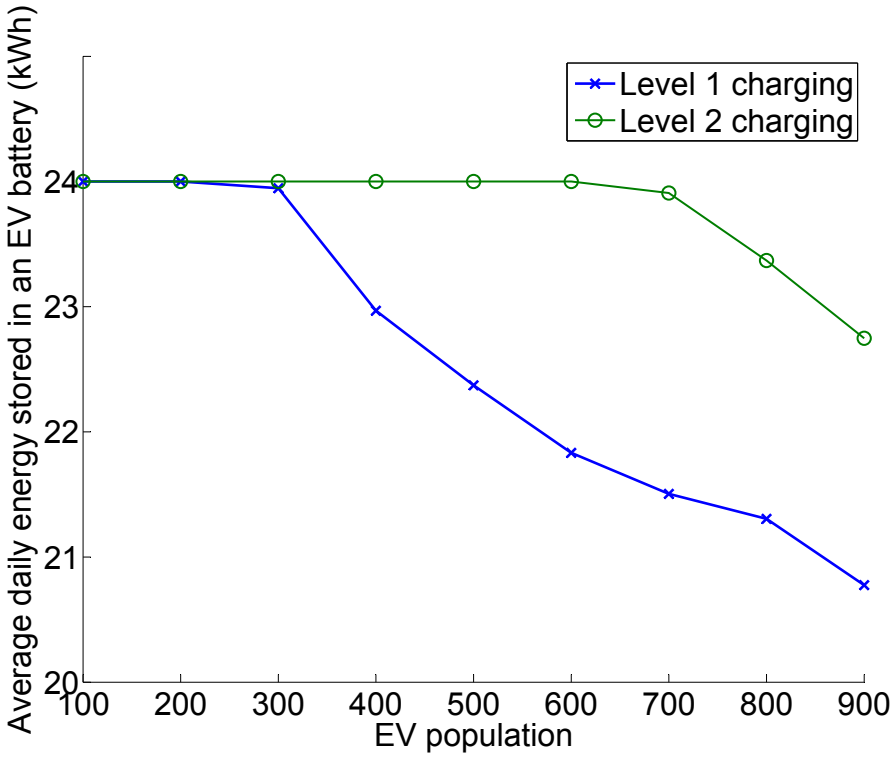


Figure 4.8: Average energy stored in an EV battery in a day versus the EV population for AC Level 1 and Level 2 chargers when the control timescale is 1 second.

Figure 4.8 shows the average daily energy stored in an EV battery for different EV population sizes using Level 1 and Level 2 chargers, when the setpoint is chosen such that we obtain an overload of less than 1kWh/day and the control timescale is set to 1 second. Observe that EV batteries are fully charged using both Level 1 and Level 2 chargers when the EV population is less than 300 (Level 2 charging only reduces the charging time). However, when the EV population exceeds 300, the system becomes overly congested; in this regime, Level 2 charging is more beneficial to EV owners than Level 1 charging, as it increases the efficiency. For example, when the EV population is 500 and all chargers are Level 2, the setpoint could be as high as 4.8MVA; this corresponds to on average 24kWh of energy transferred to EVs per day, which means that all batteries can be fully charged. Similarly, when the EV population is 500 and all chargers are Level 1, the setpoint could be as high as 4.85MVA; this corresponds to on average 22.37kWh of energy transferred to EVs per day.

## 4.10 Chapter Summary

Our work addresses line and transformer congestion arising from uncontrolled charging of EVs. Instead of upgrading distribution circuits, we investigate the use of a feedback control mechanism to limit EV charging demands to the available network capacity. Inspired by rate control algorithms in computer networks such as TCP, we design, using the dual decomposition method, a real-time distributed algorithm for EV charging control that is stable, efficient, and fair to connected EVs. The proposed distributed control algorithm solves decoupled optimization problems at smart chargers and MCC nodes in an iterative fashion.

We show through extensive numerical simulations, as well as power flow analysis on a test distribution system, that the distributed algorithm rapidly converges from large disturbances to a stable operating point in both static and dynamic settings, and does not create a major voltage problem in the test system. We find that this algorithm scales well with the size of the network and the number of EV chargers, and the controlled test system reliably accommodates a much higher EV penetration compared to the uncontrolled case. We analyze the sensitivity of this algorithm to the EV penetration level, the maximum charge power of smart chargers, and the choice of control parameters and equipment setpoints. Based on this analysis, we provide guidelines for choosing control parameters and setpoints in a distribution system of a certain size and topology.

# Chapter 5

# Optimal Control of Active End-nodes in Distribution Networks

In this chapter, we study a radial distribution system that delivers power to residential and commercial buildings and is divided into a number of balancing zones, within each zone bidirectional power flow is permitted (see Section 2.1.1). Our goal is to control EV chargers, PV inverters, and storage systems that are installed at commercial buildings and are connected to laterals feeding the commercial loads so as to achieve the utility objectives and enhance end-use performance, while preventing unacceptable voltage deviations, equipment overloads, and reverse power flows. We seek to answer the following two critical questions. How must EV chargers (and storage systems) be controlled to ensure service reliability and enhance efficiency in distribution systems with high PV penetration? Can this control increase the PV penetration rate reliably accommodated in existing distribution systems?

In this chapter we take a completely different approach from that of Chapter 4. Particularly, we design an open-loop controller, as opposed to the feedback controller developed in the previous chapter. The open-loop controller relies on a sophisticated distribution system model and end-node measurements instead of in-network measurements, and therefore, does not require deployment of expensive MCC nodes to monitor feeders and transformers. We derive optimal controls by solving a sequence of two optimization problems, one at the substation level and one at the level of balancing zones, whereas decision making was pushed down to EV chargers using decomposition theory in Chapter 4. The optimal control enables power sharing within each balancing zone and tackles voltage and reverse flow problems in addition to the equipment overloading problem.

## 5.1 Introduction

The steady fall in the price of PV systems, combined with governmental, social, and environmental incentives, has resulted in an exponential rise in the number of small-scale PV installations in power distribution networks and a substantial reduction in the carbon footprint of electricity generation. Many utilities have begun to experience impacts of a high concentration of PV systems on their distribution system planning and operation practices. Specifically, overvoltage conditions and reverse power flows that are expected when solar generation surpasses the feeder loading could cause protection coordination problems and overuse of voltage regulators and switched capacitors, shortening their expected life cycle [49].

Thus, the increasing penetration of distributed PV systems along with the growing number of EV chargers connected to distribution feeders can put reliability at risk in future.

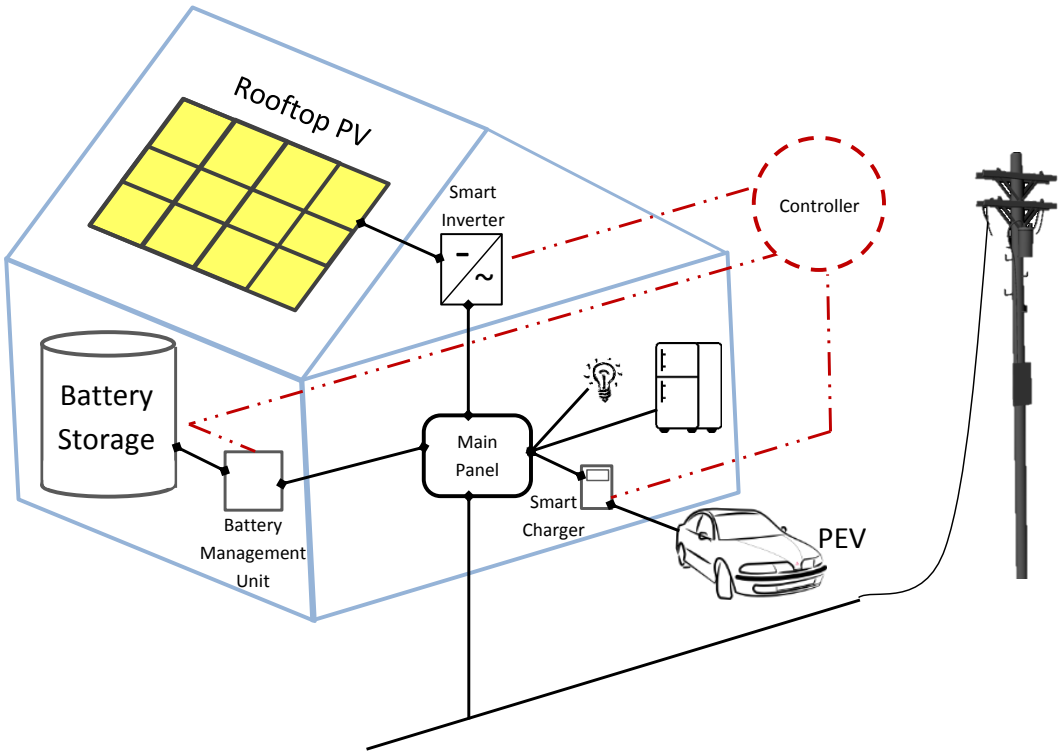


Figure 5.1: A schematic diagram of a small business with a rooftop PV system, a battery storage system, a PEV, and a number of appliances that are connected to the mains via an electrical service panel. The smart inverter, the smart EV charger, and the battery management system communicate with the upstream controller(s) over a communication network.

To overcome this imminent threat, utilities can limit PV and EV charger installations in size and number; this comes at the price of a significant reduction in efficiency of the grid. A more promising approach would be to exploit the synergy between EV chargers, storage systems, and PV inverters to reliably accommodate a higher penetration of these active end-nodes in existing distribution systems. For example, the charge power of EV chargers and storage systems located in a balancing zone can be controlled to absorb solar generation locally when it peaks. This enhances reliability, enables charging a larger population of EVs, reduces wasteful and expensive solar generation curtailment and overall carbon emissions, and most importantly eliminates the tradeoff between reliability and efficiency.

Unfortunately, existing power system controls do not provide this level of control over a large number of geographically dispersed active end-nodes. Furthermore, using *ad hoc* controls can make the distribution control system unsustainable and insecure, potentially leading to chaotic situations [92]. What is needed is a control architecture that supports fast-timescale control of thousands of active end-nodes connected to a distribution network. This is the focus of this work.

We study a radial distribution system that supplies homes and small businesses constituting a number of balancing zones. We assume that active end-nodes are installed at small businesses only[1]. Hence, EV chargers are likely to be active during the day when more solar energy can be harnessed. The active end-nodes connect to the electrical service panel of the building and communicate with the upstream controller over a proprietary network, as illustrated in Figure 5.1. Assuming that the utility is granted remote control and monitoring of active end-nodes[2] and pays for solar generation even if it is curtailed, we propose an optimal control scheme for active end-nodes that aims to achieve multiple utility-defined objectives simultaneously, subject to network and end-node constraints described in Section 5.2. This scheme enables sharing of solar generation and stored energy within each balancing zone.

The optimal control is found by solving a sequence of two optimization problems for every time slot in a decentralized fashion (at two different levels), where the length of each time slot is 1 minute during which the number of active end-nodes and household and business demands are assumed to be constant. The proposed control is *myopic* as objective functions depend only on the charge power of EV chargers, real and reactive outputs of inverters, and storage operations in the current time slot, ignoring their future and past dynamics. The myopic approach is reasonable given that EVs can drive off at any time. We define the two optimization problems and describe the operation of the decentralized scheme in Section 5.3. We introduce two local control schemes that serve as benchmarks for our scheme in Section 5.4. For performance evaluation, we run numerous simulations on a standard test distribution system for different scenarios described in Section 5.5. In Section 5.6 we present our simulation results. Specifically, we compare the control schemes in terms of the introduced objectives, quantify benefits of using storage and sharing power within balancing zones, and validate feasibility of our open-loop controller through power flow analysis.

[1] A business does not necessarily install all three technologies.

[2] Customers may relinquish control of active end-nodes in exchange for a fixed reduced electricity price.

## 5.2 Constraints and Objectives

We now specify the constraints imposed by EV chargers, PV panels, and storage systems and discuss three operational requirements of a distribution system. We also present three objectives that we take into account when designing the control system. These objectives are defined with the assumption that the utility controls the active end-nodes, *i.e.*, solar panel inverters, EV chargers, and storage systems.

### 5.2.1 End-node Constraints

We adopt the models introduced in Section 3.2 for EV charger, PV inverter, and storage systems. The operation of these end-nodes is subject to some constraints that we repeat here for completeness.

#### Inverter Constraints

Smart inverters are capable of on-demand curtailment of real power production of PV systems to prevent overloads and reverse flows in the distribution system. Furthermore, they can consume or inject reactive power to regulate distribution voltage. Real and reactive power contributions of an inverter are subject to the constraints specified in Section 3.2.2:

$$0 \leq p_i^g(t) \leq \overline{p}_i^g(t) \qquad \forall\, i \in \mathcal{J}, t \in \mathcal{T} \tag{5.1}$$

$$p_i^g(t)^2 + q_i^g(t)^2 \leq \overline{s}_i^{g2} \qquad \forall\, i \in \mathcal{J}, t \in \mathcal{T} \tag{5.2}$$

where $\overline{s}_i^g$ is the apparent power rating of the inverter and $\overline{p}_i^g(t)$ is the available solar power in time slot $t$. The available solar power is assumed to be measured just before the beginning of every time slot and the apparent power rating of the inverter is assumed to be known. Note that the lower the available solar power, the higher could be the reactive power contribution of an inverter.

#### Storage Constraints

Charge and discharge powers of a battery storage system must stay within certain bounds. These bounds depend on the rated charge and discharge capacities of the battery and its

SOC[3], as discussed in Section 3.2.3. We can write:

$$-\underline{p}_i^s(t) \leq p_i^s(t) \leq \overline{p}_i^s(t) \qquad \forall\, i \in \mathcal{S}, t \in \mathcal{T} \tag{5.3}$$

We assume that storage systems do not consume or produce reactive power.

#### Charger Constraints

We assume that the EV charging load is pure resistive. A smart charger can charge the connected EV at any rate that satisfies this constraint:

$$\underline{p}_i^e(t) \leq p_i^e(t) \leq \overline{p}_i^e(t) \qquad \forall\, i \in \mathcal{E}, t \in \mathcal{T} \tag{5.4}$$

where the upper and lower bounds are defined in Section 3.2.4. We set $\underline{p}_i^e(t)$ to zero for every charger in every time slot to ensure that there always exists a feasible control, regardless of charging deadlines and the congestion state of the network. This makes the charging service best-effort, *i.e.*, charging deadlines are not taken into account[4].

### 5.2.2 System Constraints

Control must fulfill the requirements that are crucial for reliable operation of the distribution system. These requirements are therefore modelled as hard constraints in our optimization problems.

[3] These bounds ensure that the storage SOC remains between $\underline{c}$ and $\overline{c}$.

[4] In an over-provisioned distribution network, the electric utility can offer a guaranteed charging service by enforcing a lower bound on the charge power of each charger, assuring that charging demands are met by the deadlines. The grid power is used to meet these minimum demands when solar power is unavailable.

### Power Flow Equations

We recap the linearized DistFlow equations presented in Section 3.1.2 and the bus injection equations presented in Section 3.2.5 here:

$$p_k(t) = \sum_{i:\mathbf{A}^l_{ik}=1} p^l_i(t) + \sum_{i:\mathbf{A}^e_{ik}=1} p^e_i(t) - \sum_{i:\mathbf{A}^g_{ik}=1} p^g_i(t) - \sum_{i:\mathbf{A}^s_{ik}=1} p^s_i(t) \qquad \forall\, k \in \mathcal{B} \quad (5.5)$$

$$q_k(t) = \sum_{i:\mathbf{A}^l_{ik}=1} q^l_i(t) - \sum_{i:\mathbf{A}^g_{ik}=1} q^g_i(t) - q^c_k \qquad \forall\, k \in \mathcal{B} \quad (5.6)$$

$$P_{ij}(t) = \sum_{k \in \mathcal{B}_i} p_k(t) \qquad \forall\, (i,j) \in \mathcal{L} \quad (5.7)$$

$$Q_{ij}(t) = \sum_{k \in \mathcal{B}_i} q_k(t) \qquad \forall\, (i,j) \in \mathcal{L} \quad (5.8)$$

$$v^2_j(t) = v^2_0 - 2\left( \sum_{k \in \mathcal{B}} p_k(t) \sum_{(m,n) \in \mathcal{L}^j \bigcap \mathcal{L}^k} r_{mn} + \sum_{k \in \mathcal{B}} q_k(t) \sum_{(m,n) \in \mathcal{L}^j \bigcap \mathcal{L}^k} x_{mn} \right) \qquad \forall\, j \in \mathcal{B} \quad (5.9)$$

### Voltage Limits

The service voltage must be maintained within acceptable limits to comply with the distribution system code. To ensure that the service voltage stays within these strict bounds, utilities indirectly control the voltage on the primary circuit, taking into account the expected voltage drop along the laterals. We write the voltage constraint for distribution buses as:

$$v^2_{\text{min}} \leq v^2_i(t) \leq v^2_{\text{max}} \qquad \forall\, i \in \mathcal{B}, t \in \mathcal{T} \quad (5.10)$$

where $v_{\text{min}}$ and $v_{\text{max}}$ are the lower and the upper voltage limits.

### Capacity Limits

Overloaded equipment is generally more susceptible to failure due to overheating. Thus, the equipment load should be limited to a setpoint defined by the utility. We have the following constraint for each feeder:

$$P_{ij}(t) \leq \xi_{ij} \qquad \forall\, (i,j) \in \mathcal{L}, t \in \mathcal{T} \quad (5.11)$$

We can similarly write the capacity constraint for the substation transformer, noting that this transformer supplies the total demand that is not met by local resources to maintain a constant balance between supply and demand.

$$P_0(t) \leq \xi_0 \qquad \forall\, t \in \mathcal{T} \tag{5.12}$$

where $P_0(t)$ and $\xi_0$ are the substation transformer loading in time slot $t$ and its setpoint, respectively.

#### Power Flow Direction

Reversal of real power flow can negatively impact protection coordination and operation of line voltage regulators as distribution circuits are designed with the assumption that the direction of power flow is from the substation to loads at all times. For example, reverse flow conditions can cause *network protectors*, which are installed at distribution transformers, to open unnecessarily and create problems when they try to reclose [24]. In this problem formulation, we strictly forbid reverse flows outside balancing zones. Thus, real power cannot be injected to the network at a load bus that represents the root of a balancing zone. We write this constraints as:

$$p_i(t) \geq 0 \qquad \forall\, i \in \mathcal{B}_{\mathcal{Z}}, t \in \mathcal{T} \tag{5.13}$$

Recall that $\mathcal{B}_{\mathcal{Z}}$ is the set of buses representing the root of a balancing zone.

### 5.2.3 Objectives

The utility must meet the demand of homes and businesses at all times. Additionally, it seeks to operate active end-nodes so as to maximize its revenue, assuming that it has full control over EV chargers, PV inverters, and battery management systems. The utility is also required to implement government mandates, such as expanding renewable energy generation and cutting emissions. This leads to a multi-objective optimization problem that can be solved to obtain the optimal control.

We introduce the objectives considered in this work, define a particular ordering of them, and argue that this ordering is both reasonable and necessary. The following are these objectives in descending order of importance to the utility: *1*) maximize the utility's revenue by maximizing the total power delivered to elastic loads from different sources and simultaneously allocating the available power to connected EVs in a fair manner,

*2*) minimize the curtailment of solar power, *3*) minimize the use of conventional power from the grid, thereby reducing carbon emissions. In Section 5.3, we formulate a series of two optimization problems to achieve these control objectives in the order specified above. We discuss each of these objectives below.

**Objective 1 – Maximizing Revenue through Fair Power Allocation to EV Chargers**

The primary objective of the electric utility is to maximize its revenue. Assuming that the revenue is directly proportional to the supplied power, maximizing the revenue is the same as maximizing the total supplied power. Since household and business loads have a fixed demand in every time slot, which is guaranteed to be met by the utility, a revenue-maximizing strategy is the one that maximizes the total real power allocated to active EV chargers in a given time slot[5].

There are possibly many feasible revenue-maximizing control strategies in every time slot, since real power can be distributed among active chargers in different ways, all having the same total use of real power. We prefer the allocation that is fair to the connected EVs. Similar to our approach in Chapter 4, we assume that EV owners are greedy and want to finish charging their EVs as soon as possible; therefore, at time $t$, we attribute a utility to EV owner $i$ that is equal to the charge power adopted by its charger in the current time slot, $p_i^e(t)$.

We adopt the notion of proportional fairness and formulate a global optimization problem to maximize the sum of the logarithm of the utility function for EV owners. This choice of the objective function guarantees that real power is allocated in a proportionally fair manner among active EV chargers, as discussed in Section 2.4. For notational simplicity, we denote $\log(p_i^e(t))$ by $U_i(t)$, which is an infinitely differentiable, increasing, and strictly concave function in its domain. We note that the proportionally fair allocation is indeed a revenue-maximizing allocation. This is an appealing property of proportional fairness in that it utilizes all available resources.

[5]We do not take into account the energy that can be charged into storage systems when defining the revenue-maximizing control strategy for a time slot. This is because this energy is not actually consumed and will be used at some point to supply loads (with some losses). Hence, the utility does not increase its revenue in the long run by storing energy in the distribution network.

**Objective 2 – Minimizing Solar Curtailment**

Curtailing solar generation is a forfeiture of inexpensive green energy. This motivates our choice of minimizing the curtailment of distributed solar generation, which is equivalent to maximizing the use of solar power, as the secondary objective of the electric utility. Even when solar generation exceeds the aggregate demand of a balancing zone the excess energy can be used to charge storage systems within the same balancing zone. Nevertheless, curtailment cannot be avoided at all times; excess solar generation must be curtailed when it cannot be stored or exported due to the constraints presented earlier in this section. Smart inverters are capable of curtailing solar generation in these occasions.

We note that solar curtailment does not necessarily result in a revenue loss because the utility can displace solar energy with conventional energy and stored energy to obtain the same revenue. Hence, this objective is not redundant given the revenue maximization objective.

**Objective 3 – Minimizing the Use of Conventional Power**

Displacing conventional power supplied by the substation with solar power produced instantaneously by rooftop PV systems or stored in battery storage systems in previous time slots reduces the overall cost and carbon emissions of electricity generation as well as transmission losses. Hence, the utility would strive to minimize the use of conventional power to improve the power system efficiency, reduce transmission losses, and comply with external mandates. The use of conventional power is therefore restricted to when household and business demands cannot be met entirely by PV and storage systems.

We note that this objective is not redundant given the first two objectives because conventional power can be displaced with discharged power from storage systems without having any impact on the first two objectives.

## 5.3 Optimal Control

In this section, we describe a series of two optimization problems that generate our optimal control in every time slot. We discuss how the second problem can be decomposed into a number of decoupled problems and sketch the operation of our decentralized control scheme.

### 5.3.1 Optimization Problems

We need a multi-step optimization since the three objectives cannot be satisfied at the same time without using an arbitrary scalarization, *i.e.*, a weighted sum of the objectives. In particular, reducing the use of conventional power is in conflict with the revenue-maximization objective because it can reduce the total supplied power; therefore, a two-step optimization is inevitable. We discuss these two convex optimization problems next.

#### Revenue-Maximizing Fair Allocation with Minimum Solar Curtailment

The first optimization problem is to maximize the use of solar power, while allocating the available power in a proportionally fair manner among active chargers. Since the first two objective functions of Section 5.2.3 are not conflicting, it is possible to optimize them at the same time without introducing weight terms. More specifically, for any feasible control, increasing the use of solar power does not negatively impact the optimal power allocation to EV chargers. Hence, the optimal solution to the sum of these two objectives is the solution to *any* weighted sum of these two objectives[6].

Assuming that real and reactive power consumptions of homes and businesses, the setpoint of feeders and transformers, the available solar power at the point of connection of PV systems, and the set of active end-nodes and their parameters are known in the beginning of every time slot, we pose this problem as a nonlinear convex optimization problem.

Problem (5.14) is subject to the power flow equations (Section 3.1.2), the real and reactive power injection equations for buses (Section 3.2.5), the distribution systems constraints (Section 5.2.2), and the end-node constraints (Section 5.2.1). Note that this is a nonlinear convex problem because it maximizes the sum of two concave functions, subject to constraints that define a convex set. We represent the unique proportionally fair power allocation to EV chargers in time slot $t$ by $\tilde{\mathbf{p}}^e(t)$, and the optimal real and reactive power contributions of PV inverters by $\tilde{\mathbf{p}}^g(t)$ and $\tilde{\mathbf{q}}^g(t)$, respectively. Here the upright boldface letters represent vectors.

[6]Nevertheless, algorithmically weight terms are important because they influence how fast the optimal solution is found.

Problem 1: the global problem

**Inputs**: $\mathbf{p}^l(t), \mathbf{q}^l(t), \xi, \overline{\mathbf{p}^g}(t), \overline{\mathbf{s}^g}, \overline{\mathbf{p}^e}(t), \underline{\mathbf{p}^e}(t), \overline{\mathbf{p}^s}(t), \underline{\mathbf{p}^s}(t), \mathcal{I}, \mathcal{E}, \mathcal{J}, \mathcal{S}$

---

$$\max_{\mathbf{p}^e(t), \mathbf{p}^s(t), \mathbf{p}^g(t), \mathbf{q}^g(t)} \sum_{i \in \mathcal{E}} U_i(t) + \sum_{i \in \mathcal{J}} p_i^g(t) \tag{5.14}$$

subject to

End-node Constraints $(5.1 - 5.4)$

System Constraints $(5.10 - 5.13)$

Bus Injection Equations $(5.5 - 5.6)$

Power Flow Equations $(5.7 - 5.9)$

**Minimizing the Use of Conventional Power**

Given the solution to the first problem, the second optimization problem aims at minimizing the power supplied by the grid in a time slot, which can be written as:

$$P_{\text{grid}}(t) = \sum_{i \in \mathcal{I}} p_i^l(t) + \sum_{i \in \mathcal{E}} \tilde{p}_i^e(t) - \sum_{i \in \mathcal{J}} \tilde{p}_i^g(t) - \sum_{i \in \mathcal{S}} p_i^s(t)$$

Since the three first terms in the right hand side of this equation are fixed, maximizing the total power discharged from storage systems minimizes the use of conventional power supplied by the grid. Given real and reactive power consumptions of homes and businesses, the setpoint of feeders and transformers, the solution to the first optimization problem, the available solar power at the point of connection of PVs, the set of active end-nodes, and their parameters, we pose this problem as an LP. Note that Problem (5.15) does not include end-node constraints except for storage systems. This is because the operations of other active end-nodes have been determined already.

As a practical matter, all storage systems located in the same balancing zone must be either charging or discharging in a given time slot; otherwise, control may discharge one storage system and use the energy stored in that system to charge another storage system in the same zone. The energy transfer between storage systems that are within the same zone results in waste of energy due to storage charge and discharge inefficiencies. Hence, we rule out such controls by requiring all storage systems located in the same zone to either charge or discharge in each time slot, thereby maximizing the system efficiency

Problem 2: the global problem

**Inputs**: $\mathbf{p}^l(t), \mathbf{q}^l(t), \xi, \tilde{\mathbf{p}}^g(t), \tilde{\mathbf{q}}^g(t), \tilde{\mathbf{p}}^e(t), \overline{\mathbf{p}^s}(t), \underline{\mathbf{p}^s}(t), \mathcal{I}, \mathcal{E}, \mathcal{J}, \mathcal{S}$

---

$$\max_{\mathbf{p}^s(t)} \sum_{i \in \mathcal{S}} p_i^s(t) \tag{5.15}$$

subject to

$$0 \leq p_i^s(t) \leq \overline{p}_i^s(t) \qquad i \in \mathcal{S}^D$$

$$-\underline{p}_i^s(t) \leq p_i^s(t) \leq 0 \qquad i \in \mathcal{S}^C$$

System Constraints $(5.10 - 5.13)$

Bus Injection Equations $(5.5 - 5.6)$

Power Flow Equations $(5.7 - 5.9)$

implicitly. We denote the set of storage systems that must be charged and the set of storage systems that must be discharged by $\mathcal{S}^C$ and $\mathcal{S}^D$, respectively, which are defined as:

$$\mathcal{S}^C = \left\{ i \in \mathcal{S} | \mathbf{A}_{ij}^s = 1, j \in \mathcal{B}^C \right\} \tag{5.16}$$

$$\mathcal{S}^D = \left\{ i \in \mathcal{S} | \mathbf{A}_{ij}^s = 1, j \in \mathcal{B}^D \right\} \tag{5.17}$$

where $\mathcal{B}^C$ and $\mathcal{B}^D$ are balancing zones in which every storage system must be charged and discharged, respectively. We define these two sets as:

$$\mathcal{B}^C = \left\{ j \in \mathcal{B}_{\mathcal{Z}} | \sum_{i:\mathbf{A}_{ib}^g=1} \tilde{p}_i^g(t) > \sum_{i:\mathbf{A}_{ib}^l=1} p_i^l(t) + \sum_{i:\mathbf{A}_{ij}^e=1} \tilde{p}_i^e(t) \right\} \tag{5.18}$$

$$\mathcal{B}^D = \left\{ j \in \mathcal{B}_{\mathcal{Z}} | \sum_{i:\mathbf{A}_{ib}^g=1} \tilde{p}_i^g(t) \leq \sum_{i:\mathbf{A}_{ib}^l=1} p_i^l(t) + \sum_{i:\mathbf{A}_{ij}^e=1} \tilde{p}_i^e(t) \right\} \tag{5.19}$$

This optimization problem can have multiple solutions, each minimizing the use of conventional power from the grid. We represent an optimal control for storage systems in time slot $t$ by $\tilde{\mathbf{p}}^s(t)$.

Observe that the optimization problem (5.15) is separable because no constraint couples storage systems that belong to two different balancing zones[7]. Thus, this problem

[7]We can ignore line and transformer capacity constraints that are outside balancing zones in Prob-

can be decomposed to several problems of the forms (5.20) and (5.21), each of which corresponds to a single balancing zone. Solving each of these problems can be delegated to the controller installed at the edge of the balancing zone as discussed in the next section.

Problem 2-1: the balancing zone problem: $j \in \mathcal{B}^C$
**Inputs**: $\mathbf{p}^l(t), \mathbf{q}^l(t), \xi, \tilde{\mathbf{p}}^g(t), \tilde{\mathbf{q}}^g(t), \tilde{\mathbf{p}}^e(t), \overline{\mathbf{p}^s}(t), \underline{\mathbf{p}^s}(t), \mathcal{I}, \mathcal{E}, \mathcal{J}, \mathcal{S}$

---

$$\max_{\mathbf{p}^s(t)} \sum_{i \in \mathcal{S}} p_i^s(t) \tag{5.20}$$

subject to

$$-\underline{p}_i^s(t) \leq p_i^s(t) \leq 0 \qquad i \in \mathcal{S}^C$$

System Constraints $(5.10 - 5.13)$

Bus Injection Equations $(5.5 - 5.6)$

Power Flow Equations $(5.7 - 5.9)$

Problem 2-2: the balancing zone problem: $j \in \mathcal{B}^D$
**Inputs**: $\mathbf{p}^l(t), \mathbf{q}^l(t), \xi, \tilde{\mathbf{p}}^g(t), \tilde{\mathbf{q}}^g(t), \tilde{\mathbf{p}}^e(t), \overline{\mathbf{p}^s}(t), \underline{\mathbf{p}^s}(t), \mathcal{I}, \mathcal{E}, \mathcal{J}, \mathcal{S}$

---

$$\max_{\mathbf{p}^s(t)} \sum_{i \in \mathcal{S}} p_i^s(t) \tag{5.21}$$

subject to

$$0 \leq p_i^s(t) \leq \overline{p}_i^s(t) \qquad i \in \mathcal{S}^D$$

System Constraints $(5.10 - 5.13)$

Bus Injection Equations $(5.5 - 5.6)$

Power Flow Equations $(5.7 - 5.9)$

lem (5.15). This is because 1) storage systems are not charged from the grid due to the third objective and 2) storage systems are discharged at the maximum rate due to the choice of the objective function in Problem (5.15) and this does not overload any line or transformer if we ignore the capacity constraints as Problem (5.14) had a feasible solution.

### 5.3.2 Operation of the Decentralized Control Scheme

The utility may need to control possibly thousands of PV panels, storage systems, and EV chargers using measurements collected from tens of thousands of end-nodes in the distribution network. This calls for the design of an overall architecture that enables scalable, robust, timely, and secure data transfer between measurement and control nodes. Following the discussion in Section 2.3.3, we adopt a decentralized control architecture that consists of a centralized substation controller that coordinates control with a set of controllers corresponding to balancing zones. A communication network connects the substation controller to the balancing zone controllers and to measurement devices installed at homes and businesses. These devices measure residential and commercial demands and the parameters pertaining to the active end-nodes, discussed in Section 2.3.2, and send them to upstream controllers in every time slot.

Control actions are computed jointly by the substation controller and balancing zone controllers as follows: Step 1: the substation controller receives real-time measurements from the end-nodes just before the end of every time slot and uses this information to solves the optimization problem (5.14) for the next time slot. Step 2: it then communicates the optimal control setpoints, $\tilde{\mathbf{p}}^g(t)$, $\tilde{\mathbf{q}}^g(t)$, and $\tilde{\mathbf{p}}^e(t)$, to balancing zone controllers. Step 3: depending on the optimal setpoints computed by the substation controller, the controller of every balancing zone determines whether the storage systems in that zone must charge or discharge in the next time slot and solves either the problem (5.20) or the problem (5.21). Step 4: the controller of each balancing zone sends the control decisions down to the active end-nodes in its subtree. Step 5: each active end-node carries out the control decision in the beginning of the next time slot.

## 5.4 Benchmarks

To compare the performance of our control system with schemes that are already used in the field, we use as benchmarks two fully distributed control schemes. These define controllers that run at individual businesses to control their EV charging, and their inverter output and storage operations. A controller installed at a small business independently controls active end-nodes that are installed there using local measurements. Both schemes aim to limit the output of solar inverters to meeting the local demand; thus, they curtail solar generation when it exceeds the aggregate local demand and do not allow sharing within the balancing zones. We remark that these schemes cannot control reactive power output of inverters because they are not aware of the distribution network model and

also do not observe voltage at upstream buses. Thus, voltage and congestion problems are still possible due to the operation of EV chargers. Nevertheless, these schemes serve as benchmarks for our proposed control scheme.

We note that less conservative control schemes are also used in practice today. In these schemes, smart inverters permit the export of excess solar generation to the grid, curtailing only on overvoltage, which is less strict than the local criterion studied in this work. We do not use these schemes as benchmarks in this work because we do not have the ability to model voltage at a service drop.

### 5.4.1 Local Use of Solar Power without Storage

The first scheme assumes that storage systems are not installed at small businesses, and therefore, solar generation must be curtailed when it exceeds the sum of the demand of the small business and the maximum demand of the corresponding EV charger. The local controller aims at *1*) charging the EV at the maximum rate, and *2*) minimizing solar curtailment from the local PV system, subject to the constraint that there is no export of real power to the grid. Thus, the controller implements the following rules in the given order:

$$p_i^e(t) = \overline{p}_i^e(t) \tag{5.22}$$

$$p_i^g(t) = \min\{\overline{p}_i^g(t), p_i^l(t) + p_i^e(t)\} \tag{5.23}$$

To simplify the presentation, it is assumed here that all end-nodes indexed by $i$ are connected to the small business $i$.

### 5.4.2 Local Use of Solar Power with Local Storage

The second scheme assumes that storage systems are installed at small businesses and can be charged using the surplus solar energy if needed. However, excess solar production cannot be shared with loads even in the same balancing zone; it must be stored. The local controller aims at *1*) charging the EV at the maximum rate, *2*) minimizing curtailment of solar power produced by the local PV system, and *3*) minimizing the use of conventional power from the grid, subject to the constraint that there is no export of real power to the

| Bus | 680 | 634 | 675 | 645 | 646 | 684 | 652 | 611 |
|---|---|---|---|---|---|---|---|---|
| Phase | abc | abc | abc | bc | bc | ac | a | c |
| Number of homes/businesses | 450 | 50 | 300 | 50 | 200 | 50 | 150 | 150 |
| Number of EV chargers | 20 | 10 | 10 | 10 | 10 | 10 | 10 | 10 |
| Percentage of storage systems | 10% | 5% | 5% | 5% | 5% | 5% | 5% | 5% |
| Percentage of PV systems | 10% | 5% | 5% | 5% | 5% | 5% | 5% | 5% |

Table 5.1: The parameter setting for different simulation scenarios.

grid. Thus, the controller implements the following rules in the given order:

$$p_i^e(t) = \overline{p}_i^e(t) \tag{5.24}$$

$$p_i^g(t) = \min\{\overline{p}_i^g(t), p_i^l(t) + p_i^e(t) + \underline{p}_i^s(t)\} \tag{5.25}$$

$$p_i^s(t) = \min\{\overline{p}_i^s(t), p_i^l(t) + p_i^e(t) - p_i^g(t)\} \tag{5.26}$$

As before, all end-nodes indexed by $i$ are connected to the small business $i$.

## 5.5 Simulation Scenarios

This section describes the test distribution system used in our simulations and power flow studies and specifies the parameter setting for each simulation scenario. To obtain concrete simulation results, it is necessary to make numerous assumptions about the test system, as we detail below. We have tried our best to be as realistic as possible in the choice of these simulation parameters, recognizing that our results may change if these parameter values are modified. We note, however, that the overall conclusions and insights gained from these simulations are relatively insensitive to the actual parameter choices. We present the results from extensive simulations in Section 5.6. Specifically, for a specific penetration rate of active end-nodes, we carry out 7 simulation runs, using traces obtained for 7 days in the summer as discussed below, and compute the average and the standard deviation of the parameters of interest across these runs. We set the length of each time slot to 1 minute in our simulations.

### 5.5.1 Test Distribution System

We evaluate the proposed control scheme on a variant of the IEEE 13-bus test feeder [52], which is a three-phase unbalanced radial distribution system supplied by a 5MVA substation transformer stepping down the voltage from 115kV to 4.16kV. We modify this radial system as explained next. We remind the reader that our control scheme relies on a model that considers loads and active end-nodes connected to each phase separately. However, we evaluate our scheme in a three-phase system by performing power flow analysis which considers the coupling between phases. This allows us to see how far we can push this control approach.

Figure 5.2 shows primary distribution feeders and buses that comprise this radial system. A load bus represents a transformer connection where a distribution transformer supplies a low-voltage distribution network and downstream household and business loads. We assume that each low-voltage distribution network constitutes a balancing zone, depicted by dashed red boxes in Figure 5.2. Hence, distribution transformers are installed at the edge of balancing zones. This implies that real power cannot be injected back into the network at load buses (but bidirectional flows within the balancing zone may be permitted, depending on the nature of the control scheme). Nevertheless, due to the lack of a realistic model of low-voltage distribution networks, we assume that all end-nodes within a balancing zone are aggregated at the corresponding load bus. Note that our approach can be extended to study the entire distribution grid if the low-voltage distribution network model is available.

The zero-impedance switch installed between buses 671 and 692 is normally-closed, and shunt capacitors connected to buses 675 and 611 are assumed to be always switched on. It is also assumed that loads are single-phase connected between a phase and neutral. We ignore the coupling between phases and conduct a per-phase analysis of this radial system. Specifically, we incorporate the linearized DistFlow model, the single-phase power flow model discussed in Section 3.1.2, into our optimization problems. To simplify the model of the test system that is used in our optimizations, we assume that the voltage magnitude at bus 650 is fixed at 4.16kV, ignore the substation voltage regulator, and replace the 500kVA in-line transformer between buses 633 and 634 with three 167kVA single-phase transformers. Note that power flow simulations are performed on the test system without making these simplifying assumptions.

We set the capacity of every feeder and the capacity of every transformer to 90% of its ampacity at $50°C$ and 90% of its rated capacity, respectively. As is the common case, we require bus voltages to stay within $\pm$5% of the nominal distribution voltage. We have

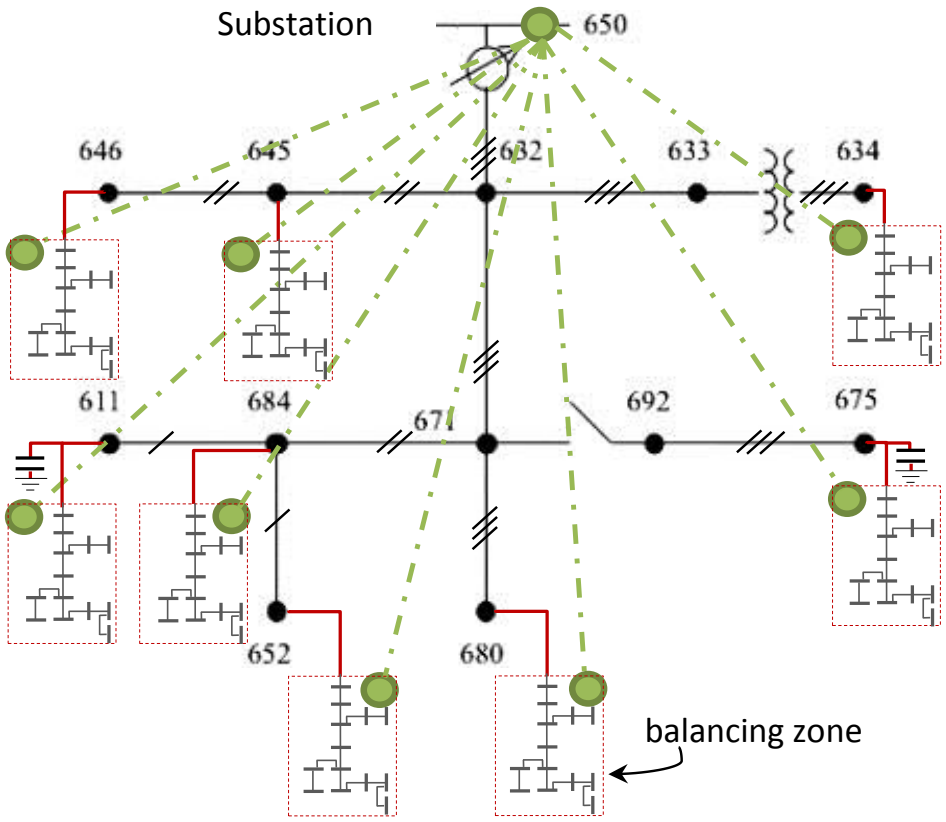


Figure 5.2: The one-line diagram of our radial test system. Balancing zones are depicted by dashed red boxes connected to selected load buses. A low-voltage distribution network within a balancing zone is connected to each load bus. A communication network that forms a logical tree (green lines) over the distribution system connects the substation controller to balancing zone controllers, depicted by green circles, and also to end-nodes.

chosen a typical layout of loads, EV chargers and PV inverters, which can be viewed as educated guesses. Table 5.1 specifies how loads are connected to our test system, noting that the figures provided in this table are per phase and node. Recall that EV chargers, PV inverters, and storage systems are installed only at small businesses and not on distribution buses.

We assume that a communication network connects household and business loads, and active end-nodes to the controller of their balancing zone, and also connects balancing zone controllers to the substation controller as discussed in Section 5.3.2. Each balancing zone controller receives near real-time measurements (*i.e.*, with a delay much smaller than 1 second) of the maximum demand of active EV chargers, the available real power at PV systems, and the maximum charge and discharge demands of storage systems from downstream active end-nodes. The controllers use these measurements as estimates of the corresponding values in the next time slot and compute the optimal control for that time slot accordingly.

### 5.5.2 Load Profiles

Our test distribution network supplies 3300 homes and businesses connected to selected buses as described in Table 5.1. To evaluate our control algorithm and study its fast timescale dynamics, we also need fine-grained measurements of the electricity demand of a large number of households, which we lack. Therefore, we generate synthetic load profiles using the Markov models developed in [6] for household electricity consumption during on-peak, mid-peak, and off-peak periods. These models are derived from fine-grained measurements of electricity consumption in 20 homes over four months. We choose 1-minute resolution for synthesizing the load profiles to match the time resolution of our solar traces and create load profiles using the models that correspond to the summer season.

We remark that using identical Markov models to generate the load profile of all homes and businesses results in a relatively smooth substation load during on-peak, mid-peak, and off-peak periods that abruptly changes as we switch to the next period. To avoid these abrupt transitions, we modulate the overall power consumption levels of our reference Markov models in every time slot such that the aggregate load at the substation resembles the Ontario demand in the first seven days of July 2014, which is shown in Figure 5.3. Specifically, we find the sum of all load profiles and compute a correction factor for every time slot by comparing the sum with the Ontario demand. We then multiply the

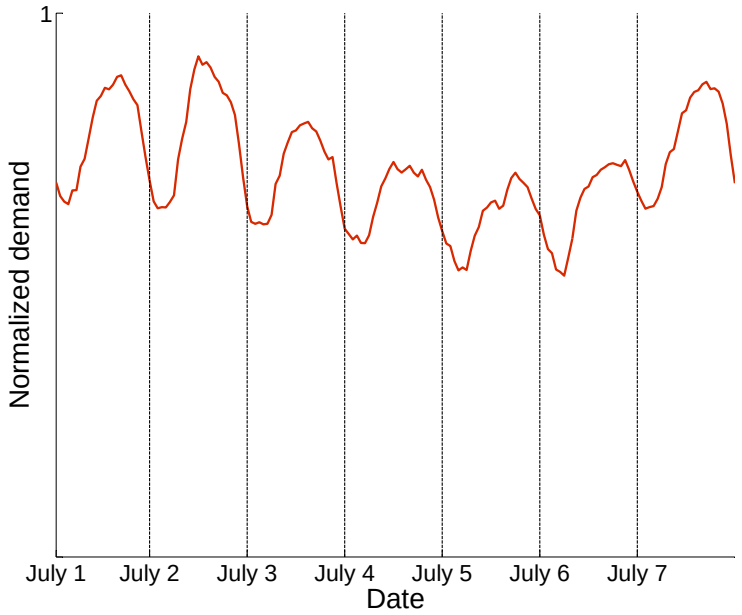


Figure 5.3: The Ontario demand (5-minute resolution) in the first week of July 2014.

consumption level of all loads in every time slot by the correction factor computed for that time slot.

We assume that the reactive power consumption of every home or business is 30% of its real power consumption in every time slot. This corresponds to a power factor of about 0.95 at the loads, which is typical for residential loads. Power flow calculations indicate that the peak demand at the substation is 4.50MW and 4.23MW with and without losses, respectively; this shows that distribution losses amount to approximately 6% of the demand. It also shows that the substation transformer is not congested over the simulation interval, in the absence of active end-nodes.

### 5.5.3 Solar Traces

We obtain 1-minute solar irradiance data for the week of July 1 to July 7, 2003 from the atmospheric radiation measurement site in Southern Great Plains [68]. We use this as a reference model to generate solar traces for the installed panels. Specifically, we scale up the reference model such that the peak available power of a single PV installation is uniformly distributed in the range 4-5kW, and set the rated apparent power capacity of PV inverters to 5kVA. We run our simulations for different numbers of PV installations,

namely 100, 200, 300, 400, and 500 panels connected to load buses as described in Table 5.1.

### 5.5.4 Storage

Storage systems are assumed to be installed at each small business with a PV installation. Hence, the number of storage systems is always equal to the number of PV systems in every simulation scenario. Table 5.1 describes the distribution of storage systems in the test system. We set the maximum charge power and the maximum discharge power of storage systems to 10kW, their energy capacity to 5kWh, and their charge and discharge efficiencies to 95%. At the beginning of every simulation, the SOC of all storage systems is assumed to be zero.

### 5.5.5 EV Model

Table 5.1 describes the manner in which 200 EV chargers are connected to load buses. We assume that EV chargers are only installed at businesses that also have PV installations and storage systems[8]. We also assume that all chargers are Level 2, thus imposing a maximum load of 7.2kW on the distribution network. A maximum of one EV is connected to each charger at a time, the capacity of an EV battery is 24kWh (*i.e.*, the capacity of a Nissan Leaf [66]), its charge efficiency is 95%, and the SOC of all EVs is 0.5 upon arrival. Hence, the initial energy demand of every EV is 12kWh.

Finally, assume that EVs arrive and connect to the chargers (located at businesses) every day starting from 8am, following a Poisson distribution with parameter $\mu = \frac{200}{90} = 2.2$ arrivals per minute. Poisson arrivals have also been used by other work in the literature [11]. We assume that EVs disconnect from the chargers 8 hours after their arrival. Thus, the number of active chargers varies over time starting from 0 at 8am, rising to the full number by approximately 9:30am and starting to decline at 4pm, reducing to 0 by approximately 5:30pm.

[8]The only exception is the scenario in which there are 100 PV panels and 100 storage systems; hence, PV panels are fewer than EV chargers. In this scenario, the other 100 EV chargers are installed at randomly selected businesses.

## 5.6 Results

In this section, we use power flow analysis to examine the effects of uncontrolled EV charging and solar generation on the modified IEEE 13-bus test system described in Section 5.6.1 and Section 5.6.2, respectively. Distribution network problems, such as overvoltage, undervoltage, equipment overloading, and reverse flow, that arise in these cases motivate the design of our scheme that simultaneously controls EV chargers, PV inverters, and storage systems to achieve the higher-level objectives discussed in Section 5.2.3, while addressing these problems. We validate through power flow analysis in Section 5.6.3 that the control computed by our scheme for every time slot is feasible. We also benchmark the performance of our control scheme with and without storage against the two local control schemes defined in Section 5.4 and quantify the benefits of sharing and using storage.

Note that we implement the proposed control scheme and carry out numerical simulations in MATLAB. We use AMPL to model the optimization problems described in Section 5.3, and CPLEX and MINOS solvers to solve linear and nonlinear convex problems in every time slot, respectively. We perform power flow analysis using the standard OpenDSS simulator [31] to compute the actual power flow in each branch and the actual voltage at each bus, thereby ensuring that our proposed control does not violate distribution network constraints. We let OpenDSS automatically control tap settings in each power flow simulation, unless otherwise stated. All simulations are run on a dedicated optimization server with a 12-core processor and 500GB of memory. We expand on our simulation framework in Appendix A.

### 5.6.1 The Effect of Uncontrolled EV charging

We first consider the case where only 200 EV chargers (and no PV or storage systems) are installed at small businesses, as described in Table 5.1. Hence, the distribution substation supplies demands of 3300 homes and businesses and 200 chargers. We study two uncontrolled EV charging scenarios in which chargers immediately start charging at their maximum rate after arrival. The first scenario assumes that all chargers are Level 1 and the second one assumes that all of them are Level 2.

We run power flow analysis for both scenarios to obtain branch flows and bus voltages. Figure 5.4 shows the effect of uncontrolled EV charging on the substation transformer loading in both scenarios in the first day of our simulation. It can be seen that uncontrolled charging of EVs in the Level 2 charging scenario overloads the substation transformer once most chargers become active. Should Level 1 charging be adopted, the transformer loading

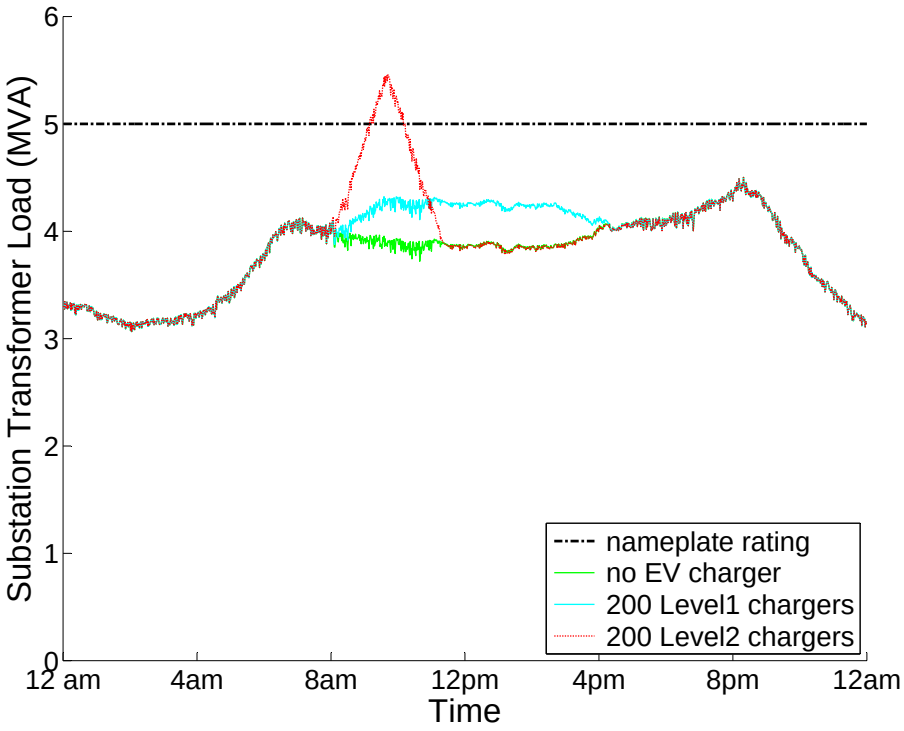


Figure 5.4: The effect of uncontrolled Level 1 and Level 2 EV charging on the substation transformer load.

does not exceed its nameplate rating. However, Level 1 charging extends the average charging time from 100 minutes to 400 minutes. Expectedly, uncontrolled charging of EVs does not result in reverse power flow in both scenarios.

We now focus on the impact of uncontrolled charging on voltage profiles. We first consider the case where regulator taps are not controlled on a fast timescale. We fix the taps to a position at which bus voltages will remain within the tolerance limits over the simulation interval, when the grid only supplies household and business demands. We specifically use the tap setting +8, neutral, and +10 (each step is 0.625%) for phase a, b, and c, respectively. Table 5.2 shows the minimum and maximum voltage levels recorded in our power flow simulations for both scenarios. It can be seen that uncontrolled Level 2 EV charging results in undervoltage at bus 646. Should tap operations be permitted as fast as once per minute to restore load voltage to normal, we see that simultaneous charging of the entire EV population does not result in any voltage problem in both scenarios.

| | 200 L1 chargers | | 200 L2 chargers | |
|---|---|---|---|---|
| | max | min | max | min |
| 650a | 1.000 | 1.000 | 1.000 | 1.000 |
| 650b | 1.000 | 1.000 | 1.000 | 1.000 |
| 650c | 1.000 | 1.000 | 1.000 | 1.000 |
| 632a | 1.038 | 1.025 | 1.038 | 1.021 |
| 632b | 0.985 | 0.969 | 0.985 | 0.968 |
| 632c | 1.046 | 1.025 | 1.046 | 1.015 |
| 671a | 1.025 | 0.998 | 1.025 | 0.992 |
| 671b | 0.983 | 0.959 | 0.983 | 0.959 |
| 671c | 1.036 | 0.998 | 1.036 | 0.980 |
| 680a | 1.020 | 0.990 | 1.020 | 0.982 |
| 680b | 0.980 | 0.953 | 0.980 | 0.953 |
| 680c | 1.031 | 0.990 | 1.031 | 0.971 |
| 633a | 1.038 | 1.024 | 1.038 | 1.019 |
| 633b | 0.984 | 0.968 | 0.984 | 0.967 |
| 633c | 1.046 | 1.024 | 1.046 | 1.013 |
| 634a | 1.033 | 1.018 | 1.033 | 1.008 |
| 634b | 0.979 | 0.962 | 0.979 | 0.956 |
| 634c | 1.042 | 1.018 | 1.042 | 1.002 |
| 692a | 1.025 | 0.998 | 1.025 | 0.992 |
| 692b | 0.983 | 0.959 | 0.983 | 0.959 |
| 692c | 1.036 | 0.998 | 1.036 | 0.980 |
| 675a | 1.023 | 0.995 | 1.023 | 0.989 |
| 675b | 0.982 | 0.956 | 0.982 | 0.956 |
| 675c | 1.035 | 0.996 | 1.035 | 0.977 |
| 645b | 0.978 | 0.959 | 0.978 | 0.955 |
| 645c | 1.042 | 1.019 | 1.042 | 1.007 |
| 646b | 0.974 | 0.954 | 0.974 | **0.949** |
| 646c | 1.040 | 1.015 | 1.040 | 1.004 |
| 684a | 1.023 | 0.995 | 1.023 | 0.988 |
| 684c | 1.034 | 0.995 | 1.034 | 0.974 |
| 652a | 1.018 | 0.988 | 1.018 | 0.979 |
| 611c | 1.033 | 0.993 | 1.033 | 0.971 |

Table 5.2: Voltage magnitudes (p.u.) per phase and node for uncontrolled EV charging scenarios without optimizing voltage regulator tap settings. Voltage limit violations are printed in bold.

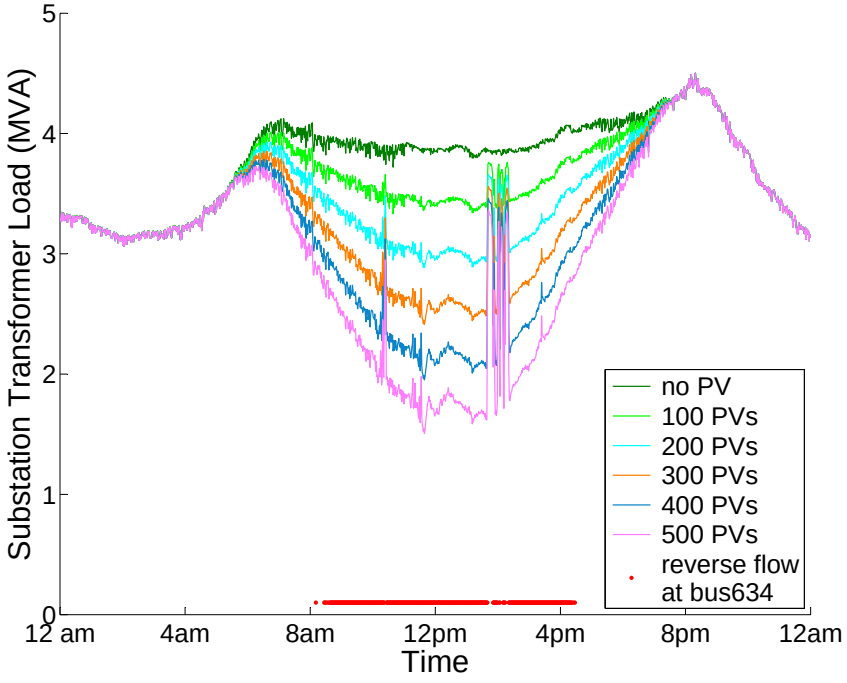


Figure 5.5: The effect of solar generation with uncontrolled inverters on the substation transformer load for different PV penetration rates for a typical day.

Nevertheless, this would cause excessive wear on the voltage regulator, which translates into higher operation and maintenance costs, and is therefore not desirable [72, 2].

### 5.6.2 The Effect of Uncontrolled Solar Generation

We now study the case where a certain population of PV panels is installed at small businesses, as described in Table 5.1. We assume that no storage or EV charger is installed in this network, PV inverters only produce real power, their real power output is not throttled by the operator, and excess solar generation can be transferred to loads in the same balancing zone. We gradually increase the PV penetration rate from 0 to 500 PVs (0–15%) and perform power flow studies for each case. Note that, in some jurisdictions, even in 2014, a penetration rate of 20% has already been achieved [71].

We first focus on the impact of uncontrolled solar generation on voltage profiles.

| | 100 PVs–3% | | 200 PVs–6% | | 300 PVs–9% | | 400 PVs–12% | | 500 PVs–15% | |
|---|---|---|---|---|---|---|---|---|---|---|
| | max | min | max | min | max | min | max | min | max | min |
| 650a | 1.000 | 1.000 | 1.000 | 1.000 | 1.000 | 1.000 | 1.000 | 1.000 | 1.000 | 1.000 |
| 650b | 1.000 | 1.000 | 1.000 | 1.000 | 1.000 | 1.000 | 1.000 | 1.000 | 1.000 | 1.000 |
| 650c | 1.000 | 1.000 | 1.000 | 1.000 | 1.000 | 1.000 | 1.000 | 1.000 | 1.000 | 1.000 |
| 632a | 1.038 | 1.025 | 1.038 | 1.025 | 1.038 | 1.025 | 1.040 | 1.025 | 1.041 | 1.025 |
| 632b | 0.985 | 0.969 | 0.985 | 0.969 | 0.985 | 0.969 | 0.987 | 0.969 | 0.989 | 0.969 |
| 632c | 1.046 | 1.025 | 1.046 | 1.025 | 1.049 | 1.025 | **1.053** | 1.025 | **1.056** | 1.025 |
| 671a | 1.025 | 0.998 | 1.025 | 0.998 | 1.025 | 0.999 | 1.026 | 0.999 | 1.028 | 0.999 |
| 671b | 0.983 | 0.959 | 0.983 | 0.959 | 0.983 | 0.959 | 0.983 | 0.959 | 0.984 | 0.959 |
| 671c | 1.036 | 0.998 | 1.036 | 0.998 | 1.041 | 0.998 | 1.047 | 0.998 | **1.053** | 0.998 |
| 680a | 1.020 | 0.990 | 1.020 | 0.990 | 1.020 | 0.990 | 1.021 | 0.990 | 1.023 | 0.990 |
| 680b | 0.980 | 0.953 | 0.980 | 0.953 | 0.980 | 0.953 | 0.980 | 0.953 | 0.981 | 0.953 |
| 680c | 1.031 | 0.990 | 1.031 | 0.990 | 1.036 | 0.990 | 1.043 | 0.990 | 1.049 | 0.990 |
| 633a | 1.038 | 1.024 | 1.038 | 1.024 | 1.038 | 1.024 | 1.040 | 1.024 | 1.041 | 1.024 |
| 633b | 0.984 | 0.968 | 0.984 | 0.968 | 0.985 | 0.968 | 0.987 | 0.968 | 0.989 | 0.968 |
| 633c | 1.046 | 1.024 | 1.046 | 1.024 | 1.049 | 1.024 | **1.053** | 1.024 | **1.056** | 1.024 |
| 634a | 1.033 | 1.018 | 1.034 | 1.018 | 1.037 | 1.018 | 1.039 | 1.018 | 1.042 | 1.018 |
| 634b | 0.979 | 0.962 | 0.981 | 0.962 | 0.984 | 0.962 | 0.987 | 0.962 | 0.990 | 0.962 |
| 634c | 1.042 | 1.018 | 1.043 | 1.018 | 1.048 | 1.018 | **1.053** | 1.018 | **1.058** | 1.018 |
| 692a | 1.025 | 0.998 | 1.025 | 0.998 | 1.025 | 0.999 | 1.026 | 0.999 | 1.028 | 0.999 |
| 692b | 0.983 | 0.959 | 0.983 | 0.959 | 0.983 | 0.959 | 0.983 | 0.959 | 0.984 | 0.959 |
| 692c | 1.036 | 0.998 | 1.036 | 0.998 | 1.041 | 0.998 | 1.047 | 0.998 | **1.053** | 0.998 |
| 675a | 1.023 | 0.996 | 1.023 | 0.996 | 1.023 | 0.996 | 1.025 | 0.996 | 1.027 | 0.996 |
| 675b | 0.982 | 0.956 | 0.982 | 0.956 | 0.982 | 0.956 | 0.982 | 0.956 | 0.983 | 0.956 |
| 675c | 1.035 | 0.996 | 1.035 | 0.996 | 1.040 | 0.996 | 1.046 | 0.996 | **1.052** | 0.996 |
| 645b | 0.978 | 0.959 | 0.978 | 0.959 | 0.980 | 0.959 | 0.983 | 0.959 | 0.986 | 0.959 |
| 645c | 1.042 | 1.019 | 1.042 | 1.019 | 1.046 | 1.019 | **1.051** | 1.019 | **1.053** | 1.019 |
| 646b | 0.974 | 0.954 | 0.974 | 0.954 | 0.977 | 0.954 | 0.980 | 0.954 | 0.983 | 0.954 |
| 646c | 1.040 | 1.015 | 1.040 | 1.015 | 1.044 | 1.015 | 1.048 | 1.015 | **1.052** | 1.015 |
| 684a | 1.023 | 0.995 | 1.023 | 0.995 | 1.023 | 0.996 | 1.025 | 0.996 | 1.027 | 0.996 |
| 684c | 1.034 | 0.995 | 1.034 | 0.995 | 1.040 | 0.995 | 1.047 | 0.995 | **1.054** | 0.995 |
| 652a | 1.018 | 0.988 | 1.018 | 0.988 | 1.019 | 0.988 | 1.022 | 0.988 | 1.025 | 0.988 |
| 611c | 1.033 | 0.993 | 1.033 | 0.993 | 1.040 | 0.993 | 1.047 | 0.993 | **1.054** | 0.993 |

Table 5.3: Voltage magnitudes (p.u.) per phase and node for uncontrolled solar generation scenarios without optimizing voltage regulator tap settings. Voltage limit violations are printed in bold.

Similar to the case of uncontrolled EV charging, we assume that regulator taps are not controlled on a fast timescale. We fix the taps using the same setting described in Section 5.6.1. Table 5.3 shows the minimum and maximum voltage levels recorded in our power flow simulations. It can be seen that overvoltage occurs at several buses, such as 634 and 645, when the number of PV installations exceeds 400. Should tap operations be permitted as fast as once per minute, our studies show that voltage does not increase beyond the permissible threshold at these penetration rates, even in the case of 500 PV systems. Again, we remark that voltage regulators are meant to be controlled infrequently and this would cause excessive wear on them.

Expectedly, distribution lines and transformers are not overloaded in our simulations because distributed solar generation reduces their load. Instead, reverse flow is observed at buses 634, 645, and 684 when the number of PV installations exceeds 200. Figure 5.5 shows the effect of uncontrolled solar generation on the substation transformer load for different penetration rates and the direction of power flow at bus 634 in the case of 500 PV systems. We see that the net load decreases drastically during the day when solar power is available and ramps up again in the evening; this is widely known as the 'duck curve' [19]. Furthermore, it can be seen that real power flows from bus 634 towards bus 632 in most time slots when the sun is shining. This reverse flow can cause severe problems discussed in [100, 48]. Interestingly, most EVs are connected to chargers at small businesses in this time interval, suggesting that the synergy between EV chargers and PV inverters could enhance power system reliability and address network problems that are likely to occur at high EV and PV penetration rates. This motivates the design of our control scheme.

### 5.6.3 Evaluating the Proposed Control

We compare our control scheme with the two local control schemes introduced in Section 5.4. Recall that in all three schemes, both EVs and PV systems are present. In the schemes with local control, only local observations are used to make control decisions, whereas in our scheme, a central controller coordinates decisions. Moreover, in the local control schemes, PV panels are not allowed to inject power into the balancing zone, but in our scheme, power sharing is allowed within each balancing zone. Figure 5.6 shows the total available solar power and the total real power output of PV inverters for different control schemes, when 100 PV panels and 100 storage systems are connected to the test distribution network. It can be seen that with our control it is possible to use all of the solar energy available in every time slot. This is because excess solar generation can

always be stored or consumed by loads that are in the same balancing zone at this PV penetration rate. Observe that the two local control schemes use much less solar power due to curtailments, especially when storage is unavailable.

When the number of PV installations (and the number of storage systems) increases to 400, our scheme is no longer capable of meeting the upper bound and curtailment becomes inevitable in some time slots. This can be seen in Figure 5.7. We attribute abrupt changes in the total real power output of PV inverters when our control is implemented to changes in the number of active chargers, load fluctuations, reverse flow restrictions, and storage capacity constraints. Nevertheless, the proposed control results in much less curtailment compared to the other two schemes as shown in Figure 5.8. The same observation is made when the number of PV installations increases to 500.

We now compare the performance of our control scheme when storage is unavailable with the other three control schemes. Figure 5.8 shows that the average amount of solar energy curtailed by different schemes over the period of a day. Our control does not result in solar curtailment when there are fewer than 300 PV/storage systems, or when there are fewer than 200 PV systems (but no storage). Even when the number of PV installations increases to 400 and 500, respectively, the proposed control results in on average 90.9% and 78.3% less curtailment compared to the first local control scheme, and 85.3% and 65.7% less curtailment compared to the second local control scheme. Furthermore, simulation results suggest that sharing is more effective in reducing curtailment than using even 5kWh storage per PV location. This result is very insightful for electric utilities in that sharing is cost-free unlike expensive storage systems.

We also compare the control schemes in terms of their use of conventional power supplied by the grid. Figure 5.9 shows that the proposed control scheme reduces the use of conventional power by displacing it with solar power. Note that the four control schemes are similar in terms of the energy supplied to EVs since all of them fully charge EVs by their deadlines in our simulation scenarios. However, if deadlines were set earlier, our scheme would allocate power to connected EVs in a proportionally fair manner, while local control schemes do not provide fairness and can result in starvation.

Finally, our power flow studies find that the proposed open-loop controller does not cause *any* voltage, congestion, or reverse flow problem in all simulation scenarios. As an example of the resulting operation, Figure 5.10 shows the substation loading over the first day of our simulation. It can be seen that our control successfully prevents overloads, confirming that using setpoints that are 10% below the nameplate ratings is sufficient

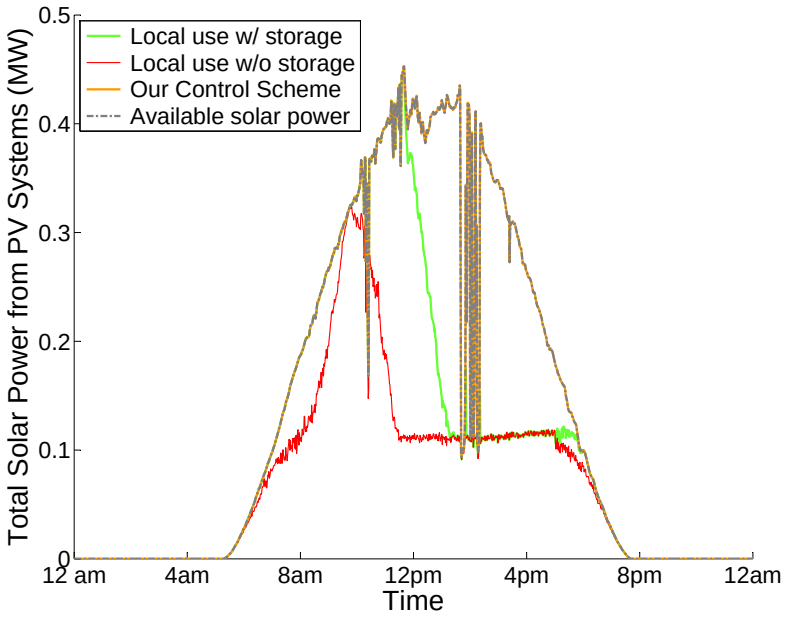


Figure 5.6: Total power output of PV inverters over a day for different control schemes in the case that 100 PV panels are deployed in the distribution network.

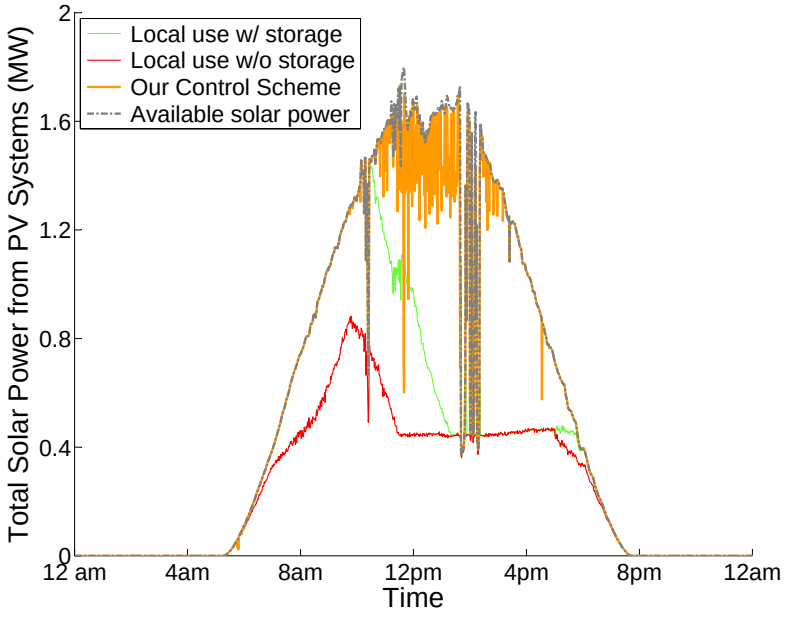


Figure 5.7: Total power output of PV inverters over a day for different control schemes in the case that 400 PV panels are deployed in the distribution network.

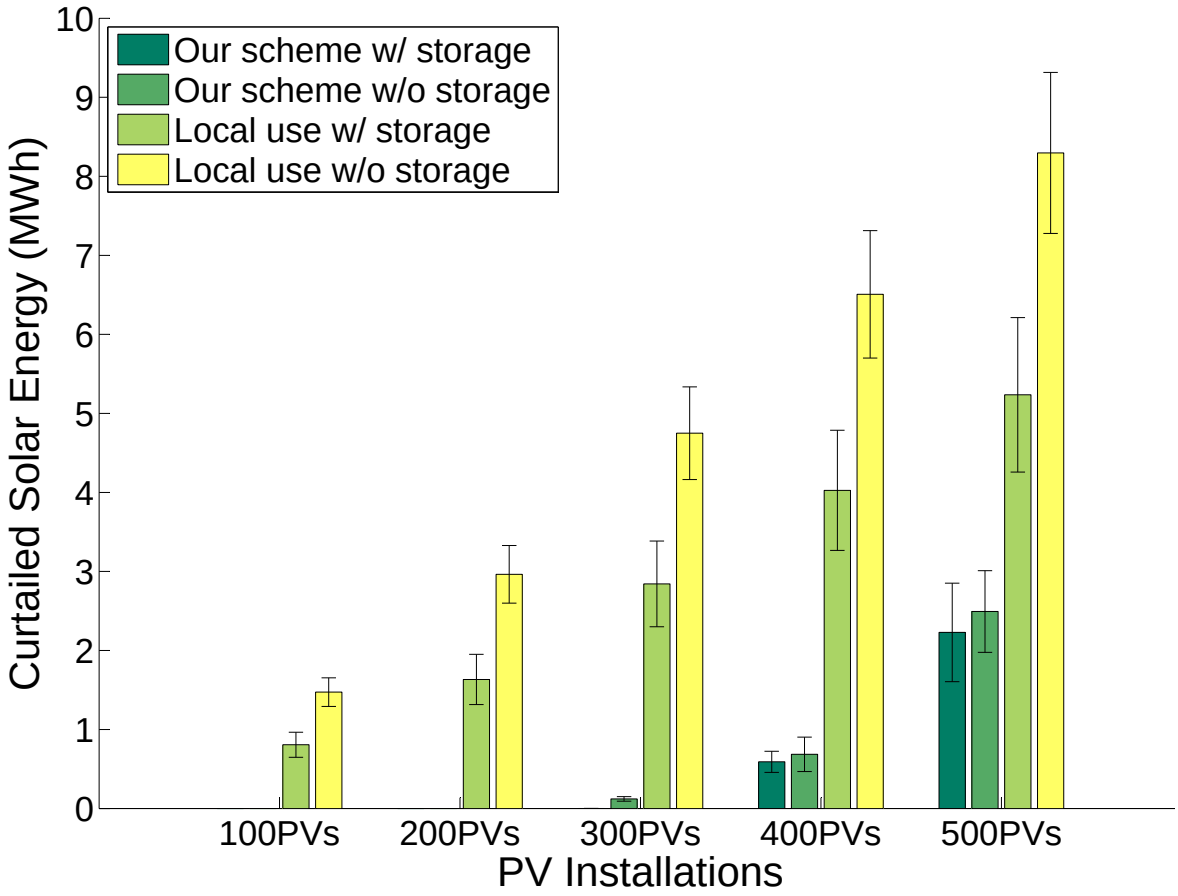


Figure 5.8: Average solar energy curtailed by different control schemes over the period of a day (lower is better). Error bars represent one standard error.

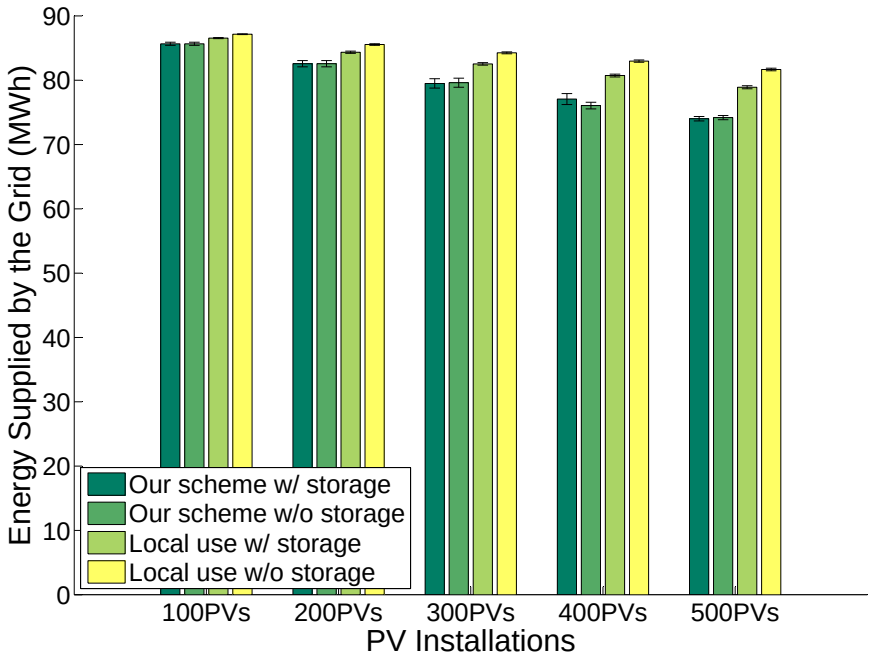


Figure 5.9: Average use of conventional energy by different control schemes over the period of a day (lower is better). Error bars represent one standard error.

to compensate for inaccuracies of the simplified DistFlow model[9]. We note that we have tried higher equipment setpoints, *e.g.*, we set them equal to the nameplate ratings and 5% below the nameplate ratings, and have witnessed in these cases they often lead to infeasible problems in our simulations. Thus, the results are sensitive to the choice of using 90% of the rated equipment capacity as the setpoint.

### Scalability of the Proposed Control Scheme

We now briefly discuss scalability of the proposed control scheme. The optimal control is found efficiently (in less than 1 second) on our server in scenarios with less than 400 PV

[9]Electric utilities have a rough estimate of resistive losses in their distribution circuits, enabling them to appropriately choose the equipment setpoints.

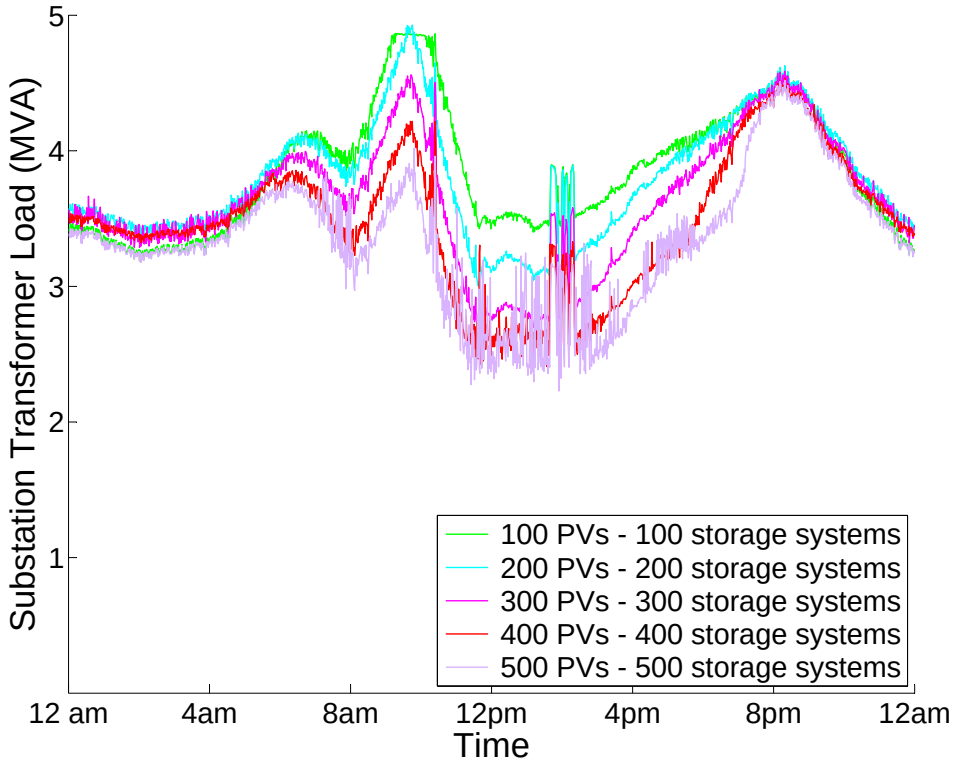


Figure 5.10: Substation transformer loading over a day for 200 EV chargers and different PV and storage penetration rates using the proposed control.

installations and 400 storage systems. However, should the number of active end-nodes increase even further, solving the first optimization problem takes up to 30 seconds, while the second optimization problem is still solved efficiently, in less than a few seconds. This implies that a fully distributed control scheme similar to the one designed in Chapter 4, is essential to control active end-nodes when their penetration increases to a certain level. We discuss this further in Section 7.2.2.

## 5.7 Chapter Summary

Many utilities in Europe and North America are experiencing the effects of high penetration of distributed PV systems and EVs on their radial distribution systems. Future distribution systems are anticipated to accommodate even higher penetrations of these

technologies, threatening service reliability, impairing power quality, and reducing efficiency of these systems under existing planning and operation paradigms. Our work uses the synergy between EV chargers and PV inverters to cancel out their effects on distribution feeders and simultaneously achieve the objectives defined by the utilities. Using the optimal control framework, we develop a decentralized scheme to control EV chargers, PV inverters, and storage systems that are connected to low-voltage distribution networks. Our control is myopic, relies on end-node measurements, and requires the distribution network model. It enables power sharing within the balancing zones and is designed to address potential voltage, reverse flow, and congestion problems in distribution systems.

We show through extensive simulations and power flow studies on a radial test feeder that the proposed control successfully addresses voltage, reverse flow, and congestion problems, maximizes the utility's revenue, allocates available power in a proportionally fair manner among active EV chargers, harnesses as much solar energy as possible using storage and sharing, and minimizes the use of conventional power.

# Chapter 6

# Optimal Policies for Solar-Powered Charging Stations

In this chapter, we explore the EV charge scheduling problem in the context of a public solar-powered charging station with multiple charging points and a grid connection. We assume that the charging station cannot export excess solar power to the grid and its grid connection is such that the peak charging demand can be reliably accommodated. Thus, we do not model the effect of simultaneous EV charging or fluctuating solar generation at this station on voltage profiles and branch flows in the distribution network.

## 6.1 Introduction

The cost of solar power generation has fallen tremendously over the past few years [27], causing global installations to increase by over 50 percent a year since 2006 [61]. In 2013, the installed cost of best-in-class rooftop solar photovoltaic systems fell to less than $4 per watt of peak capacity for U.S. residential customers, and studies suggest that it will fall to $2.30 by 2015 and to $1.60 by 2020 [61]. This makes solar power attractive even if subsidies disappear entirely. In view of this steep cost reduction and the widespread introduction of EVs to the mass market, we envision the widespread use of solar generation to meet the EV charging demand.

Currently, only a limited number of charging stations are available for public use. However, the increasing penetration of short-range plug-in EVs into the power grid in recent years is motivating the rapid development of public charging infrastructure. We anticipate that in the near future a large number of charging stations will be supplied by solar power, which peaks at almost the same time that most EVs are parked and plugged in to chargers at public and workplace charging stations. These charging stations are likely to have a grid connection in addition to the on-site solar photovoltaic system. The grid can back up intermittent solar generation, creating a reliable supply mix. In spite of this, solar power is expected to be the primary supply source in these charging stations for economic and environmental reasons.

The grid connection enables the CSP to give a worst-case guarantee to its customers since conventional power can be used to charge EVs even when the incoming solar radiation is low. Specifically, the CSP guarantees that EV batteries are charged up to a certain SOC by their deadlines, regardless of the amount of solar energy available in the charging interval. Nevertheless, the CSP may not be able to meet charging demands entirely by the deadlines as the charging station grid connection has a certain rated capacity, which cannot be exceeded.

Customers typically choose a tight deadline thinking that it gives them priority over

others. They need to understand the impact of charging deadlines on the charging cost and the service they receive. In fact, the later the deadlines are, the more solar energy would be available for EV charging, reducing the use of conventional energy and associated costs. Hence, extending charging deadlines would decrease the overall cost, *i.e.*, the energy procurement cost or the carbon footprint, of the charging service, and is therefore beneficial to the CSP and potentially to the customers if more energy can be stored in their EV batteries.

To investigate the relationship between charging deadlines, customer satisfaction, and the total cost of the charging service in a grid-connected solar charging station, we develop a charging strategy based on a series of optimization problems. Assuming perfect knowledge of daily solar radiation and EV mobility, this strategy minimizes the total cost of the charging service for given deadlines, leverages solar generation to store more energy into EV batteries than when solar power is unavailable, and allocates the available power in a *proportionally fair* manner among EVs with different arrival times and energy demands. This provides a benchmark for evaluating the impact of different deadlines in terms of the resultant cost and average customer satisfaction, enabling us to quantify the benefits of extending the deadlines from the perspective of the CSP and customers.

The rest of this chapter is organized as follows. We present our model of a solar charging station and attribute a utility to each customer in Section 6.2. We formulate three optimization problems to determine the optimal charging strategy in Section 6.3 and describe our simulation scenarios in Section 6.4. Using real traces of solar power generation, we numerically evaluate the three-way tradeoff between the carbon footprint of EV charging, the deadlines, and the average customer utility in Section 6.5. In one specific case, we identify three different regimes, each corresponding to a range of deadlines, and discuss whether the CSP or EV owners would benefit from extending the deadlines in each regime.

## 6.2 System Overview

Consider a grid-tied public charging station with multiple identical chargers. Suppose the chargers become active or inactive only at the beginning of a time slot and consume constant real power over a time slot when they are active. We denote the real power consumption of charger $i$ in time slot $t$ by $p_i^e(t)$. The charging station is supplied by the grid and a PV system with installed capacity $G^{\max}$, as illustrated in Figure 6.1. The PV system is connected to the charging station via an inverter that produces real power only.

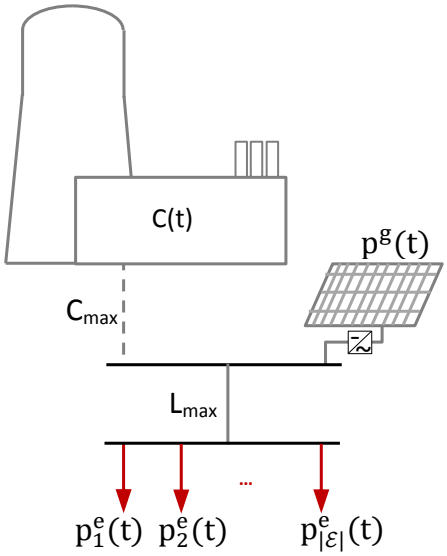


Figure 6.1: A schematic diagram of a grid-connected solar charging station with multiple chargers represented by red arrows.

The real power output of the inverter is assumed to be fixed in each time slot. We denote the real power output of the inverter in time slot $t$ by $p^g(t)$, where $p^g(t) \leq G^{\max}$ for all $t$.

We denote the conventional power consumed by the charging station in time slot $t$ by $C(t)$. This power is carried by a line that connects the charging station to the grid and is rated at $C^{\max}$; thus, $C(t) \leq C^{\max}$. A protective relay ensures that the direction of the real power flow in this line is from the grid to the charging station at all times. We assume that the charging station can be supplied simultaneously by the PV system and the grid. The line that connects EV chargers to both supply sources is rated at $L^{\max}$. We assume that $L^{\max} \geq C^{\max}$. Hence, a maximum of $C^{\max}$ is available to chargers without solar generation, while a maximum of $\min\{L^{\max}, C^{\max} + G^{\max}\}$ is available to chargers, taking into account the real power output of the inverter. Note that solar generation is curtailed by the inverter when $p^g(t) > L^{\max}$.

We assume that there are enough chargers for all EVs at this station. Let $a_i$ be the time slot in which charger $i$ becomes active, following an EV arrival. We assume that each customer sets the charging deadline to be $d$ time slots after the arrival, *i.e.*, the beginning of time slot $a_i + d$, and the corresponding EV charger becomes inactive and stops charging once the deadline is passed[1]. We denote the charging demand of this EV upon arrival

[1]We assume that all customers pick the same value of $d$ irrespective of their arrival time.

by $e_i$. The CSP cannot guarantee that charging demands of EVs are met entirely by their deadlines because the available energy from both sources may not be enough. Thus, the minimum demand of each charger is set to zero in every time slot. The charge power of EV charger $i$ belongs to the interval $[0\ \overline{p}_i^e]$ at all times.

We represent the set of all time slots in the charging interval by $\mathcal{T}$ and the set of time slots in which charger $i$ is active by $T_i = [a_i, \cdots, a_i + d - 1]$. We define the indicator function $\mathbb{1}_{T_i}$ on the set $T_i$ as:

$$\mathbb{1}_{T_i}(t) = \begin{cases} 1 & \text{if } t \in T_i \\ 0 & \text{otherwise} \end{cases} \tag{6.1}$$

### 6.2.1 Customer Utility

We attribute a utility to each customer of the charging station. We assume that customers keep their EV connected to the charger until the deadline they specify at the connection time is passed. Hence, it is reasonable to assert that the customer utility increases with the amount of energy stored in their EV battery by this deadline. We define the utility of a customer using charger $i$ as:

$$u_{i,d} = \frac{\sum_{t \in T_i} p_i^e(t)}{e_i} = \frac{\sum_{t \in \mathcal{T}} p_i^e(t) \times \mathbb{1}_{T_i}(t)}{e_i} \tag{6.2}$$

where $u_{i,d}$ is a normalized value belonging to the interval $[0\ 1]$. The customer utility is one if the EV battery is fully charged by the deadline.

We adopt the notion of proportional fairness discussed in Section 2.4. The proportionally fair solution is the one that maximizes the sum of the logarithm of the utility function of all customers. Observe that $\log(u_{i,d})$ is infinitely differentiable, increasing, and strictly concave on the interior of its domain.

### 6.2.2 Cost Function

We model the cost of the charging service as an increasing convex function of the total amount of conventional energy used over the charging interval, *i.e.*, $\sum_{t \in \mathcal{T}} C(t)$. We denote the cost function by $f$, noting that it could represent the procurement cost of conventional energy or the carbon footprint associated with a charging schedule. We adopt a linear cost function in this work.

## 6.3 Optimization Problems

We now formulate a sequence of three convex optimization problems to find, for a given deadline, a proportionally fair charging schedule that minimizes the cost associated with the charging service and guarantees a utility to customers that is higher than the utility they would have obtained in the worst case without solar generation. We propose an offline algorithm that solves these optimization problems in the given order to compute this schedule, assuming perfect knowledge of solar generation and EV arrival times over the charging interval. This algorithm can be used in practice to determine a sub-optimal charging schedule using predictions of solar generation and EV arrival times over the charging interval.

We formulate three optimization problems to avoid combining the three objective functions into a single one using an arbitrary linear scalarization. The solution to the first problem is the utility of every customer for a given deadline $d$ without using solar power (the worst case). It is indeed the worst case since a charging station without the PV system is limited to $C^{\max} \leq L^{\max}$ and the resultant charging schedule would have the highest cost. Thus, the first problem gives us a lower bound on the utility that each EV should expect for a given deadline $d$. We refer to this as the minimum service requirement. The second problem determines how conventional power should be used to minimize the cost, while meeting the minimum service requirements. The solution to the third optimization problem is a proportionally fair allocation of solar and conventional power to EV chargers over the charging interval. The total cost of this charging schedule cannot exceed the solution of the second optimization problem and it is required to meet the minimum service requirements obtained by solving the first optimization problem.

We describe each of these optimization problems next.

### 6.3.1 Worst Case Customer Utility

In Problem 1, we compute the utility of every customer, assuming that solar power is unavailable and conventional power is allocated to active chargers in a proportionally fair manner. To solve this problem, we need to know EV arrival times, their initial charging demands, and the constraints imposed by the charging station and chargers. We denote the solution of this problem by $\mathbf{u}^*_{i,d}$, which is the utility that each customer attains in the worst case assuming a fair scheduling algorithm.

Optimization Problem 1
**Inputs**: $\mathbf{e}_i, \mathbb{1}_{T_i}(t), \overline{\mathbf{p}}_i^e, C^{\max}, \mathcal{E}, \mathcal{T}$

$$\max_{\mathbf{p}^e(t)} \sum_{i\in\mathcal{E}} \log u_{i,d} \tag{6.3}$$

$$\text{s.t.} \quad u_{i,d} \leq 1 \qquad \forall i \in \mathcal{E} \tag{6.4}$$

$$\sum_{i\in\mathcal{E}} p_i^e(t) \times \mathbb{1}_{T_i}(t) \leq C^{\max} \qquad \forall t \in \mathcal{T} \tag{6.5}$$

$$0 \leq p_i^e(t) \leq \overline{p}_i^e \qquad \forall t \in \mathcal{T},\ i \in \mathcal{E} \tag{6.6}$$

Since the grid is the only supply source in the worst case, the available power for EV charging is limited to $C^{\max}$ in this case.

### 6.3.2 The Minimum Charging Cost to Meet Service Requirements

Given the minimum service requirement of each customer and available solar power in every time slot, Problem 2 determines the cost-minimizing use of conventional power over the charging interval to meet the minimum service requirements (*i.e.*, to ensure that the utility of every customer is not less than the utility they would get in the worst case). We denote the optimal use of conventional power in time slot $t$ by $C_d^*(t)$.

Note that Constraint (6.9) is an inequality constraint because the actual use of solar power might be less than $p^g(t)$ due to the possibility of curtailment. Particularly, solar generation is curtailed if $p^g(t) > \sum_{i\in\mathcal{E}} \overline{p}_i^e \times \mathbb{1}_{T_i}(t)$ or $p^g(t) > L^{\max}$.

### 6.3.3 Fair Allocation of Available Power to EV Chargers

In Problem 3, we determine the charge power of every charger in every time slot and also the use of conventional power in every time slot. Specifically, we find a proportionally fair allocation of available power to EV chargers that meets the minimum service requirements and ensures that its total cost is no more than $f(\sum_{t\in\mathcal{T}} C_d^*(t))$. Hence, to solve this problem we need to know $C_d^*(t)$ and $\mathbf{u}_{i,d}^*$ in addition to EV arrival times, their initial charging

Optimization Problem 2
**Inputs**: $\mathbf{e}_i, \mathbf{u}^*_{i,d}, \mathbb{1}_{T_i}(t), p^g(t), \overline{\mathbf{p}}^e_i, C^{\max}, L^{\max}, \mathcal{E}, \mathcal{T}$

---

$$\min_{\mathbf{p}^e(t), C(t)} f(\sum_{t\in\mathcal{T}} C(t)) \tag{6.7}$$

$$\text{s.t.} \quad u^*_{i,d} \leq u_{i,d} \leq 1 \qquad \forall i \in \mathcal{E} \tag{6.8}$$

$$\sum_{i\in\mathcal{E}} p^e_i(t) \times \mathbb{1}_{T_i}(t) \leq C(t) + p^g(t) \qquad \forall t \in \mathcal{T} \tag{6.9}$$

$$\sum_{i\in\mathcal{E}} p^e_i(t) \times \mathbb{1}_{T_i}(t) \leq L^{\max} \qquad \forall t \in \mathcal{T} \tag{6.10}$$

$$0 \leq C(t) \leq C^{\max} \qquad \forall t \in \mathcal{T} \tag{6.11}$$

$$0 \leq p^e_i(t) \leq \overline{p}^e_i \qquad \forall t \in \mathcal{T},\ i \in \mathcal{E} \tag{6.12}$$

Optimization Problem 3
**Inputs**: $\mathbf{e}_i, \mathbf{u}^*_{i,d}, \mathbb{1}_{T_i}(t), p^g(t), \overline{\mathbf{p}}^e_i, C^*_d(t), L^{\max}, \mathcal{E}, \mathcal{T}$

---

$$\max_{\mathbf{p}^e(t), C(t)} \sum_{i\in\mathcal{E}} \log u_{i,d} \tag{6.13}$$

$$\text{s.t.} \quad u^*_{i,d} \leq u_{i,d} \leq 1 \qquad \forall i \in \mathcal{E} \tag{6.14}$$

$$\sum_{i\in\mathcal{E}} p^e_i(t) \times \mathbb{1}_{T_i}(t) \leq C(t) + p^g(t) \qquad \forall t \in \mathcal{T} \tag{6.15}$$

$$\sum_{i\in\mathcal{E}} p^e_i(t) \times \mathbb{1}_{T_i}(t) \leq L^{\max} \qquad \forall t \in \mathcal{T} \tag{6.16}$$

$$f(\sum_{t\in\mathcal{T}} C(t)) \leq f(\sum_{t\in\mathcal{T}} C^*_d(t)) \tag{6.17}$$

$$0 \leq C(t) \leq C^{\max} \qquad \forall t \in \mathcal{T} \tag{6.18}$$

$$0 \leq p^e_i(t) \leq \overline{p}^e_i \qquad \forall t \in \mathcal{T},\ i \in \mathcal{E} \tag{6.19}$$

demands, the available solar power in every time slot, and the constraints imposed by the charging station and chargers. We remark that the utility that each customer attains can be greater than what they would have attained in the worst case given this problem formulation.

## 6.4 Simulation Scenarios

Our simulation involves a public EV charging station with a PV system and a grid connection, serving a finite population of customers that charge their EVs at this station. The charging station has a certain number of Level 1 chargers (a maximum load of 1.8kW per charger). The number of chargers is assumed to be equal to the number of customers that use this service; hence, a customer can always find an available charging spot upon arrival. The customers arrive at the charging station every day after 7am, plug in their EV upon arrival, and set the deadline to $x$ hours after their arrival, where $x$ takes value from the set $\{4, 4.5, \cdots, 10.5, 11\}$. We set the length of every time slot to five minutes and model EV arrivals using a Poisson distribution with parameter $\lambda = 2.08$ per time slot so that on average, 50 EVs arrive in two hours. We assume that all EVs have a 24kWh battery and their SOC at the arrival time is 0.5; thus, their initial demand is 12kWh.

We use one-minute resolution solar irradiance data from the US Virgin Islands Bovoni 2 measurement station [67] and scale it to obtain the maximum solar power of $G^{\max}$. We set $L^{\max}$ to 90kW, and assume that the cost associated with the use of conventional power is linearly proportional to the amount of conventional energy consumed over the charging interval[2]. We study three cases described in the following section.

## 6.5 Results

In this section, we solve the convex optimization problems using AMPL modelling language and the Minos solver, running on a server with two six-core Intel Xeon processors, to find the minimum cost of EV charging along with the average customer utility for a given population of EVs and a solar irradiation time series. For a certain size of EV population, we simulate an ensemble of 10 runs of EV charging with randomly generated arrival patterns as described in the previous section. We report the mean and the standard deviation for the parameters of interest over the simulation runs.

[2]The cost associated with the use of conventional power does not vary with time in our model.

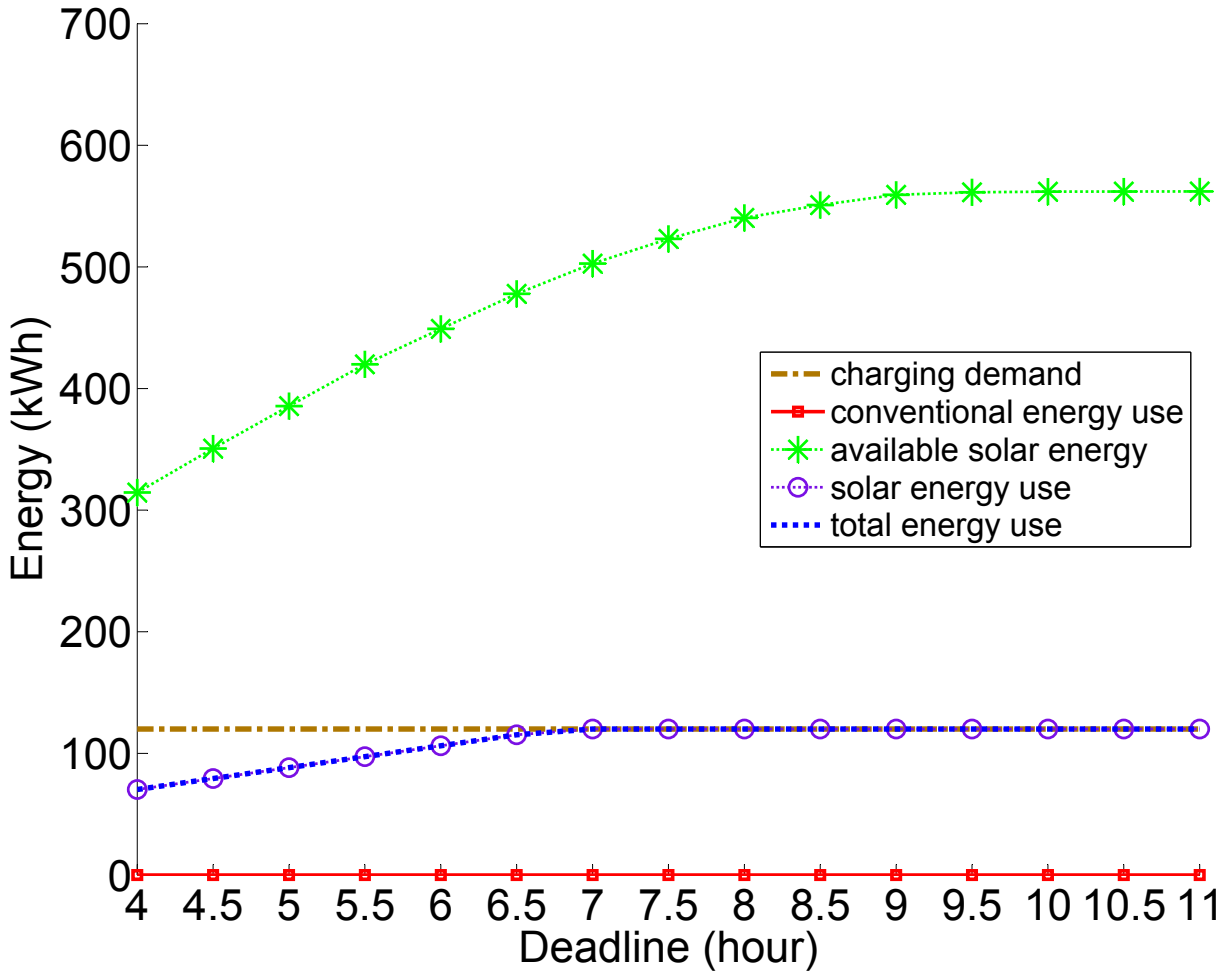


Figure 6.2: Average energy supplied by different sources for different deadlines in multiple simulation runs when EV population is 10, $G^{\max} = 80kW$, and $C^{\max} = 10kW$.

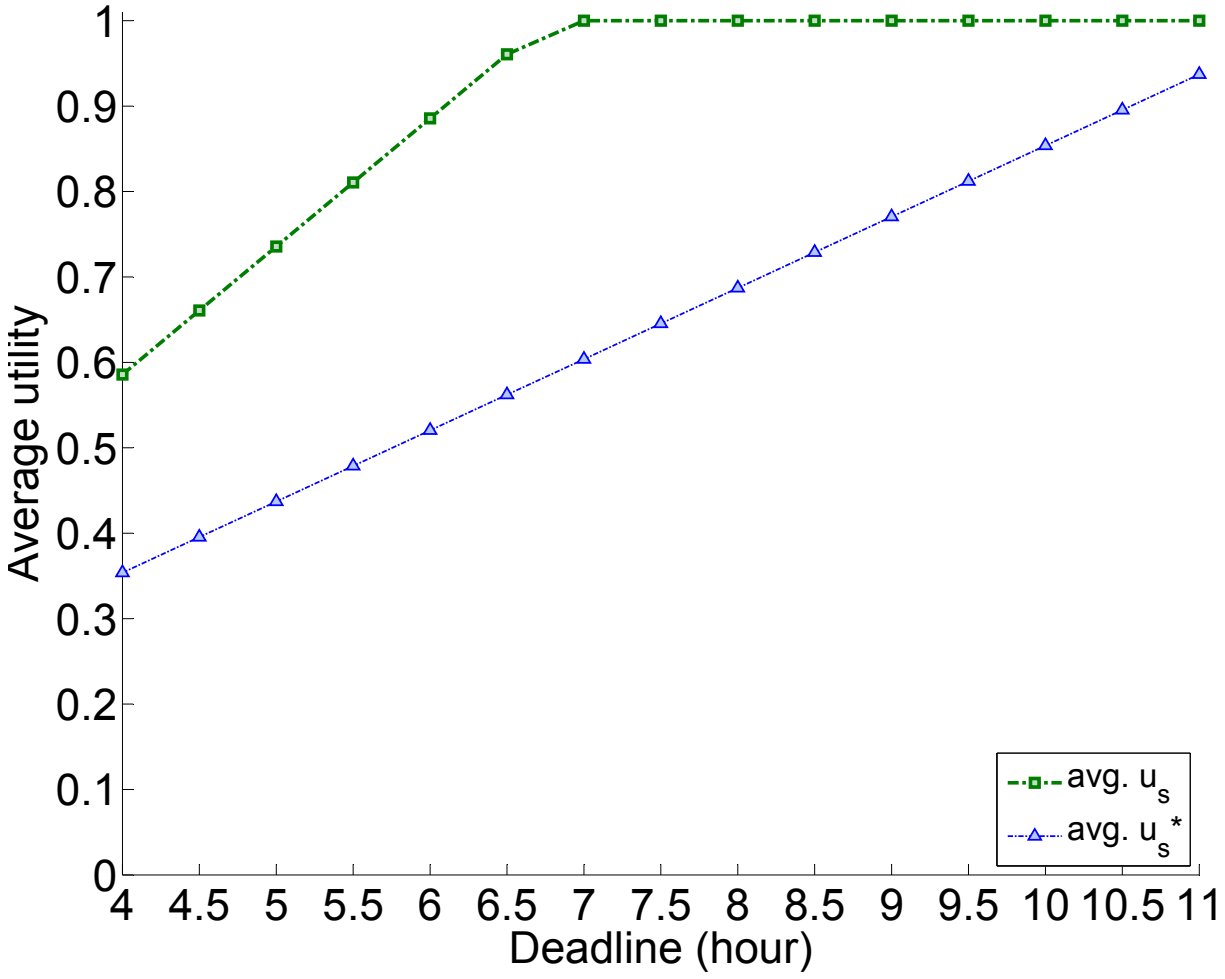


Figure 6.3: Average customer utility, $u_{s,d}$, obtained by solving Problem 3 and the average worst-case utility, $u^*_{s,d}$ for different deadlines when EV population is 10, $G^{\max} = 80kW$, and $C^{\max} = 10kW$.

### 6.5.1 Plenty of Solar Power

We first assume that the PV system is huge compared to the charging demand; hence, the optimal strategy relies entirely on solar power to meet the minimum service requirements. Specifically, if there is enough solar power to obtain $C_d^*(t) = 0$ in every time slot, all customers can attain a utility that is higher than the utility they attain in the worst case.

To see this, suppose that the installed capacity of the PV system is 80kW and $C^{\max} = 10$kW. With this parameter setting, the average worst-case utility of customers is relatively low. Now if the EV population is 10, the total EV charging demand would be $10 \times 24 \times 0.5 = 120$kWh. Figure 6.2 depicts the simulation results for different charging deadlines. It can be seen that the proposed charging strategy meets the minimum service requirements for all values of the deadline by relying entirely on solar energy; this results in zero cost and is therefore the optimal solution. Note that the use of solar energy grows with the deadline until all EVs can be fully charged; this happens when the deadline is in seven hours.

Figure 6.3 shows the average utility and the average worst-case utility of customers. The proportionally fair power allocation algorithm gives every customer a utility which is much higher than the worst-case utility. Note that the average utility reaches one when the deadline is seven hours after arrivals, indicating that all EVs are fully charged at this point.

Since the cost of EV charging is zero for all values of $d$, customers can attain a higher utility by extending their deadlines from four hours to seven hours without increasing the cost. A further extension of the deadlines does not benefit anyone in this case.

### 6.5.2 Limited Solar Power

We now turn our attention to when there is insufficient solar energy; thus, some amount of conventional energy must be used, in addition to the available solar energy, to satisfy the minimum service requirements. This would be the case, for example, when the installed capacity of the PV system is 40kW, $C^{\max} = 50$kW, and the EV population is 50 (the total charging demand is $50 \times 24 \times 0.5 = 600$kWh).

Figure 6.4 shows simulation results for different charging deadlines. The amount of solar energy available for EV charging increases with the deadline until sunset, and all the available solar energy is used for EV charging by the algorithm. However, since the available solar energy is insufficient to meet the minimum service requirements, the use

of conventional energy also increases with the deadline. In fact, its rate of increase is higher than that of solar energy when the deadline is shifted to the evening.

The blue curves with triangle and cross markers in Figure 6.5 show the average customer utility obtained by solving Problem 3 and the average worst-case utility for customers found in Problem 1, respectively. Observe that the average customer utility is always higher than the average worst-case utility and it increases with the deadline, but never reaches one.

In this case, extending the charging deadline increases the average customer utility, but this comes at the price of increasing the cost of the charging service, especially when the deadline moves to the evening. We believe that this tradeoff is very useful for the CSP. For example, if the cost of the charging service should not exceed a certain threshold, then the CSP would be required to enforce a lower bound on charging deadlines.

### 6.5.3 Plenty of Conventional Power

We finally study the case when the amount of solar energy is insufficient (similar to the previous case); but, this time the capacity of the charging station grid connection is chosen such that customers obtain a considerably higher utility in the worst case compared to the previous case. To see this, we need to increase $C^{\max}$ to 80kW. Other parameters are identical to the previous case described in Section 6.5.2.

To differentiate this case from the previous case, we first look at the utilities. The red curves with circle and asterisk markers in Figure 6.5 show the average customer utility obtained by solving Problem 3 and the average worst-case utility for customers found in Problem 1, respectively. Observe that customers attain a higher utility as we increase the deadline, until the deadline reaches 7.5 hours after arrivals. After this point, every EV is fully charged and the average utility remains at one.

Figure 6.6 shows the simulation results for different charging deadlines. We witness three different behaviours in this case identified by three regimes. The first regime corresponds to the case that EV batteries are not fully charged and the optimal charging strategy uses almost all the available solar energy in addition to some amount of conventional energy to satisfy minimum service requirements. Thus, the same tradeoff between the average customer utility and the cost of EV charging exists in this regime. In the second regime, all EVs are fully charged and increasing the deadline only results in using more

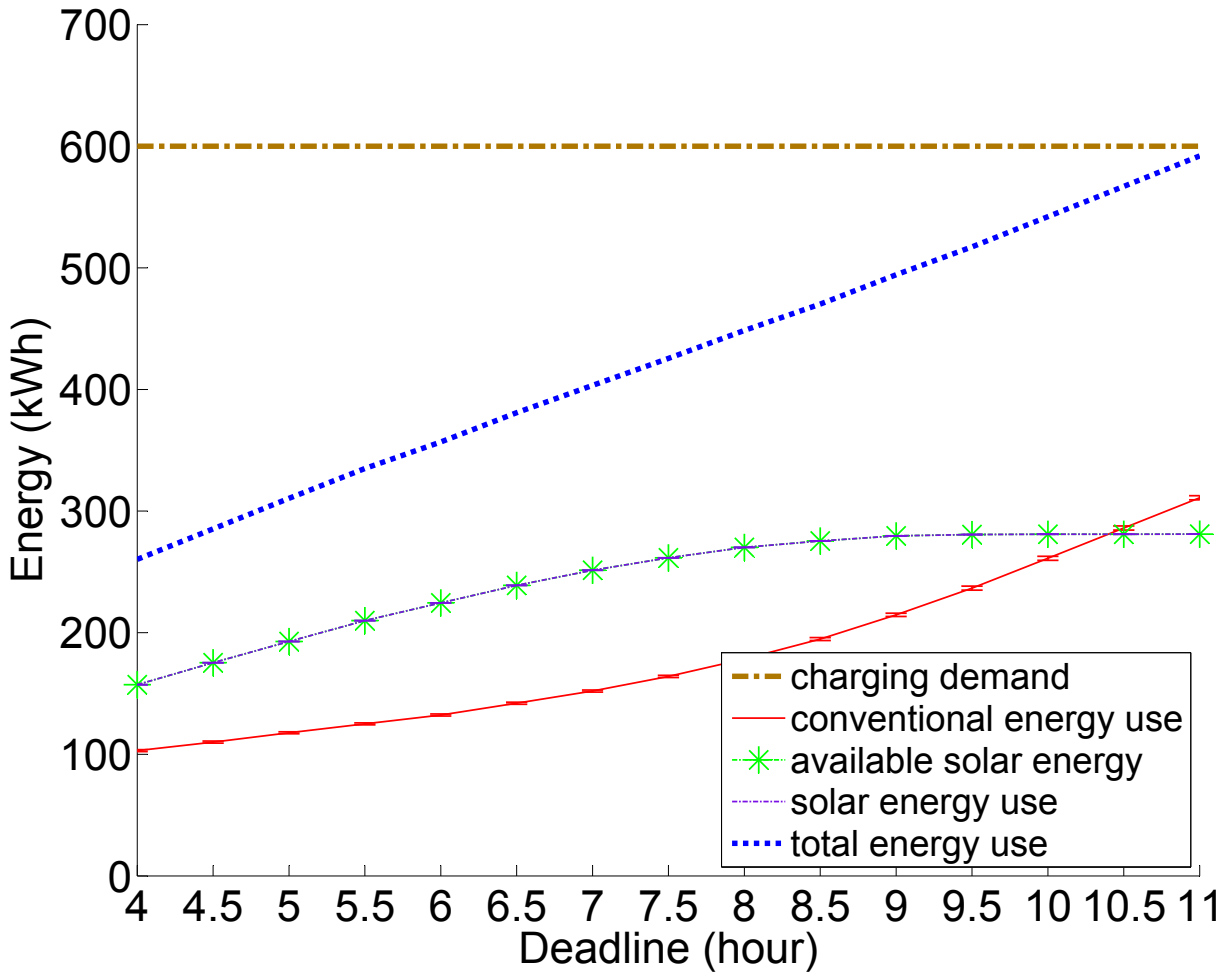


Figure 6.4: Average energy supplied by different sources for different deadlines in multiple simulation runs when EV population is 50, $G^{\max} = 40kW$, and $C^{\max} = 50kW$. Note that error bars represent one standard error.

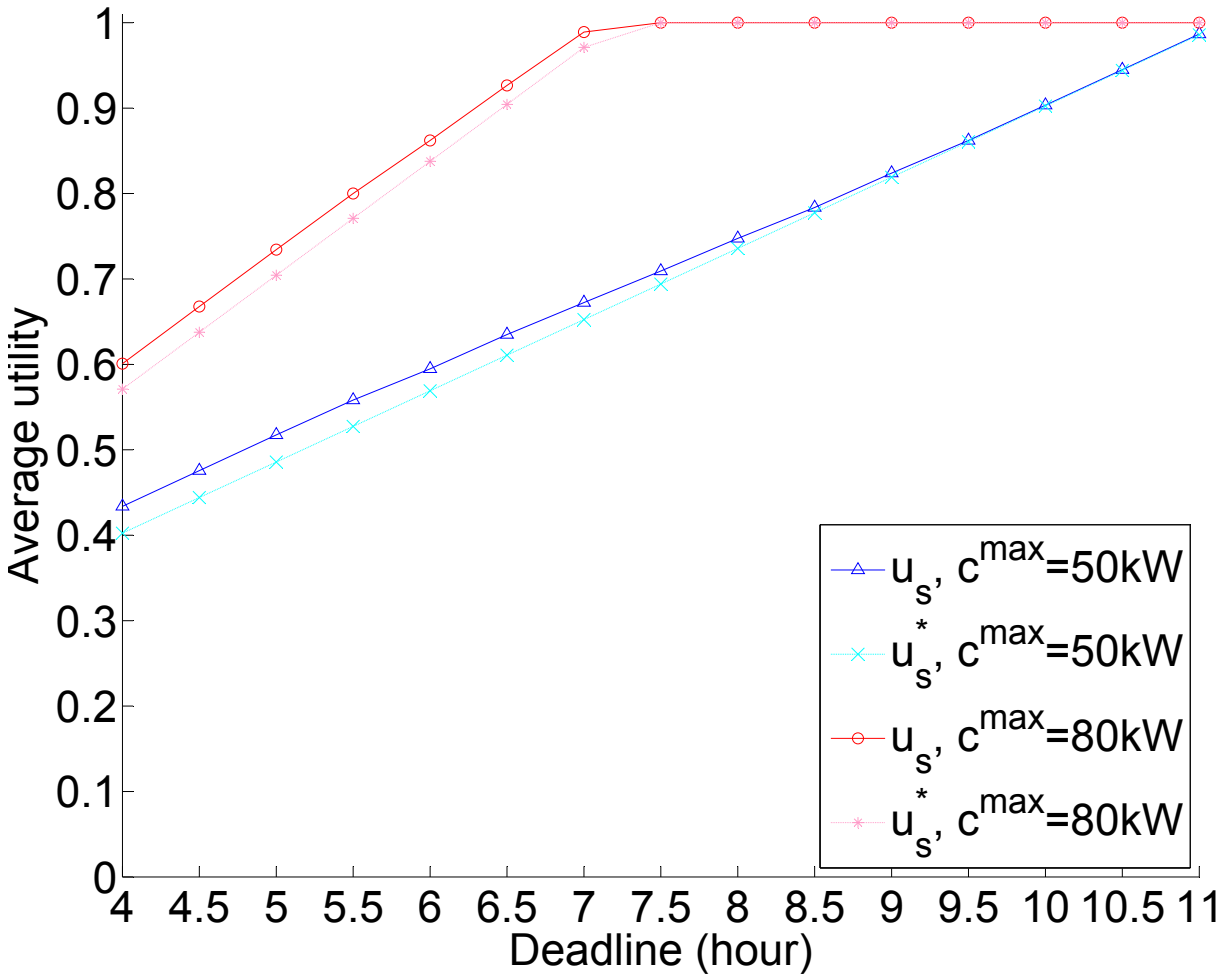


Figure 6.5: Average customer utility, $u_{s,d}$, obtained by solving Problem 3 and the average worst-case utility, $u^*_{s,d}$ for different deadlines and two different values of $C^{\max}$ when EV population is 50 and $G^{\max} = 40kW$.

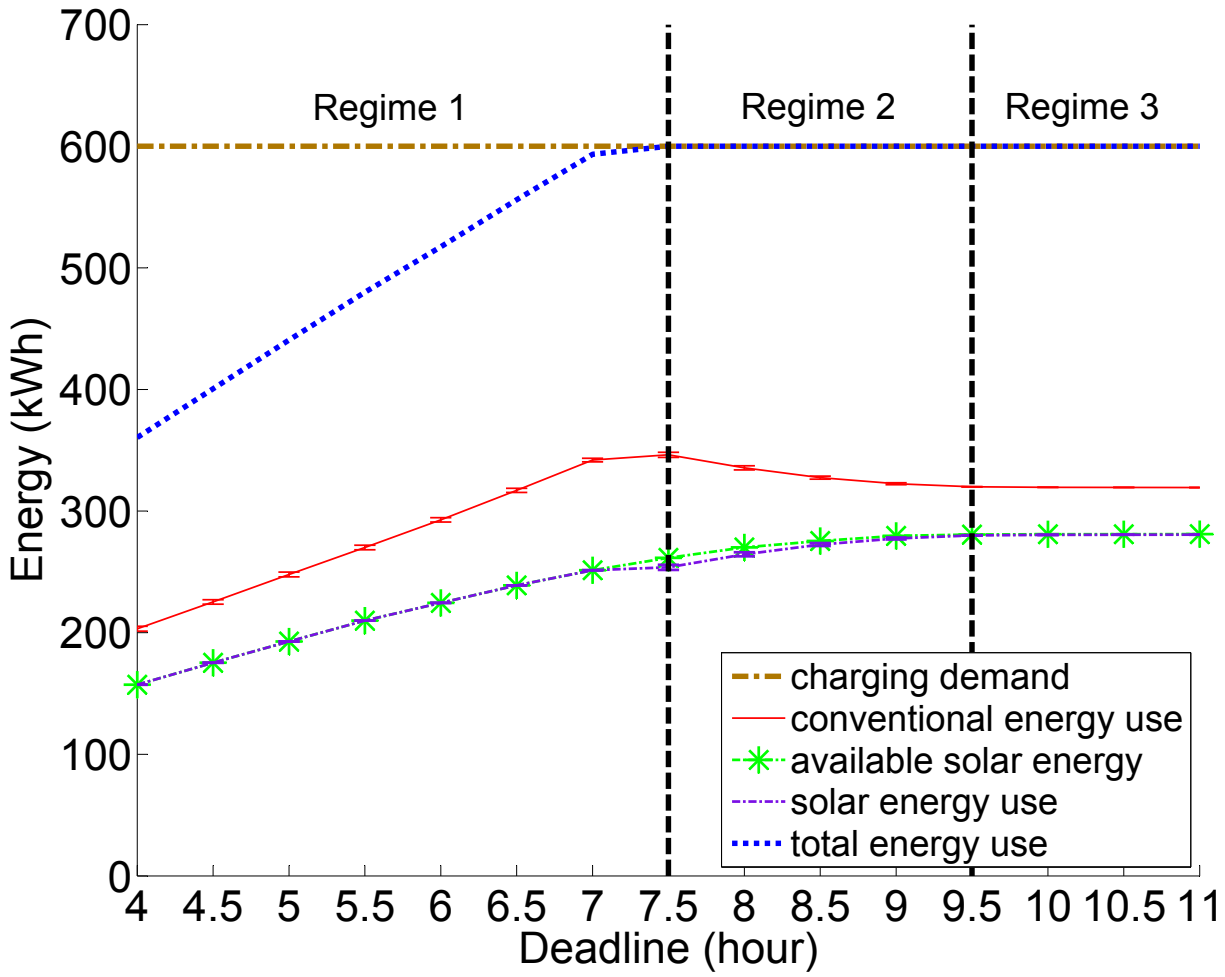


Figure 6.6: Average energy supplied by different sources for different deadlines in multiple simulation runs, when EV population is 50, $G^{\max} = 40kW$, and $C^{\max} = 80kW$. Note that error bars represent one standard error.

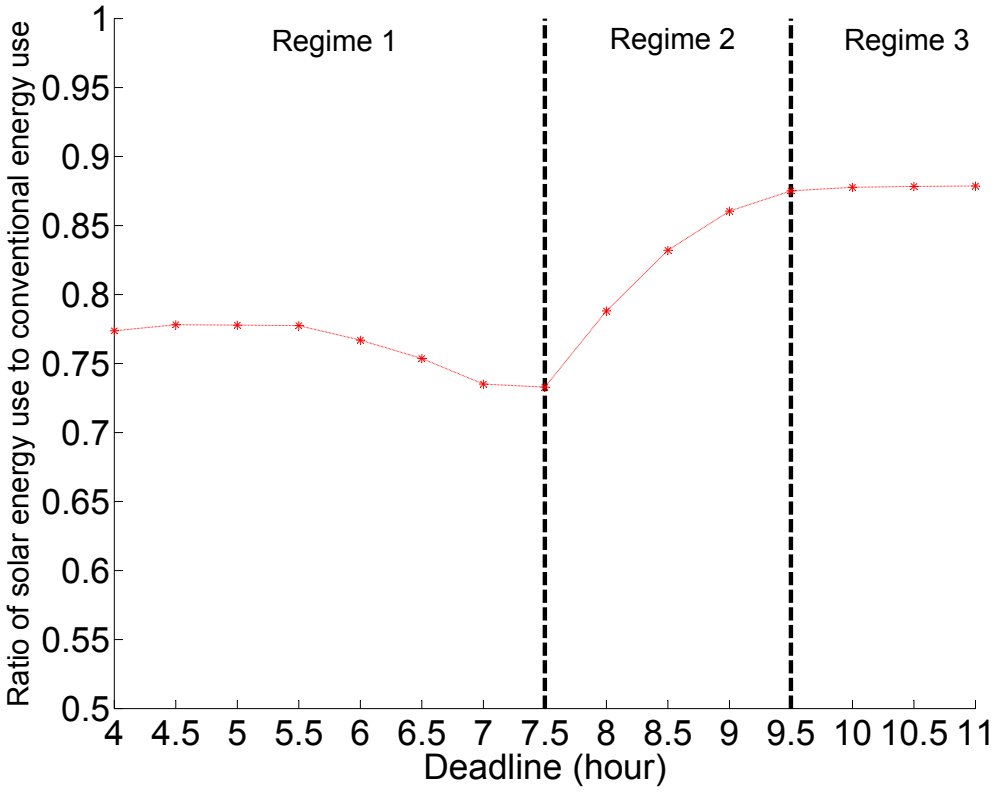


Figure 6.7: Regime switching happens as the deadline increases. In this case, the EV population is 50, $G^{\max} = 40kW$, and $C^{\max} = 80kW$.

solar energy for charging EVs. Therefore, the proposed strategy replaces some amount of conventional energy with solar energy to further reduce the cost without affecting the customer utility. In this regime, extending the deadlines does not benefit the customers, although it helps reduce the overall cost of EV charging (in the favour of the CSP). Finally, in the third regime extending the deadlines does not benefit the customers and does not reduce the cost of EV charging since no more solar energy is available late in the evening.

Figure 6.7 shows the difference between these three regimes. In particular, it shows the ratio of the used solar energy to the used conventional energy determined by the algorithm. It can be seen that this ratio does not vary much in the first regime because the use of both supply sources increases at approximately the same rate. However, in the second regime this ratio grows noticeably as the algorithm replaces conventional power by solar power. This ratio converges to an asymptotic value in the last regime.

## 6.6 Chapter Summary

Solar power is becoming competitive with conventional power in many jurisdictions. Powering public EV charging stations using local solar generation is a promising application because solar power peaks at almost the same time that utilization of these stations peaks, creating an opportunity to absorb the available solar energy without the need for storage and to reduce the cost of EV charging. In this context, we quantified the benefits of shifting EV charging deadlines from the perspective of the CSP and customers. We proposed an offline algorithm that relies on daily solar radiation and EV mobility forecasts for computing a proportionally fair charging schedule that satisfies the minimum service requirements with the minimum cost. We implement this algorithm and run numerical simulations using real traces of solar power generation to show how extending the deadlines could change the customer utility and the use of conventional power.

# Chapter 7

# Conclusion and Future Work

This chapter concludes the thesis. In Section 7.1, we summarize contributions of our work. We outline existing challenges and several directions for future work in Section 7.2 and present concluding remarks in Section 7.3.

## 7.1 Summary

Each distribution feeder in the smart grid will soon connect thousands of EV chargers, inverter-based PV systems, and dedicated storage systems, collectively referred to as active end-nodes. Many utilities have become seriously concerned about potential impacts of the increasing penetration of active end-nodes on reliability and efficiency of their distribution systems. Studies suggest that excessive overloads, voltage deviations, bidirectional power flows, loss of coordination among power electronic devices that operate on the same feeder, and many other reliability and power quality-related issues can occur even at a low penetration of active end-nodes. This highlights the urgent need for new planning and operation practices that take active end-nodes into account.

The focus of this thesis has been on a control framework, especially in the last mile of distribution networks, to mitigate emerging operational and technical problems and fulfill various environmental, societal, and business objectives. Exploiting the availability of low-cost broadband communications in the distributing network, and pervasive monitoring of distribution equipment and loads, we introduced a novel control framework for active end-nodes. Our framework simultaneously achieves multiple control objectives, relying on real-time measurements as opposed to long-term predictions. Thus, it increases the degree of penetration of active end-nodes that can be reliably accommodated in existing power systems.

These control solutions are inspired by the design of well-established resource allocation and flow control algorithms that have been developed for the Internet. For example, we have extended the notion of proportional fairness to the EV charging problem and designed a TCP-like feedback control mechanism for EV chargers. It is worth noting that our proposed control mechanisms are developed as extensions of the mechanisms that are currently in place for balancing the grid. We summarize our contributions below.

### 7.1.1 Summary of Contributions

We studied control of active end-nodes in two different contexts: a radial distribution system and a grid-connected public EV charging station powered by on-site solar generation.

In the first context, we considered the case where EV chargers are the only type of active end-nodes connected to the radial distribution system and the case where inverter-based PV systems and battery storage systems are connected to the distribution system as well. We presented a thorough analysis of uncontrolled EV charging and solar PV generation in the context of the distribution system, motivating the need for control. We then proposed two real-time decentralized algorithms to solve multi-objective multi-constraint control problems for active end-nodes on a fast timescale in the distribution system. Using realistic load and solar generation traces and stochastic EV arrivals and departures, we showed that these real-time algorithms simultaneously achieve several objectives without violating power system constraints. In the second context, we proposed a scheduling algorithm for the public EV charging station where scalability is not a concern.

Specifically, we developed a TCP-inspired distributed feedback control mechanism for fair power allocation to smart EV chargers without causing feeder and transformer overloads in Chapter 4. What distinguishes this scheme from other EV charging schemes that deal with distribution network problems is that our control mechanism does not depend on power flow calculations; it is instead based on real-time measurements of feeder and transformer loading. The resulting control actions are sent to downstream EV chargers to independently adjust their charge power. We proved that this control is stable if household demands and the number of active chargers are constant. We then showed that this result can be extended to the case where household demands and the number of active chargers are fixed during a time slot and only change from one time slot to another. Detailed power flow analysis confirms that optimal control computed in this way does not overload feeders and transformers in a test distribution system.

The synergy between solar PV generation and EV chargers is used in Chapter 5 to tackle distribution system problems, increasing the potential penetration rate of both PV systems and EVs in the existing power system. We developed a decentralized control mechanism for active end-nodes based on linearized power flow equations for radial systems and real-time measurements of loads and states of the active end-nodes. Given that the underlying optimization problems are convex, the optimal control can be found both quickly and efficiently. This control is fair to active EV chargers, and permits sharing of solar power and the use of storage systems within a balancing zone, thereby reducing solar curtailment and the use of conventional power from the grid. We showed using numerical simulations that this control outperforms control schemes that limit solar generation to the local demand in terms of solar curtailment and conventional energy use. Our power flow analysis confirms that this control does not cause overloads, overvoltage and undervoltage conditions, or reverse flows.

Turning our attention to the public EV charging station powered by on-site solar

generation, we formulated a series of fixed-horizon centralized optimization problems to compute a cost-minimizing EV charging strategy in an offline fashion in Chapter 6. This strategy minimizes the total cost of the charging service when given a set of deadlines, leveraging solar generation to store energy in EV batteries, and allocates the available power in a proportionally fair manner among EVs with different arrival times and energy demands. This control strategy serves as a benchmark for comparing different deadlines in terms of the resultant cost and average customer satisfaction. We analyzed the three-way tradeoff between the carbon footprint of EV charging, the charging deadline, and the average customer utility. This motivates CSPs to request longer charging deadlines from 'greener' customers.

In summary, the control mechanisms proposed in this thesis simultaneously achieve various user-level and system-level objectives. This is a nontrivial task as these objectives are often competing.

## 7.2 Existing Challenges and Future Work

We present existing challenges and avenues for future work in this section.

### 7.2.1 Using a Faster Distributed Algorithm to Control EV Charging

In Chapter 4 we used the projected gradient descent algorithm to solve the master optimization problem iteratively. Gradient descent algorithms can potentially exhibit slow convergence. This reduces the convergence speed of our feedback controller to optimality, thereby reducing efficiency of the power system and increasing the equipment maintenance cost and failure risk due to possible excursions of equipment loading above its nameplate rating[1].

Other first-order methods have been proposed in the literature to solve the NUM problem using a distributed algorithm [101, 107]. Some of these methods exhibit significant improvement in the convergence speed compared to the gradient descent method. We plan to use an efficient distributed first-order method that does not require nonlocal information in the design of our controller.

[1] In recent work, an anytime algorithm is proposed for real-time control of EV chargers [77]. This algorithm produces feasible results in every iteration using communications between the substation, protective devices, and EV chargers, thereby eliminating excursions of equipment loading above its nameplate rating.

### 7.2.2 TCP-style Control for Active End-nodes

In Chapter 5, we have used the simplified DistFlow to estimate voltage and reactive power in the distribution system. Exploiting real-time measurements of loads and the state of active end-nodes, we solve a series of two open-loop optimization problems to find control in every iteration. This requires using a centralized algorithm to solve the first optimization problem, which has coupling constraints. This algorithm is clearly not scalable.

What we need is a TCP-like feedback control mechanism for active end-nodes. A potential solution approach would be to decompose the centralized optimization problem that depends on linear power flow equations, which relates active and reactive power consumptions at end-nodes to bus voltages, to obtain decoupled problems that are coordinated by a master problem using Lagrangian multipliers. This enables to develop a simple feedback control mechanism for active end-nodes based on in-network rather than end-node measurements. This control would be fully distributed and is therefore more scalable compared to the proposed open-loop control mechanism. Designing this control mechanism is complicated because there are many coupled variables and coupling constraints.

### 7.2.3 Generalizing to Unbalanced Multi-phase Distribution Systems

We solve power flow equations separately for each phase of the distribution network to obtain optimal control decisions in Chapters 4 and 5. However, distribution networks are usually unbalanced and ignoring the coupling between different phases introduces some error into our analysis. A possible direction for future work is to substitute this model with a distribution power flow model for unbalanced multi-phase networks, similar to the linear approximation proposed in [35] or the generic distribution power flow model proposed in [72]. This unbalanced power flow model is more accurate for distribution systems and will also permit us to balance phase loads.

We note that loads are typically modeled as voltage dependent components in distribution systems. To simplify power flow calculations, we used the constant power load model in Chapter 5. A better load model is also a fruitful avenue for future work.

### 7.2.4 Optimizing Switching Operations of Load Tap Changers and Capacitors

Conventional distribution system operation has been chiefly concerned about voltage and reactive power control using local measurements with distribution loss minimization being the operational objective in most cases. This is generally achieved by solving a distribution optimal power flow problem to control operations of transformer LTCs and switched capacitors [72].

Recall that the optimization problems solved in Chapter 5 to compute optimal control of active end-nodes also involves power flow calculations for the distribution system. This indicates the possibility of incorporating transformer LTCs and switched capacitors into our control problem to jointly optimize operations of EV chargers, solar PV inverters, storage systems, and switching operations of taps and capacitors. A similar approach has been taken in [83] to control EV chargers and taps and capacitor switching decisions. The main challenge here is that active end-nodes, and LTCs and capacitors must be controlled on two different timescales; thus, combining them into a single control problem requires careful consideration of the control timescales.

This is a step toward designing a comprehensive large-scale control architecture for distribution systems.

### 7.2.5 Model Predictive Control for the Public EV Charging Station

Instead of using fixed horizon optimization in Chapter 6, which suffers from obsolete and infeasible control decisions due to long-term prediction errors, an alternative would be to use receding horizon optimization that takes advantage of short term predictions and the newly updated state of the system to arrive at improved optimal controls for the current time slot, and repeats this process for the next time slot after updating the state of the system using most recent measurements and shifting forward the prediction horizon. This yields EV charging control decisions that are closer to theoretically optimal decisions in terms of the cost and the use of solar power, compared to current charging schedules computed ahead of time based on potentially inaccurate predictions. Hence, the MPC framework can be used to control charging of a finite EV population in the context of a public charging station.

## 7.3 Concluding Remarks

The increasing penetration of elastic loads and distributed renewable generation, along with the introduction of measurement, communication, and control technologies in power distribution systems has several implications. Specifically, pervasive measurement and communication increases interactions between customers, system operators, and independent producers, providing new opportunities to improve reliability, as well as cost and carbon efficiency of the grid. Additionally, the integration of active end-nodes into low-voltage residential distribution networks introduces several new environmental, societal, and business objectives for which the grid has not been designed originally. We believe that control plays a key role in accomplishing these goals. However, existing grid controls are incapable of solving multi-objective multi-constraint problems that involve a large number of active end-nodes and new control solutions have not been defined yet to achieve recently introduced objectives of the active end-nodes. This work attempts to fill this gap in the literature by developing fast timescale control mechanisms for active end-nodes.

Despite the novelty of our approach, it has certain limitations. In particular, proposed control mechanisms only work for balanced radial systems, the underlying power flow model is approximate and could therefore result in suboptimal or infeasible control decisions, the convergence speed of the gradient decent algorithm used in the design of the feedback controller is slow in most cases, and the decentralized control algorithm does not scale well with the size of the network and the number of active end-nodes. These limitations present ample opportunities for future work.

# References


[1] K.H. Abdul-Rahman, S.M. Shahidehpour, M. Aganagic, and S. Mokhtari. A practical resource scheduling with OPF constraints. *Power Systems, IEEE Transactions on*, 11(1):254–259, Feb 1996.

[2] Y.P. Agalgaonkar, B.C. Pal, and R.A. Jabr. Distribution voltage control considering the impact of pv generation on tap changers and autonomous regulators. *Power Systems, IEEE Transactions on*, 29(1):182–192, Jan 2014.

[3] C. Ahn, C.T. Li, and H. Peng. Optimal decentralized charging control algorithm for electrified vehicles connected to smart grid. *J. Power Sources*, 196(2):10369–10379, 2011.

[4] AMPL Optimization. AMPL. http://ampl.com/products/ampl/.

[5] M. Amrhein and P.T. Krein. Dynamic simulation for analysis of hybrid electric vehicle system and subsystem interactions, including power electronics. *Vehicular Technology, IEEE Transactions on*, 54(3):825–836, May 2005.

[6] O. Ardakanian, S. Keshav, and C. Rosenberg. Markovian models for home electricity consumption. In *Proceedings of the 2nd ACM SIGCOMM workshop on Green networking*, pages 31–36, 2011.

[7] O. Ardakanian, S. Keshav, and C. Rosenberg. Real-time distributed control for smart electric vehicle chargers: From a static to a dynamic study. *Smart Grid, IEEE Transactions on*, 5(5):2295–2305, Sept 2014.

[8] O. Ardakanian, C. Rosenberg, and S. Keshav. Realtime distributed congestion control for electrical vehicle charging. *SIGMETRICS Performance Evaluation Review*, 40(3):38–42, January 2012.

[9] O. Ardakanian, C. Rosenberg, and S. Keshav. Distributed control of electric vehicle charging. In *ACM e-Energy*, pages 101–112, 2013.

[10] O. Ardakanian, C. Rosenberg, and S. Keshav. Quantifying the benefits of extending electric vehicle charging deadlines with solar generation. In *IEEE Smart Grid Communications*, pages 620–625, 2014.

[11] S. Bae and A. Kwasinski. Spatial and temporal model of electric vehicle charging demand. *Smart Grid, IEEE Transactions on*, 3(1):394–403, March 2012.

[12] S. Bansal, M.N. Zeilinger, and C.J. Tomlin. Plug-and-play model predictive control for electric vehicle charging and voltage control in smart grids. In *IEEE Conference on Decision and Control*, pages 5894–5900, 2014.

[13] M.E. Baran, H. Hooshyar, Zhan Shen, and A. Huang. Accommodating high PV penetration on distribution feeders. *Smart Grid, IEEE Transactions on*, 3(2):1039–1046, June 2012.

[14] M.E. Baran and F.F. Wu. Network reconfiguration in distribution systems for loss reduction and load balancing. *Power Delivery, IEEE Transactions on*, 4(2):1401–1407, Apr 1989.

[15] M.E. Baran and F.F. Wu. Optimal capacitor placement on radial distribution systems. *Power Delivery, IEEE Transactions on*, 4(1):725–734, Jan 1989.

[16] M.E. Baran and F.F. Wu. Optimal sizing of capacitors placed on a radial distribution system. *Power Delivery, IEEE Transactions on*, 4(1):735–743, Jan 1989.

[17] T.A. Becker, I. Sidhu, and B. Tenderich. Electric vehicles in the United States: A new model with forecasts to 2030, August 2009.

[18] D.P. Bertsekas and J.N. Tsitsiklis. *Parallel and distributed computation: numerical methods*. Prentice-Hall, Inc., Upper Saddle River, NJ, USA, 1989.

[19] California ISO. Fast Facts. http://www.caiso.com/Documents/FlexibleResourcesHelpRenewables_FastFacts.pdf, Retrieved on June 1, 2015.

[20] California New Car Dealers Association. California auto outlook. http://www.cncda.org/CMS/Pubs/Cal_Covering_4Q_14.pdf, February 2015.

[21] D.S. Callaway and I.A. Hiskens. Achieving controllability of electric loads. *Proceedings of the IEEE*, 99(1):184–199, Jan 2011.

[22] S. Chen and L. Tong. iEMS for large scale charging of electric vehicles: Architecture and optimal online scheduling. In *IEEE Smart Grid Communications*, pages 629–634, 2012.

[23] K. Clement-Nyns, E. Haesen, and J. Driesen. The impact of charging plug-in hybrid electric vehicles on a residential distribution grid. *Power Systems, IEEE Transactions on*, 25(1):371–380, Feb 2010.

[24] M.H. Coddington, B. Kroposki, T. Basso, K. Lynn, D. Sammon, M. Vaziri, and T. Yohn. Photovoltaic systems interconnected onto secondary network distribution systems-success stories. Report NREL/TP-550-45061, National Renewable Energy Laboratory, April 2009.

[25] N. DeForest, J. Funk, A. Lorimer, B. Ur, I. Sidhu, P. Kaminsky, and B. Tenderich. Impact of widespread electric vehicle adoption on the electrical utility business - threats and opportunities, August 2009.

[26] S. Deilami, A.S. Masoum, P.S. Moses, and M. A S Masoum. Real-time coordination of plug-in electric vehicle charging in smart grids to minimize power losses and improve voltage profile. *Smart Grid, IEEE Transactions on*, 2(3):456–467, Sept 2011.

[27] The Economist. Sunny Uplands: Alternative energy will no longer be alternative. http://www.economist.com/news/21566414-alternative-energy-will-no-longer-be-alternative-sunny-uplands, Retrieved on April 1, 2014.

[28] Electric Vehicles Initiative and International Energy Agency. Global EV Outlook. http://www.iea.org/evi/Global-EV-Outlook-2015-Update_1page.pdf, 2015.

[29] Agora Energiewende. The German Energiewende and its climate paradox. Report 038/04-A-2014/EN, Agora Energiewende, April 2014.

[30] EPIA. Global market outlook for photovoltaics 2014–2018. http://www.epia.org/news/publications/global-market-outlook-for-photovoltaics-2014-2018/, June 2014.

[31] EPRI. Simulation Tool – OpenDSS. http://smartgrid.epri.com/SimulationTool.aspx.

[32] Z. Fan. A distributed demand response algorithm and its application to PHEV charging in smart grids. *Smart Grid, IEEE Transactions on*, 3(3):1280–1290, Sept 2012.

[33] M. Farivar, L. Chen, and S. Low. Equilibrium and dynamics of local voltage control in distribution systems. In *IEEE Conference on Decision and Control*, pages 4329–4334, Dec 2013.

[34] M. Farivar, R. Neal, C. Clarke, and S. Low. Optimal inverter VAR control in distribution systems with high PV penetration. In *IEEE PES General Meeting*, pages 1–7, July 2012.

[35] L. Gan. *Distributed Load Control in Multiphase Radial Networks*. Phd thesis, California Institute of Technology, 2015.

[36] L. Gan, U. Topcu, and S Low. Optimal decentralized protocol for electric vehicle charging. *Power Systems, IEEE Transactions on*, 28(2):940–951, May 2013.

[37] L. Gan, A. Wierman, U. Topcu, N. Chen, and S.H. Low. Real-time deferrable load control: handling the uncertainties of renewable generation. In *ACM e-Energy*, pages 113–124, 2013.

[38] Q. Gong, S. Midlam-Mohler, V. Marano, and G. Rizzoni. Study of PEV charging on residential distribution transformer life. *Smart Grid, IEEE Transactions on*, 3(1):404–412, March 2012.

[39] X. Guan, Q. Zhai, and A. Papalexopoulos. Optimization based methods for unit commitment: Lagrangian relaxation versus general mixed integer programming. In *IEEE PES General Meeting*, volume 2, pages 1095–1100, July 2003.

[40] H. Hao, B.M. Sanandaji, K. Poolla, and T.L. Vincent. Aggregate flexibility of thermostatically controlled loads. *Power Systems, IEEE Transactions on*, 30(1):189–198, Jan 2015.

[41] R. Hermans, M. Almassalkhi, and I. Hiskens. Incentive-based coordinated charging control of plug-in electric vehicles at the distribution-transformer level. In *American Control Conference (ACC)*, pages 264–269, 2012.

[42] G.T. Heydt. The impact of electric vehicle deployment on load management straregies. *Power Apparatus and Systems, IEEE Transactions on*, PAS-102(5):1253–1259, May 1983.

[43] C.A. Hill, M.C. Such, D. Chen, J. Gonzalez, and W.M. Grady. Battery energy storage for enabling integration of distributed solar power generation. *Smart Grid, IEEE Transactions on*, 3(2):850–857, June 2012.

[44] A.D. Hilshey, P. Rezaei, P.D.H. Hines, and J. Frolik. Electric vehicle charging: Transformer impacts and smart, decentralized solutions. In *IEEE PES General Meeting*, pages 1–8, 2012.

[45] HydroOne. peaksaver PLUS. http://www.hydroone.com/peaksaver, Retrieved on June 1, 2015.

[46] International Energy Agency. CO2 Emissions from Fuel Combustion. http://www.iea.org/publications/freepublications/publication/CO2EmissionsFromFuelCombustionHighlights2014.pdf, 2014.

[47] R. Jin, B. Wang, P. Zhang, and P.B. Luh. Decentralised online charging scheduling for large populations of electric vehicles: a cyber-physical system approach. *International Journal of Parallel, Emergent and Distributed Systems*, 28(1):29–45, February 2013.

[48] F. Katiraei and J.R. Agüero. Solar PV integration challenges. *Power and Energy Magazine, IEEE*, 9(3):62–71, May 2011.

[49] F. Katiraei, C. Sun, and B. Enayati. No inverter left behind: Protection, controls, and testing for high penetrations of PV inverters on distribution systems. *Power and Energy Magazine, IEEE*, 13(2):43–49, March 2015.

[50] F. Kelly. Charging and rate control for elastic traffic. *European transactions on Telecommunications*, 8(1):33–37, 1997.

[51] F.P. Kelly, A.K. Maulloo, and D.K.H. Tan. Rate control for communication networks: Shadow prices, proportional fairness and stability. *Journal of the Operational Research Society*, 49(3):237–252, March 1998.

[52] W.H. Kersting. Radial distribution test feeders. In *IEEE Power Engineering Society Winter Meeting*, volume 2, pages 908–912 vol.2, 2001.

[53] W.H. Kersting. *Distribution System Modeling and Analysis, Third Edition*. Taylor & Francis, 2012.

[54] S. Keshav and C. Rosenberg. How Internet concepts and technologies can help green and smarten the electrical grid. *SIGCOMM Computer Communication Review*, 41:109–114, January 2011.

[55] D. Lew et al. Wind and solar curtailment. Report NREL/CP-5500-60245, National Renewable Energy Laboratory, September 2013.

[56] Q. Li, T. Cui, R. Negi, F. Franchetti, and M.D. Ilic. On-line decentralized charging of plug-in electric vehicles in power systems, 2011.

[57] T. Li and M. Shahidehpour. Price-based unit commitment: a case of lagrangian relaxation versus mixed integer programming. *Power Systems, IEEE Transactions on*, 20(4):2015–2025, Nov 2005.

[58] J.A.P. Lopes, F.J. Soares, and P.M.R. Almeida. Integration of electric vehicles in the electric power system. *Proceedings of the IEEE*, 99(1):168–183, 2011.

[59] S.H. Low and D.E. Lapsley. Optimization flow control. I. Basic algorithm and convergence. *Networking, IEEE/ACM Transactions on*, 7(6):861–874, Dec 1999.

[60] Z. Ma, D.S. Callaway, and I.A. Hiskens. Decentralized charging control of large populations of plug-in electric vehicles. *Control Systems Technology, IEEE Transactions on*, 21(1):67–78, Jan 2013.

[61] McKinsey. The disruptive potential of solar power. http://www.mckinsey.com/insights/energy_resources_materials/the_disruptive_potential_of_solar_power, Retrieved on April 7, 2014.

[62] N. Mehboob, C. Canizares, and C. Rosenberg. Day-ahead dispatch of PEV loads in a residential distribution system. In *IEEE PES General Meeting*, pages 1–5, July 2014.

[63] A. Meier. *Electric Power Systems: A Conceptual Introduction*. Wiley-IEEE Press, 2006.

[64] A.D. Mills et al. Understanding variability and uncertainty of photovoltaics for integration with the electric power system. Report LBNL-2855E, Lawrence Berkeley National Laboratory, December 2009.

[65] Tesla Motors. Tesla Gigafactory. http://www.teslamotors.com/gigafactory, Retrieved on June 1, 2015.

[66] Nissan. Nissan Leaf. http://www.nissan.ca/en/electric-cars/leaf/versions-specs/version.s.html, Retrieved on June 1, 2015.

[67] NREL. The Measurement and Instrumentation Data Center (MIDC), US Virgin Islands Bovoni 2. http://www.nrel.gov/midc/usvi_bovoni2/, Retrieved on April 1, 2014.

[68] NREL. Atmospheric radiation measurement program. http://www.nrel.gov/midc/arm_rcs/, Retrieved on September 1, 2014.

[69] B. Nykvist and M. Nilsson. Rapidly falling costs of battery packs for electric vehicles. *Nature Climate Change*, 2015.

[70] D.P. Palomar and M. Chiang. A tutorial on decomposition methods for network utility maximization. *Selected Areas in Communications, IEEE Journal on*, 24(8):1439–1451, Aug 2006.

[71] Giles Parkinson. Rooftop solar to cut total grid demand to zero in South Australia. http://reneweconomy.com.au/2015/rooftop-solar-to-cut-total-grid-demand-to-zero-in-south-australia-32943, Retrieved on June 20, 2015.

[72] S. Paudyal, C.A. Canizares, and K. Bhattacharya. Optimal operation of distribution feeders in smart grids. *Industrial Electronics, IEEE Transactions on*, 58(10):4495–4503, Oct 2011.

[73] L. Pieltain Fernández, T.G.S. Román, R. Cossent, C.M. Domingo, and P. Frías. Assessment of the impact of plug-in electric vehicles on distribution networks. *Power Systems, IEEE Transactions on*, 26(1):206–213, Feb 2011.

[74] K. Qian, C. Zhou, M. Allan, and Y. Yuan. Modeling of load demand due to EV battery charging in distribution systems. *Power Systems, IEEE Transactions on*, 26(2):802–810, May 2011.

[75] S. Rahman and G.B. Shrestha. An investigation into the impact of electric vehicle load on the electric utility distribution system. *Power Delivery, IEEE Transactions on*, 8(2):591–597, Apr 1993.

[76] Deutsche Bank Market Research. 2014 outlook: Let the second gold rush begin. http://www.deutschebank.nl/nl/docs/Solar_-_2014_Outlook_Let_the_Second_Gold_Rush_Begin.pdf, January 2014.

[77] J. Rivera, C. Goebel, and H. Jacobsen. A distributed anytime algorithm for real-time ev charging congestion control. In *ACM e-Energy*, pages 67–76, 2015.

[78] N. Rotering and M. Ilic. Optimal charge control of plug-in hybrid electric vehicles in deregulated electricity markets. *Power Systems, IEEE Transactions on*, 26(3):1021–1029, Aug 2011.

[79] SAE. SAE J1772 Standard. http://www.sae.org/smartgrid/chargingspeeds.pdf, Retrieved on April 7, 2014.

[80] S. Shao, M. Pipattanasomporn, and S. Rahman. Challenges of PHEV penetration to the residential distribution network. In *IEEE PES General Meeting*, pages 1–8, 2009.

[81] S. Shao, M. Pipattanasomporn, and S. Rahman. Demand response as a load shaping tool in an intelligent grid with electric vehicles. *Smart Grid, IEEE Transactions on*, 2(4):624–631, Dec 2011.

[82] S. Shao, M. Pipattanasomporn, and S. Rahman. Grid integration of electric vehicles and demand response with customer choice. *Smart Grid, IEEE Transactions on*, 3(1):543–550, March 2012.

[83] I. Sharma, C. Canizares, and K. Bhattacharya. Smart charging of PEVs penetrating into residential distribution systems. *Smart Grid, IEEE Transactions on*, 5(3):1196–1209, May 2014.

[84] E. Sortomme, M.M. Hindi, S.D.J. MacPherson, and S.S. Venkata. Coordinated charging of plug-in hybrid electric vehicles to minimize distribution system losses. *Smart Grid, IEEE Transactions on*, 2(1):198–205, March 2011.

[85] R. Srikant. *The Mathematics of Internet Congestion Control (Systems and Control: Foundations and Applications)*. Birkhauser, 2004.

[86] S. Studli, E. Crisostomi, R. Middleton, and R. Shorten. AIMD-like algorithms for charging electric and plug-in hybrid vehicles. In *Electric Vehicle Conference (IEVC), 2012 IEEE International*, pages 1–8, 2012.

[87] W. Su and M.Y. Chow. Computational intelligence-based energy management for a large-scale PHEV/PEV enabled municipal parking deck. *Applied Energy*, 96(0):171–182, 2012.

[88] X. Su, M.A.S. Masoum, and P.J. Wolfs. Optimal PV inverter reactive power control and real power curtailment to improve performance of unbalanced four-wire LV distribution networks. *Sustainable Energy, IEEE Transactions on*, 5(3):967–977, July 2014.

[89] A. Subramanian, M. Garcia, A. Dominguez-Garcia, D. Callaway, K. Poolla, and P. Varaiya. Real-time scheduling of deferrable electric loads. In *American Control Conference (ACC), 2012*, pages 3643–3650, June 2012.

[90] O. Sundström and C. Binding. Optimization methods to plan the charging of electric vehicle fleets. In *Proceedings of the International Conference on Control, Communication and Power Engineering*, pages 28–29, 2010.

[91] J. Taft and P. De Martini. Cisco Systems – Ultra Large-Scale Power System Control Architecture. http://www.cisco.com/web/strategy/docs/energy/control_architecture.pdf, October 2012.

[92] J. Taft and P. De Martini. Ultra-large scale control architecture. In *IEEE PES Innovative Smart Grid Technologies (ISGT)*, pages 1–6, Feb 2013.

[93] The Edison Foundation IEI. Utility-Scale Smart Meter Deployments. http://www.edisonfoundation.net/iei/Documents/IEI_SmartMeterUpdate_0914.pdf, September 2014.

[94] M. Thomson and D.G. Infield. Network power-flow analysis for a high penetration of distributed generation. *Power Systems, IEEE Transactions on*, 22(3):1157–1162, Aug 2007.

[95] J. Tomić and W. Kempton. Using fleets of electric-drive vehicles for grid support. *J. Power Sources*, 168(2):459–468, 2007.

[96] K. Turitsyn, N. Sinitsyn, S. Backhaus, and M. Chertkov. Robust broadcast-communication control of electric vehicle charging. In *IEEE Smart Grid Communications*, pages 203–207, 2010.

[97] K. Turitsyn, P. Sulc, S. Backhaus, and M. Chertkov. Distributed control of reactive power flow in a radial distribution circuit with high photovoltaic penetration. In *IEEE PES General Meeting*, pages 1–6, July 2010.

[98] United States Department of Energy. One million electric vehicles by 2015. http://www.eere.energy.gov/vehiclesandfuels/pdfs/1_million_electric_vehicles_rpt.pdf, February 2011.

[99] J.G. Vlachogiannis. Probabilistic constrained load flow considering integration of wind power generation and electric vehicles. *Power Systems, IEEE Transactions on*, 24(4):1808–1817, Nov 2009.

[100] R.A. Walling, R. Saint, R.C. Dugan, J. Burke, and L.A. Kojovic. Summary of distributed resources impact on power delivery systems. *Power Delivery, IEEE Transactions on*, 23(3):1636–1644, July 2008.

[101] E. Wei, A. Ozdaglar, and A. Jadbabaie. A distributed newton method for network utility maximization–I: Algorithm. *Automatic Control, IEEE Transactions on*, 58(9):2162–2175, Sept 2013.

[102] C.K. Wen, J.C. Chen, J.H. Teng, and P. Ting. Decentralized plug-in electric vehicle charging selection algorithm in power systems. *Smart Grid, IEEE Transactions on*, 3(4):1779–1789, Dec 2012.

[103] A.J. Wood and B.F. Wollenberg. *Power Generation, Operation, and Control*. Wiley, 2 edition, 2012.

[104] Y. Xu and F. Pan. Scheduling for charging plug-in hybrid electric vehicles. In *IEEE Conference on Decision and Control*, pages 2495–2501, Dec 2012.

[105] H. Yaïche, R.R. Mazumdar, and C. Rosenberg. A game theoretic framework for bandwidth allocation and pricing in broadband networks. *IEEE/ACM Trans. Networking*, 8(5):667–678, 2000.

[106] M. Yilmaz and P.T. Krein. Review of battery charger topologies, charging power levels, and infrastructure for plug-in electric and hybrid vehicles. *Power Electronics, IEEE Transactions on*, 28(5):2151–2169, May 2013.

[107] M. Zargham, A. Ribeiro, A. Ozdaglar, and A. Jadbabaie. Accelerated dual descent for network flow optimization. *Automatic Control, IEEE Transactions on*, 59(4):905–920, April 2014.

[108] T. Zhang, W. Chen, Z. Han, and Z. Cao. Charging scheduling of electric vehicles with local renewable energy under uncertain electric vehicle arrival and grid power price. *Vehicular Technology, IEEE Transactions on*, 63(6):2600–2612, July 2014.

# APPENDICES

# Appendix A

# A Simulation Framework for Active End-node Control

Evaluating the mechanisms proposed for the control of active end-nodes in the smart grid requires a simulation framework that supports four principal functions:

- Creating large-scale scenarios with several stochastic variables
- Simulating the operation of the control scheme and communications between control nodes and measurement devices
- Solving optimization problems to determine control decisions
- Performing power flow calculations for a distribution system with active end-nodes

Several software programs exist for performing each of these functions; however, these programs usually support different scripting languages and their input and output formats are not compatible with each other in most cases. This calls for the design of a unified simulation framework that integrates existing simulators, coordinates their execution, and provides a simple API for creating simulation scenarios and instantiating models and variables.

To implement and validate the control schemes proposed in this thesis, we have developed a simulation framework that combines a sophisticated electrical system simulation tool for distribution systems, called OpenDSS [31], with a powerful optimization tool for modelling and solving optimization problems, called AMPL [4]. The simulation engine written in MATLAB coordinates the execution of these two simulators and enables

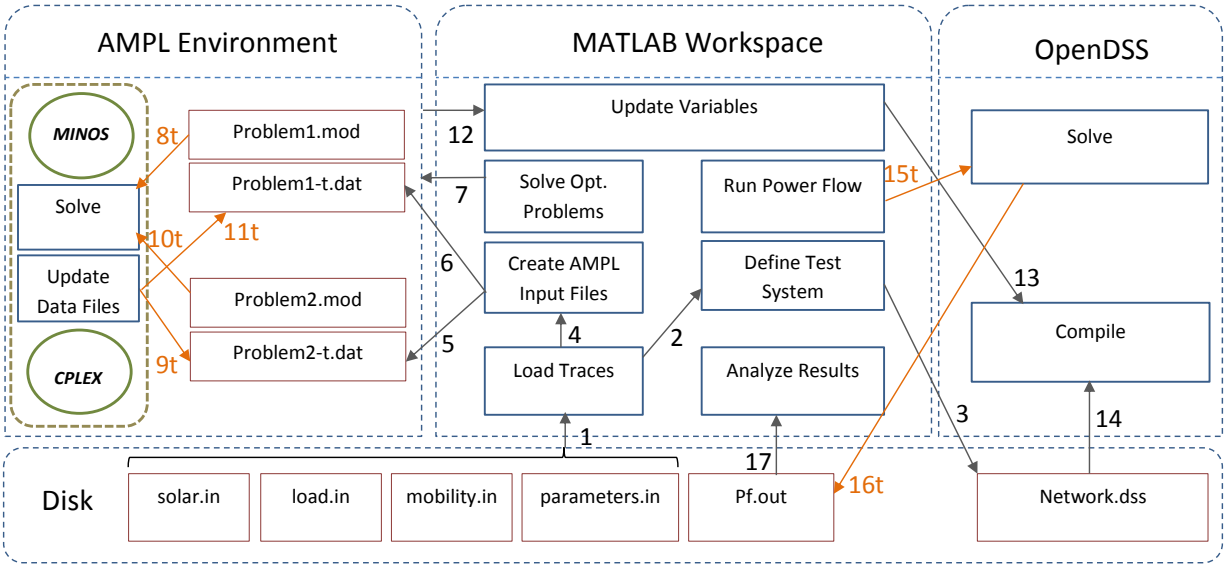


Figure A.1: A system diagram of our simulation framework.

users to specify a test distribution network, model loads and active end-nodes, generate random traces, and run discrete-time simulations for a certain time period. We describe components of this simulation framework and the flow of data and control between these components next, noting that the power flow simulator, the optimization package, and the simulation engine do not need to run on the same machine.

## A.1 Components

Figure A.1 shows the components of our simulation framework. The arrows depict data and control flows, the red boxes represent data and configuration files stored on the disk, and the blue boxes represent functions and scripts. The arrows are numbered based on their execution order, noting that those that must be executed in every time slot are labeled with a number followed by the letter 't'.

For each simulation run, the MATLAB simulator builds the distribution system and active end-node models using parameters specified in the input files. It creates the `network.dss` file and writes AMPL data files `problem1-t.dat` and `problem2-t.dat` for every time slot. The simulator then calls the AMPL solver to load optimization models and

data files and solve the two optimization problems serially for every time slot. Specifically, for a given time slot $t$, the AMPL solver solves the first optimization problem based on values provided in `problem1-t.dat` and appends its optimal solutions to `problem2-t.dat`. It then solves the second optimization problem to obtain the optimal storage operations for each balancing zone. The optimal solutions are used to update the data files for the next time slot.

Once optimal control decisions are found, they are sent to the simulation engine. Consequently, the MATLAB simulator updates its local variables and send control decisions along with other parameters to OpenDSS. The power flow simulator then loads the `network.dss` file and compiles the test system model. It performs power flow calculations for every time slot and writes bus voltages and branch flows to the `pf.out` file. The simulation engine is notified when power flow studies are done to check the feasibility of control decisions and generate plots. This concludes a simulation run.

## A.2 Functions

The following functions have been written in MATLAB:

| | |
|---|---|
| **Load Traces** | Reads data files from disk. These files include load profiles for residential and commercial customers, solar traces, and randomly generated EV mobility traces. |
| **Define Test System** | Loads the IEEE 13-bus test system model, modifies its parameters, and creates 'network.dss', which will be used by OpenDSS. |
| **Create AMPL Input Files** | Creates AMPL data files, each describing input parameters of an optimization problem defined for a single time slot. |
| **Solve Opt. Problems** | Runs a script that invokes the AMPL solvers to find optimal control decisions for every time slot in the simulation interval. |
| **Update Variables** | Fetches optimal control decisions that are found by AMPL, updates variables in the MATLAB workspace, and changes the 'network.dss' file accordingly. |
| **Run Power Flow** | Calls OpenDSS to preform power flow calculations for every time slot, to check feasibility of optimal control decisions, |

and to compute branch flows, bus voltages, and transformer loadings.

**Analyze Results** Examines voltage profiles and branch flows that are computed by OpenDSS, generates plots, and writes the output back to the disk.

The Bash scripts defined in the AMPL environment:

**Solve** Loads the optimization problem model (a *.mod file), initializes its parameters by reading the data file that corresponds to the current time slot (a *.dat file), passes options to the appropriate solver, solves the linear or nonlinear convex problem, and stores the optimal solution.

**Update Data Files** Updates model parameters using the optimal control and appends them to the data file of the next time slot.

Finally, the Component Object Model (COM) interface of OpenDSS permits us to run several commands and also call the following functions from our MATLAB simulator:

**Compile** Compiles the test distribution system model which is described in 'network.dss'.

**Solve** Runs power flow analysis to compute unknown variables, given a set of known variables for the specified distribution system. The unknown variables are usually bus voltages and power flows.

## A.3 Files

We now describe the files that are accessed by our MATLAB simulator, the OpenDSS module, or the AMPL environment.

**network.dss** Contains the distribution network model. This file is read by OpenDSS.

**problemX.mod** Describes an optimization problem model (objective functions, constraints, and input variables) in the AMPL language.

| | |
|---|---|
| **problemX-t.dat** | Contains input variables for an optimization problem for time slot $t$. |
| **load.in** | Contains daily load profiles for a certain number of homes and businesses. |
| **solar.in** | Contains incoming solar irradiance data for a certain number of days. |
| **mobility.in** | Contains arrival and departure times for a certain population of EVs. |
| **parameters.in** | Contains different simulation parameters, such as the network topology, bus association matrices, and parameters pertaining to active end-nodes. |
| **pf.out** | Contains the result of power flow calculations for every time slot. |